UNIVERSITY OF CALIFORNIA

Los Angeles

A Kinetic Rate Model Simulation
of the Initial Stages of
Thin Film Nucleation and Growth
Under Low-Energy Particle
Bombardment

A dissertation submitted in partial satisfaction of the

requirements for the degree

Doctor of Philosophy in Nuclear Engineering
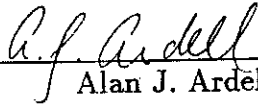
by

Charles Arnold Stone, IV

1990

The dissertation of Charles Arnold Stone, IV is approved.

M. Abdou

Mohamed A. Abdou
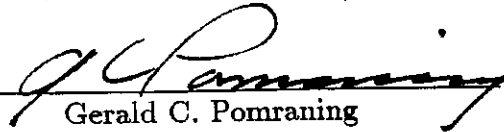
A. J. Ardell
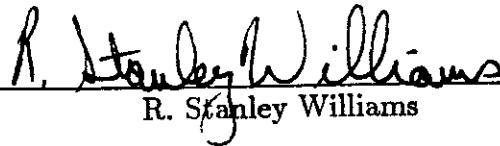
Alan J. Ardell

G. C. Pomraning

Gerald C. Pomraning

R. Stanley Williams

R. Stanley Williams

Nasr M. Ghoniem

Nasr M. Ghoniem
Committee Chair

University of California, Los Angeles

1990

Dedication

For Rocky and Smiley

Contents

List of Tables

List of Figures

List of Symbols

Uppercase Symbols

A_i	polymer which contains i-mers
A_n	polymer which contains n-mers
A_{n+i}	polymer which contains $(n+i)$-mers
$C(x,t)$	discrete x-atom cluster density $[\#/\text{cm}^2]$
$C_{agg}(t)$	$\sum_{x=2}^{\infty} C(x,t)$, the aggregate cluster density $[\#/\text{cm}^2]$
$C_b(1,t)$	bound single atom density $[\#/\text{cm}^2]$
$C_{con}(x,t)$	continuum-cluster distribution function $[\#/\text{cm}^2]$
$C_{mob}(1,t)$	mobile single atom density $[\#/\text{cm}^2]$
$C_{Norm}(x,t)$	Normal distribution for continuum clusters $[\#/\text{cm}^2]$
$C_{sm}[\rho(x,t),t]$	continuum-cluster distribution function in standard measure $[\#/\text{cm}^2]$
$C_T(t)$	single Trap density $[\#/\text{cm}^2]$
C_T°	$C_T(t=0)$, initial Trap density at time $t=0$ $[\#/\text{cm}^2]$
$C_{tot}(t)$	total density of continuum clusters $[\#/\text{cm}^2]$
E	energy of the monoenergetic, single-particle deposition source [eV]
E_a	adsorption energy for mobile single atoms [eV]

E_d	diffusion energy for mobile single atoms [eV]
E_d^T	diffusion energy for single Traps [eV]
E_{des}	desorption energy required to separate an adsorbed atom from the substrate [eV]
E_{diff}	diffusion energy which must be expended to move an adsorbed atom from one binding site to another on the substrate [eV]
E_{eject}	energy required to eject a single atom off the substrate [eV]
E_i	used to denote one of the activation energies E_d, E_d^T, E_a, or E_T [eV]
$E_{i\,Base}$	reference condition "Base Value" activation energies listed in Section 5.1 [eV]
E_T	activation energy for releasing bound single atoms from Trap sites [eV]
M	stabilizing catalyst for polymer interaction
$M_n(t)$	n^{th} central moment of the continuum-cluster distribution function
$M_2(t)$	the second moment (i. e., variance) of the continuum-cluster distribution function
N	number of moments used to reconstruct the continuum-cluster distribution function
N_{sites}	number of available substrate lattice sites [$\#/cm^2$]
$P_m(x)$	set of orthogonal polynomials
S	entropy
T	substrate temperature [K]
T_m	melting temperature of a deposited coating [K]
X_c	transition cluster size, defined as the smallest size described by the continuum distribution [atoms]
$X_{depos}(t)$	net number of particles deposited per unit substrate area [$\#/cm^2$]

E_d diffusion energy for mobile single atoms [eV]

E_d^T diffusion energy for single Traps [eV]

E_{des} desorption energy required to separate an adsorbed atom from the substrate [eV]

E_{diff} diffusion energy which must be expended to move an adsorbed atom from one binding site to another on the substrate [eV]

E_{eject} energy required to eject a single atom off the substrate [eV]

E_i used to denote one of the activation energies E_d, E_d^T, E_a, or E_T [eV]

$E_{i\,Base}$ reference condition "Base Value" activation energies listed in Section 5.1 [eV]

E_T activation energy for releasing bound single atoms from Trap sites [eV]

M stabilizing catalyst for polymer interaction

$M_n(t)$ n^{th} central moment of the continuum-cluster distribution function

$M_2(t)$ the second moment (i.e., variance) of the continuum-cluster distribution function

N number of moments used to reconstruct the continuum-cluster distribution function

N_{sites} number of available substrate lattice sites [$\#/cm^2$]

$P_m(x)$ set of orthogonal polynomials

S entropy

T substrate temperature [K]

T_m melting temperature of a deposited coating [K]

X_c transition cluster size, defined as the smallest size described by the continuum distribution [atoms]

$X_{depos}(t)$ net number of particles deposited per unit substrate area [$\#/cm^2$]

xiv

X_{max}	size of largest cluster modeled by the Discrete System [atoms]
$Z(t)$	fractional substrate surface coverage

Lowercase Symbols

$a(1)$	diameter of the deposit species [cm]
$a(x)$	diameter of an x-atom cluster [cm]
a_o	diameter of a substrate atom [cm]
a_m	expansion coefficient used in generalized Fourier series
a_T	diameter of a single Trap [cm]
c_{mn}	expansion coefficient used in orthogonal polynomials, $P_m(x)$
$e\phi$	plasma potential [eV]
$f(x)$	exact distribution
$\tilde{f}(x)$	approximation of $f(x)$
$g(x,t)$	a general function
$\langle g(x,t) \rangle$	a general function, appropriately averaged over the unknown continuum-cluster distribution function
i	a subscript denoting either T, m, b, or x which represents Traps, mobile single atoms, bound single atoms, or x-atom clusters, respectively
kT	substrate temperature [eV]
kT_e	electron temperature [eV]
$n(t)$	cluster density depicted in Figure 3.1 [#/cm^2]
$n_{max}(t)$	maximum value of the cluster density shown in Figure 3.1, achieved during the saturation stage [#/cm^2]
$p(E)$	average number of surface defects produced by each deposited particle

$p(x)$ an appropriate measure or prior probability

q single-particle deposition rate [$\#/\text{cm}^2/\text{sec}$]

r growth exponent, $0 \leq r < 1$

t time [sec]

t_o initial time for the Discrete System of kinetic clustering equations [sec]

t^* initial time for the Hybrid System of kinetic clustering equations, where $t^* > t_o$ [sec]

$w(x)$ an appropriate weight function (based on orthogonality condition)

x number of atoms in a cluster

$\langle x \rangle (t)$ average size of continuum clusters [atoms]

x_s the smallest cluster size used during the Constrained MEP reconstruction

Greek Uppercase Symbols

Γ diffusion coefficient [cm^2/sec]

$\Theta(z)$ step function; $\Theta(z) = 1$ for $z \geq 0$, but zero otherwise

Λ_o evaporation energy of the adsorbed species, characterizing the binding of the deposited atoms to one another [eV]

Greek Lowercase Symbols

$\beta_{m,i}$ size factor for mobile single atoms migrating with species i

$\beta_{T,i}$ size factor for mobile single Traps migrating with species i

$\gamma_{m,i}$ motion factor for mobile single atoms migrating with species i

$\gamma_{T,i}$	motion factor for mobile single Traps migrating with species i
δ_{ab}	$\delta_{ab} = 1$ if $a = b$, but zero otherwise
$\theta(j,t)$	moment ratio function
$\lambda(E)$	mean free path for single-atom re-solution [cm]
λ_k	Lagrange multipliers
ν_o	characteristic vibration frequency [sec^{-1}]
ν_1	average vibrational frequency for both mobile single-atom and single-trap diffusive "hops" in all directions on the substrate [sec^{-1}]
ν_2	characteristic vibration frequency [sec^{-1}]
$\nu_a = \tau_a^{-1}$	frequency at which mobile single atoms evaporate off the substrate [sec^{-1}]
$\nu_{diss}(x, E)$	frequency at which energetic particle bombardment dissociates x-atom clusters into $(x - 1)$-atom clusters and mobile single atoms [sec^{-1}]
$\nu_{imp}(x)$	frequency at which direct impingement of the deposit on x-atom clusters produces $(x + 1)$-atom clusters [sec^{-1}]
$\nu_{imp,T}$	frequency at which direct impingement of the deposit on single Traps creates bound single atoms [sec^{-1}]
$\nu_{m,i}(t)$	frequency at which mobile single atoms aggregate with species i on the substrate [sec^{-1}]
$\nu_T = \tau_T^{-1}$	frequency at which thermal oscillations release bound single atoms from Trap sites [sec^{-1}]
$\nu_{T,i}(t)$	frequency at which mobile single Traps aggregate with species i on the substrate [sec^{-1}]
$\xi_1(t)$	special nucleation frequency function [sec^{-1}]
$\xi_n(t)$	general nucleation frequency function [sec^{-1}]
π	dimensionless constant 3.141592654 ...

$\rho(x,t)$	cluster "size" in standard measure
$\phi_n(t)$	general drift frequency function $[\text{sec}^{-1}]$
$\psi_n(t)$	general dispersion frequency function $[\text{sec}^{-1}]$

Calligraphic Symbols

$\mathcal{A}_j(t)$	expansion coefficients used to reconstruct the continuum distribution
$\mathcal{D}(x,t)$	dispersion frequency $[\text{sec}^{-1}]$
$\mathcal{F}(x,t)$	drift frequency $[\text{sec}^{-1}]$
$\mathcal{H}_j(z)$	Chebyshev-Hermite polynomials
$\mathcal{J}(x,t)$	nucleation current $[\#/\text{cm}^2/\text{sec}]$
$\mathcal{J}(X_c,t)$	nucleation current going into the continuum $[\#/\text{cm}^2/\text{sec}]$
$\mathcal{M}_n$	the nth moment of the general function, $f(x)$
$\mathcal{R}$	region of integration

Acronyms

BCM	Binary Collision Model
EAM	Embedded Atom Method
FIM	Field Ion Microscopy
IBSD	Ion-Beam Sputtering Deposition
M&M's	Plain or peanut chocolate candies that come in the six assorted colors of black, brown, red, orange, yellow, and green. The yellow ones are my favorites. Red and green usually predominate during the Christmas season.
MANDMD	M&M's Discrete

MANDMH	M&M's Hybrid
MBE	Molecular Beam Epitaxy
MD	Molecular Dynamics
MEP	Maximum Entropy Principle
Ph. D.	Doctor of Philosophy, also known as that elusive gold ring that so many of us diligently strive for. When used in conjunction with B. S. and M. S., it also connotates "Piled Higher and Deeper".
PISCES	Plasma-Interaction Surface-Component Experimental Station
REDEP	REDEPosition of sputtered material
RF	Radio Frequency
RHS	Right-Hand Side
SOS	Solid-On-Solid
TEM	Transmission Electron Microscopy
TRIM	TRansport of Ions in Matter
TRIMCSR	TRIM with Collision cascade, Sputtering, and Replacement/Relocation events
TRIM.SP	SPuttering version of TRIM
TRIPOS	TRansport of Ions in POlyatomic Solids
UCLA	University of California, Los Angeles

Odds & Ends!

2-D	two-dimensional
3-D	three-dimensional
$\langle\ \rangle$ symbols	used to denote quantities which have been appropriately averaged over the continuum and evaluated at $x = \langle x \rangle(t)$
#$@*!?	I do not believe these remarks were found in the original version of the King's English

Acknowledgements

Goal achievement is a major measure of one's life, but even more so is being able to achieve them while still maintaining a strong feel for friends and other people.

CHARLES ARNOLD STONE, III

16 December, 1988

The variety of people, places, and events which have touched my life over the past 27 years all exert their influence in the literary prose which constitutes this dissertation. When I first told my father that I planned on attending graduate school, his reply consisted of the following two words: "Good" and "Luck". As such, I have never regarded my graduate studies as a direct means to some desired end; instead, the pursuit of a Ph. D. is something that I just decided *to do*. Consequently, my interests have focused on the complete *experience* that higher education offers, rather than mere cerebral delusions. This dissertation represents only one small aspect of this total experience.

It is not my intention to distract the reader with citations of the activities or predicaments I have ventured in as a result of my extracurricular pursuits. Nonetheless, allow me to offer the following remarks as a preface to the work which follows. No matter how bizarre or esoteric your interests may seem, document your results or share your insights with others so that future generations may enjoy the

fruits of your endeavors. Always strive to be yourself, and, within reason, always do what you want to do and believe in. More importantly, foster a greater sense of self-awareness and the world in which we live.

Since this dissertation represents a formal exposé of my scientific inquiry, a number of people should be recognized which have assisted in my development. First and foremost, I would like to acknowledge Professors Paul Turinsky, John Gilligan, and Michael Doster, three of my undergraduate mentors at North Carolina State University. The standards of excellence this triumvirate demanded enabled me to develop the skills and attitude needed for entering graduate school. Turinsky's vitality, Gilligan's composure, and Doster's thoroughness are key elements that I have tried to uphold in my own studies.

Secondly, I would like to thank all of the American taxpayers whose contributions provided me with a Magnetic Fusion Energy Technology Fellowship, sponsored by the U. S. Department of Energy through Oak Ridge Associated Universities. Craig Williamson and Gene Nardella deserve a special note of appreciation for sticking their necks out for me on a number of occasions, always supporting my interests. Thanks for showing me that real life forms can exist behind the bureaucratic facades which dot our society.

Dennis Croessmann and John Whitley gave me the opportunity to refine my experimental prowess during the summer of 1986 at Sandia National Labs in Albuquerque. In addition to warning me about the coyotes and snakes during some of my lunchtime runs, as well as pointing out which red buttons NOT to touch, Dennis and John showed me that science can really be fun. Ah, yes, it seems just yesterday I was taking data from the Electron Beam Test System with musical excerpts from Dokken echoing in the background. I can still remember Dennis chewing me out for being late to the lab one morning, and somewhere amongst my collection of artifacts is a video tape of vaporization experiments, complete

with Whitley and the boys singing television theme songs in the distance.

A note of gratitude is extended to Professor Bob Conn who helped me make the transition to UCLA in 1986. Although he did not influence my decision to come west, he did provide me with the clairvoyance and perception needed to resolve some of my own uncertainties at the time. I have never regretted my decision!

Chuck Kessel, a former office mate and 1987 UCLA graduate, shared many a Van de Kamp chocolate chip cookie with me as well as his insight on what I *should* be doing while in graduate school. Thanks for the guidance as well as the secret spaghetti recipe.

Dr. Frank D'Accone, Chair of the UCLA Musicology Department, will always have a place in my heart for exposing me to some of the greatest musical treasures in the world. Why a succession of little black dots dispersed within a setting of five parallel lines transfixes my senses still puzzles me. I only wish that I had more time to marvel in this muse.

Martin Vicanek, a post doc from the Institut für Theoretische Physik in Braunschweig, FRG, spent a year with our group from September 1989 – August 1990. During his tenure, Martin's interest in my work showed me how valuable collaborative research can be. A true friend, it's no telling how many times I called him to relay the message to the rest of the group that I would be late for the weekly meeting (usually due to the fact that I was out cycling somewhere during the early morning hours). Martin still remains oblivious to my famous "key caper" that he fell victim to, and is still probably wondering why I called my Discrete System code (discussed in Section 4.2.1), MANDMD, and my Hybrid System code (discussed in Section 4.2.2), MANDMH. Hey Martin, if you need a hint, just open a bag of M&M's! One of these days, I will publish these results in the **Journal of Computational Arts**, assuming that I eventually get around to starting this

publication. A thousand thanks for the guitar; I only wish that I had a career that it would serve me well in. In closing, remember the three "A's" and "Wha, Wha"!

Philip Chou, a research scientist in the fusion group at UCLA, is a unique individual that I have come to greatly respect and appreciate over time. His ability in answering some of my most perplexing off-the-wall computational questions still ceases to amaze me. If only his tennis game was better! I hope one day he learns how to eat barbequed chicken with the correct table manners (i.e., keep the barbeque sauce *on* the bird, not all over your face).

It is often stated that scheduling the final defense is much more difficult than actually defending one's dissertation. For my case, this turned out to be all too true. Consequently, I would like to personally thank each one of my dissertation committee members for rearranging their demanding schedules to accomodate my defense. Thank you Professors Abdou, Ardell, Ghoniem, Pomraning, and Williams for helping me beat the Fall deadline.

Jerry Pomraning deserves a special tip of my hat for giving my research a much needed kick-in-the-pants earlier this summer. Although the ogre gave me a hard time and ridiculed my work to his heart's content, his comments and criticisms helped me immensely, forcing me to re-evaluate my approach and strengthen my guard in the process. Hopefully, he will no longer beckon me as a "#$@*!? grad student" any more.

Last but not least, I save the final praise and recognition for my advisor, Nasr Ghoniem. Although we have encountered many trials and tribulations over the years, he has always kept me rolling, if not always in a forward direction. His ability and willingness to actively work *with* me through my studies and research stand as testament to his professional values. Through his tutelage, I have been able to take advantage of numerous opportunities within the scientific community

and have come to realize the privilege of being a scientist and pursuing fundamental research. Most importantly, he has given me the personal freedom to explore my own aspirations, both in and outside of academia. Nasr, my only hope is that you have learned as much from me as I have from you.

CHUCK STONE

30 November, 1990

VITA

Charles Arnold Stone, IV

18 June, 1963   Born in Burlington, North Carolina

1985   B. S., Nuclear Engineering
North Carolina State University
Raleigh, North Carolina

1986   M. S., Nuclear Engineering
University of Wisconsin
Madison, Wisconsin

PUBLICATIONS AND PRESENTATIONS

C. A. Stone
The PULSTAR Reflood Problem
Presented at the ANS Eastern Regional Student Conference,
University of Florida, Gainesville, Florida, 4-7 April, 1985.

C. A. Stone
Neutron Population Studies in a D-T Fueled Fusion Device
Presented at the ANS Eastern Regional Student Conference,
University of Florida, Gainesville, Florida, 4-7 April, 1985.

C. A. Stone IV, C. D. Croessmann, and J. B. Whitley
*REFLEX: An Energy Deposition Code That Models the Effects
of Electron Reflection During Electron Beam Heating Tests*
Sandia National Lab Report, SAND87-1954, January, 1988.

C. A. Stone IV, C. D. Croessmann, and J. B. Whitley
*Vaporization Studies of Plasma Interactive Materials in Simu-
lated Plasma Disruption Events*
Sandia National Lab Report, SAND87-0313, March, 1988.

C. A. Stone

Modeling Thin Film Formation by Energetic Atom Deposition

Presented at the TMS Fall Meeting, Chicago, Illinois, 25-29 September, 1988.

C. A. Stone

Modeling Erosion and Redeposition of Plasma-Interactive Materials in Fusion Reactors

Presented at the Magnetic Fusion Energy Technology Student Conference, Los Alamos, New Mexico, 23-25 October, 1988.

C. A. Stone and N. M. Ghoniem

Modeling the Early Stages of Thin Film Formation by Energetic Atom Deposition

Metall. Trans. A **20A**, 2609 (1989).

C. A. Stone

The Effects of Cluster Size-Dependent Aggregation on Thin Film Formation

Presented at the 11th International Vacuum Congress, Cologne, Federal Republic of Germany, 25-29 September, 1989.

C. A. Stone and N. M. Ghoniem

The Effects of Cluster Size-Dependent Aggregation on Thin Film Formation

Vacuum **41**, 1111 (1990).

C. A. Stone and M. Vicanek

Surface Atomic Cluster Formation Under Low Energy Ion Bombardment

Presented at the NATO Advanced Study Institute on *Interaction of Charged Particles with Solids and Surfaces*, Alicante, Spain, 6-18 May, 1990.

C. A. Stone

The Influence of Low-Energy Particle-Surface Interactions on the Initial Stages of Thin Film Formation

Presented at the American Vacuum Society's 37th National Symposium, Toronto, Canada, 8-12 October, 1990.

C. A. Stone and N. M. Ghoniem

The Influence of Low-Energy Particle-Surface Interactions on the Initial Stages of Thin Film Formation

To be published in J. Vac. Sci. Technol. A, May/June 1991.

ABSTRACT OF THE DISSERTATION

A Kinetic Rate Model Simulation of the Initial Stages of Thin Film Nucleation and Growth Under Low-Energy Particle Bombardment

by

Charles Arnold Stone, IV

Doctor of Philosophy in Nuclear Engineering

University of California, Los Angeles, 1990

Professor Nasr M. Ghoniem, Chair

The initial stages of thin film formation under low-energy particle bombardment are modeled by a system of kinetic rate equations which describe atomic clustering phenomena. Specifically, a set of discrete kinetic rate equations, used to model small atomic clusters, is coupled to a set of kinetic moment equations which describe the size distribution function of large atomic clusters. These moments are derived from a Fokker-Planck equation which is an equivalent continuum limit of the discrete kinetic clustering equations.

Cluster growth and decay are assumed to proceed via single-particle transitions. The model incorporates aggregation, desorption, and direct impingement

processes, and growth behavior is investigated as a function of cluster size. Low-energy particle-surface interactions and their impact on the growing film are studied by modeling surface defect production, cluster dissociation, and sputtering mechanisms. Coalescence reactions are not considered, thus the model is only valid for the early stages of nucleation and growth.

A sensitivity analysis, which assesses the influence of important model parameters on the computational results, demonstrates the strength of the modeling approach. Thermal particle deposition studies compare favorably with analytical solutions and experimental measurements, and are also used to study the role of pre-existing surface defects on the nucleation kinetics. Energetic particle deposition studies illustrate the influence of surface defect production and cluster dissociation on the early stages of thin film formation.

Results from this statistical approach demonstrate that the model describes the major features of the initial stages of thin film nucleation and growth. Only a few equations are needed to model simple atomic clustering, the total number not being dictated by the size of the largest cluster. Energetic particle deposition is shown to be remarkably different from thermal particle deposition as exemplified by the differences in calculated size distributions and nucleation kinetics. One of the novel features of this type of modeling approach is that it provides unique information about the cluster size distribution that might help experimentalists measure new kinetic clustering parameters.

Chapter 1

Introduction

A number of energetic particle deposition processes are currently being used for surface modification and thin film production purposes. These processes use a high vacuum system to condense superthermal free particles onto a host substrate material, or alternatively, stimulate the deposition process by some means of energetic particle bombardment. As a result, energetic deposition techniques can influence film growth with a variety of synergistic effects that are absent during thermal deposition [1]. These effects impact both the substrate and the growing film, and include such physical mechanisms as sputtering, implantation, reflection, defect production, collisional mixing, and heating. If a plasma assists the deposition, the nature and chemistry of the deposited species can also be changed. Consequently, thin film formation with energetic particle bombardment is fundamentally different from atomistic deposition processes involving only thermal particles.

Energetic ions have been used in a variety of deposition applications. Ion-beam deposition systems deposit ionized material directly onto a surface. Similar to ion-beam deposition is ionized cluster-beam deposition, in which a cluster of atoms is ionized and accelerated toward a substrate. Upon impact on the substrate, the cluster dissociates into individual atoms. In ion-beam sputtering deposition

1

(IBSD), an ion beam is used to sputter a solid target; these sputtered target atoms then modify the surface to be processed. Reactive ion-beam sputtering deposition is similar in principle to IBSD, but reactive molecules are introduced during the deposition process, either in the ion beam or in the gaseous phase. Dual-beam sputtering deposition is also similar to IBSD; however, an additional ion beam is used to directly bombard the growing film. An excellent review of these ion-beam processes and their applications can be found in Reference [2].

Energetic particle deposition methods which use plasmas include radio frequency (RF) bias sputtering, magnetron sputtering, triode sputtering, ion plating, activated reactive evaporation, and plasma-enhanced chemical vapor deposition [3]. These plasma processing technologies have significantly enhanced the semiconductor fabrication industry [4]. Additionally, investigations of the surface modification of materials by plasma bombardment have been performed in order to develop plasma-interactive components for fusion reactor systems [5,6,7].

The high energies of the bombarding species actually damage a surface by creating near-surface defects and partially destroying a growing film. Nonetheless, numerous benefits of energetic particle deposition processes manifest themselves in the final surface characteristics of the produced film. The surface mobility of energetic atoms is higher than corresponding thermal deposition techniques; thus, epitaxial films can be produced at lower substrate temperatures. Superior coating adhesion is also achieved because of ion-beam mixing at the film-substrate interface. From an industrial point of view, such processes alter the mechanical, chemical, electrical, optical, and tribological features of a surface [8]. The surfaces created can have high wear and corrosion resistance, reduced friction, improved fatigue performance, good adhesive properties, hard diamond-like characteristics, and desirable electrical and optical features.

From an engineering perspective, the energetic particle deposition problem is fundamentally related to the erosion and redeposition phenomena present in magnetic fusion devices. Magnetic fusion reactors generate power by using magnetic fields to confine an energetic plasma in a toroidal vacuum chamber. Since this confinement is not perfect, the plasma can escape and interact with the vacuum chamber, resulting in sputtering and erosion of the inner wall surface. Sputtered wall atoms can be ionized in the plasma edge and then transported along the magnetic field lines back to the eroded wall regions. Consequently, the net erosion rate, i. e., sputtering minus redeposition, must be analyzed to choose the proper surface materials for plasma-interactive components. From this standpoint, the redeposition phenomena can be studied as an energetic particle deposition process.

Reviews of previous atomistic deposition studies have tried to assess the nucleation and growth of thin films prepared by thermal deposition methods [9,10]. Theoretical models of thermal deposition have shown consistency with experimental observations of nucleation and growth. Various assumptions must invariably be made to simplify the computational task and thus, models of varying degrees of complexity have been proposed. In complicated experimental procedures, thin film synthesis has often been considered a black art [11]; nonetheless, the theoretical attempts at modeling thermal particle deposition have helped in clarifying the relationships between atomistic processes and the macroscopic properties of thin films.

For energetic particle deposition processes, one needs to assess the impact of low-energy (e. g., ≤ 300 eV) neutral and charged particle species on a growing film, as well as the impact of energetic clusters. The physical understanding of low-energy plasma-surface interactions will play a vital role in fusion reactor design and engineering, due to the important coupling between plasma-edge processes and the

3

properties of the confined core plasma. Ion scattering measurement experiments have been developed for the analysis of well-characterized noble gas and metal ion beams over the energy range of 20 to 10,000 eV [12], which should provide insight into particle-surface interactions over energy ranges of interest in energetic particle deposition studies. Nonetheless, comprehensive theoretical treatments on the influence of low-energy particle-surface interactions on the initial stages of thin film formation have not yet developed to the author's knowledge.

The purpose of this dissertation is to develop a comprehensive theoretical model to investigate the initial stages of thin film nucleation and growth under low-energy particle bombardment. Fundamental atomic processes will be identified and described by a set of kinetic rate equations which can be solved to yield information about the resultant thin film growth kinetics and structure. Such a study should assist in the design of deposition processes to produce desired surface characteristics, as well as provide insight into the redeposition phenomena which can enhance component lifetimes in magnetic fusion reactors. Important atomistic processes can be identified and thus related to macroscopic surface features.

Chapter 2 focuses on a brief review of previous experimental and theoretical studies of thin film formation. Distinctions are made between thermal and energetic particle depositions. Chapter 3 provides a general discussion of the important kinetic processes and basic temporal stages which characterize thin film growth. These concepts are used in Chapter 4 to develop a kinetic model which describes the early stages of thin film formation under low-energy particle bombardment. A sensitivity analysis is performed in Chapter 5 to assess the influence of important model parameters on the computational results. The model is then used in Chapter 6 to study thermal particle deposition phenomena, while Chapter 7 concentrates on energetic particle effects. Results from these simulations are

4

used to draw conclusions about the influence of low-energy particle bombardment on the initial stages of thin film growth.

Chapter 2

Previous Studies of Thin Film Formation

Over the past few decades, advances in science and technology have led to progressively more detailed experimental and theoretical investigations of thin film formation. Improvements in vacuum technology, deposition systems, and in-situ diagnostic techniques have given experimentalists a means of producing a wide variety of films with well-characterized structures. Simple analytical theories of thin film formation have been supplemented by more sophisticated numerical models with the advent of high speed computers. Together, these experimental and theoretical studies have provided valuable insight in understanding the features of thin solid films.

2.1 Thermal Deposition Studies

2.1.1 Thermal Deposition Experiments

The experimental literature on the nucleation and growth of thin films is so vast that a really thorough summary is beyond the scope of this dissertation. References [10] and [13] provide earlier reviews of these studies. Consequently, this Section will focus on recent developments in the field.

To demonstrate the basic concepts of thin film formation, Donohoe and Robins' classical nucleation experiment [14] will be discussed. In this experiment, gold atoms were deposited at a constant rate onto a freshly cleaved NaCl substrate held at a fixed temperature. The experiment was performed in an ultra-high vacuum environment to ensure that only pure Au atoms impinged on the NaCl with thermal energies. The experimental procedure consisted of making a series of deposits of different time durations under the same conditions of deposition rate and substrate temperature. High-resolution transmission electron microscopy was used to determine the number density of Au nuclei present in each deposit. Figure 2.1 displays a series of these electron micrographs obtained with a deposition rate of 10^{13} atoms/cm^2/sec at 250°C. Evaluation of these micrographs reveals the dependence of the number of nuclei upon time, as shown in Figure 2.2.

Figure 2.1 indicates that the nucleation of Au on NaCl is primarily a homogeneous process. Where the spatial distribution is quite obviously nonrandom, as in the case of the various straight lines of clusters in micrographs (a) – (d), it is clear that heterogeneous nucleation is occurring at cleavage steps on the NaCl substrate. Figure 2.2 indicates that the density of nuclei passes through a maximum and then decreases slowly over time. This behavior has been attributed to clusters coalescing with each other. At the time of this maximum density, the gold clusters are approximately 150 Å in diameter. The increase in the density (short time scale) corresponds to the end of the nucleation stage, while the eventual decline (long time scale) represents the coalescence stage. From these experiments, the nucleation rate, the saturation concentration, and the cluster size can be measured as a function of time, substrate temperature, and deposition rate. These results can be understood quite well in terms of a kinetic theory of cluster growth, and lead to a deeper understanding of the physics associated with

7
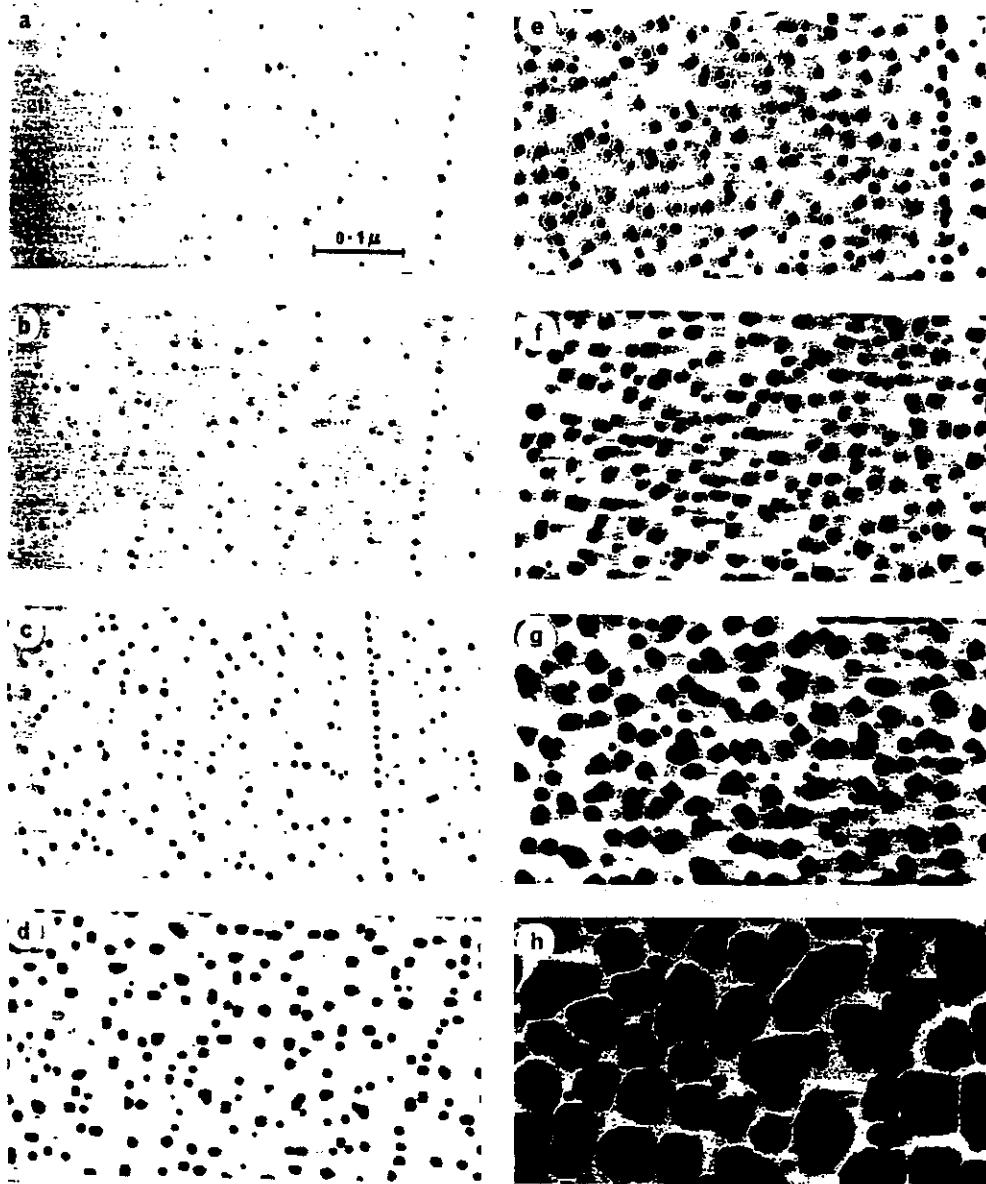
Figure 2.1. Electron micrographs of Au deposits on NaCl formed with a deposition rate of 10^{13} atoms/cm^2/sec, a substrate temperature of 250°C, and deposition times of (a) 0.5, (b) 1.5, (c) 4, (d) 8, (e) 10, (f) 15, (g) 30, and (h) 85 minutes. From Reference [14].
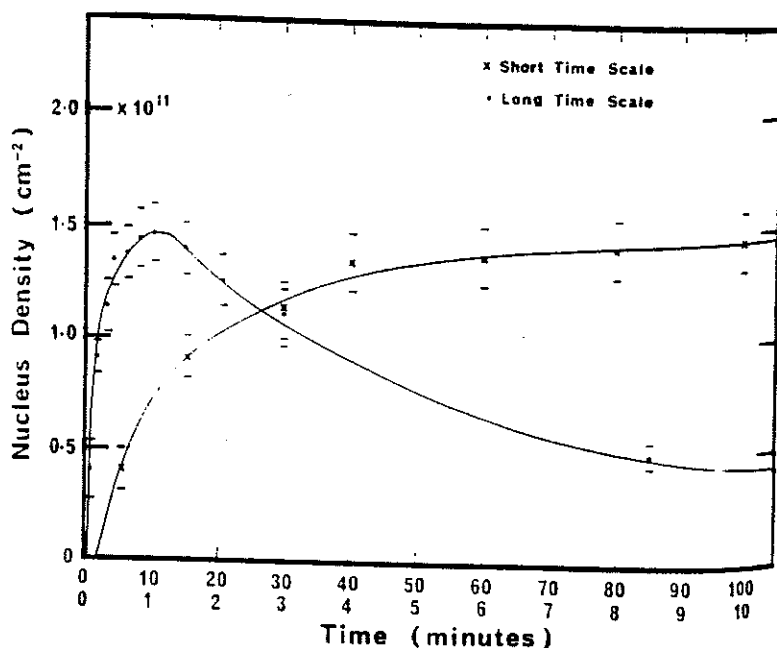
Figure 2.2. Number density of nuclei versus deposition time, plotted on two time scales, for Au deposited on NaCl at a deposition rate of 10^{13} atoms/cm^2/sec and a substrate temperature of 250°C. From Reference [14].

the initial stages of growth.

Although such nucleation experiments may seem easy to perform, it should be noted that the direct observation of very small clusters is not a trivial problem. Various diagnostic tools have been developed [9] to quantitatively study the nucleation and growth of thin films; however, each has its advantages and limitations. Mass spectrometry is a powerful way of measuring the total number of atoms condensed as a function of time, adsorption stay times, and adsorption energies. Wagner and Voorhoeve [15] used mass spectrometry to study the growth of Cd on clean W substrates. They discovered that the Cd-W system is a case of layer-by-layer growth where the adsorption energy decreases by a factor of two within the first 3 or 4 monolayers to the bulk Cd value. Voorhoeve and Wagner [16] also used mass spectrometry to study the influence of monolayer quantities

9

of hydrogen and oxygen on the Cd-W system. Although hydrogen had no effect, less than a monolayer of oxygen was able to act as a nucleation barrier, strongly reducing the Cd growth rate.

Field ion microscopy (FIM) can be used for the direct observation of condensation, as well as subsequent diffusion, desorption, and possible cluster formation. The main drawback to the method is that the area under examination is severely restricted, hence limiting the utility of the method. Nonetheless, several refractory metal systems have been examined with this technique. Using FIM, the migration and interactions of Ta, Mo, W, Re, Ir, and Pt on W have been studied [17,18,19,20,21]. FIM has also been used to study epitaxy of the first layers of Pd, Pt, Rh, and Ir on Ir and Rh over a wide temperature range [22].

Those stages of condensation in which coherent layers or extended clusters have already been formed can easily be observed by transmission electron microscopy (TEM). TEM has been successfully used to study the deposition of noble metals on alkali halides [14,23,24,25,26] and other insulators [27,28,29], the growth of semiconductor layers [30,31], and the condensation of rare gas crystals [32]. Although TEM can be used to obtain information about the density and sizes of stable clusters, it cannot be used to determine single-atom densities or adsorption times.

From an experimental point of view, the saturation density (i. e., maximum number) of growing clusters is much easier to measure than the detailed time development of the number of nuclei. The first in-situ observations on the growth of thin films deposited in an electron microscope were reported by McLauchlan [33] in 1950. In this study, Ag, Au, Cd, and Zn were deposited on amorphous substrates held at room temperature or slightly above. A sudden appearance of many nuclei, which in time grew, was observed. It was concluded that high

10

nucleation rates caused the nuclei density to saturate very quickly. Using an improved experimental configuration, Poppa [34] used in-situ electron microscopy to study the heterogeneous nucleation of Bi and Ag on amorphous SiO and carbon substrates. In both the Bi and Ag experiments, Poppa found that the steady state nucleation rate and the saturation density of growing nuclei both increased with an increasing deposition rate or lower substrate temperature, accompanied by a shorter induction time before appreciable nucleation was noticeable. Halpern [35] discovered that the saturation density of growing nuclei depends on the growth rate of cluster "islands" formed initially on the substrate. Matthews [36] observed that the presence of adsorbed impurities on a substrate leads to an increase in the saturation density. This was attributed to a reduced mobility of the deposited species as it encountered impurities, and the consequent decrease in its effective diffusion length.

Several recent experimental studies have focused on the early stages of nucleation and growth of metal clusters [37,38,39,40,41,42]. It is generally observed that the cluster size varies about an average value which increases with the amount of deposited material. Chapon and Henry [43] and Donohoe and Robins [14] have demonstrated that the migration and coalescence of small-size clusters play a prominent role in cluster nucleation, even at room temperatures. Most of the available experimental evidence shows that nucleation is rapidly dominated by growth of clusters resulting from migration, coalescence, and adatom capture processes.

It is interesting to note that various cluster shapes have been observed in clustering experiments. Hamilton and Logel deposited Ag on amorphous carbon and found that the resulting Ag clusters had a flattened, hemispherical shape[44, 45,46]. Other shapes such as rafts [47], chain-like designs [48], and icosahedral

11

structures [49] have also been experimentally observed.

Theoretical considerations allow one to predict whether a growing cluster will develop as a 2- or 3-D entity. Let Λ_o be the evaporation energy of the adsorbed species, characterizing the binding of the deposited atoms to one another; E_{des} the desorption energy required to separate an adsorbed atom from the substrate; and E_{diff} the diffusion energy which must be expended to move an adsorbed atom from one binding site to another on the substrate. Thermodynamic considerations [50] predict that 3-D clusters form if $\Lambda_o \geq 3\,E_{des}$, whereas 2-D clusters form if $\Lambda_o \leq 3\,(E_{des} - E_{diff})$. In intermediate cases the growth will be 2-D or 3-D, depending on the geometry of the substrate and film lattices. Sodium deposited onto a tungsten (100) surface has been shown to exhibit 2-D growth over 80 monolayers of film thickness [50]. The gold on NaCl result [14] displayed in Figure 2.1 is a case of pure 3-D cluster growth.

Activation energies also determine the structure of thin films grown on a substrate. It is generally accepted that there are three growth modes possible in the simplest cases where interdiffusion does not occur [51]. In the island growth mode, the condensing atoms are more strongly bound to each other than to the substrate. Island growth is typically important for metals and semiconductors grown on insulators. Layer growth occurs if the condensing atoms are more strongly bound to the substrate than to each other. Layer growth is important in homoepitaxy deposition. The third growth mode is a combination of the layer plus island modes. The general feature of this mode is that virtually any impediment to continuous layer growth results in the formation of islands on top of an intermediate layer. This mixed mode is the rule rather than the exception in heteroepitaxy, and can be expected to be important in semiconductor systems. Figure 2.3 schematically illustrates these three growth modes.
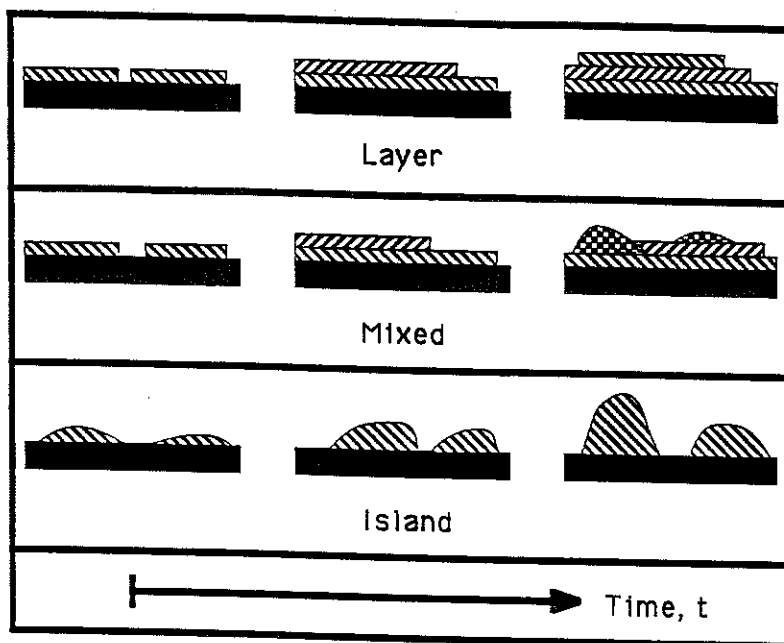
Figure 2.3. Schematic representation of three experimentally observed thin film growth modes.

The advent of new superconducting compounds has recently sparked an interest in multilayer film synthesis. Superconducting Bi-Sr-Ca-Cu-O thin films have been prepared by multilayer deposition from elemental metal sources [52]. Chang et al. [53,54] have also used a multilayer technique for depositing superconducting thin films of $YBa_2Cu_3O_7$ and the non-superconducting Y_2BaCuO_7 phase. Applications of new and improved superconductor compounds will be determined by how easily they are fabricated into useful forms.

2.1.2 Thermal Deposition Theories

Theoretical studies of thin film formation have been performed in order to predict trends and explain phenomena observed in deposition experiments. Theoretical models of thermal deposition have shown consistency with experimental observations on nucleation and growth, readily predicting measured nucleation rates

and saturation densities. Moreover, theoretical models also have the capability of simulating the evolution and structure of growing thin films. Because of the many processing and material parameters which can be changed, models which are calibrated for specific experiments can be used to plan measurements in the most important regimes.

Several theoretical studies of the nucleation process have been made. The approaches used are usually classified as either classical [55,56,57], if classical continuum thermodynamics is used, or atomistic [58,59,60,61,62,63] if the interactions between individual atoms are considered. Classical nucleation theory describes the processes involved in terms of thermodynamic, macroscopic variables such as surface tension, heat of evaporation, and the formation energy of the critical nucleus. The question that arises is how much significance one can attribute to such macroscopic variables if they are applied to nuclei consisting of only a few atoms. Atomistic theories are based on microscopic properties such as binding, migration, and desorption energies; aggregation rates; and capture probabilities. Since atomic clustering mechanisms govern the thin film formation process, an atomistic description is the appropriate modeling choice.

In 1924, Frenkel [59] proposed a theory of condensation that made use of only atomic variables. Frenkel thought that the process of condensation could be interpreted by only considering the formation of pairs of atoms. In 1962, Walton [60] used statistical mechanics to develop the first atomistic formulation of nucleation theory. According to Walton's theory, a stable cluster is an agglomeration of atoms with a greater probability to grow than to decay and consisting of at least one more atom than the critical nucleus. Walton's work was concerned primarily with predicting nucleation rates under conditions where an equilibrium population of single atoms initially existed on the substrate.

Zinsmeister [61] extended Frenkel's approach (which included single atoms and atom pairs only) to aggregates of any larger size. In Zinsmeister's work, single atoms arrive at a substrate, remain there for a certain length of time, and have a certain degree of mobility. Collisions occur between the individual atoms, giving rise to the formation of pairs and, by addition of more single atoms, of aggregates of continually higher order. At the same time, these aggregates are also subject to dissociation processes. A series of simultaneous kinetic rate equations was used to describe the density of these aggregate clusters.

In this study [61], Zinsmeister assumes that direct impingement of the depositing species on a growing cluster is negligible. He also neglects the dissociation of large clusters. Assuming that the substrate is covered by a constant single-atom population, Zinsmeister solves rate equations for the aggregate cluster densities by using an asymptotically equivalent expression for the exact solution. In a second study [62], Zinsmeister again neglects direct impingement effects and the dissociation of higher order aggregates; however, the single atom density is now assumed to be time dependent. In order to solve the resulting series of simultaneous rate equations, Zinsmeister has to assume that the adatom capture cross-section of a growing cluster is constant, independent of its size. Solution of these equations reveals that the single atom density changes with time over three distinct regions as follows: (1) linear growth, (2) constant, and (3) $t^{-1/3}$ decrease. A third study [63], which calculates the size distribution of the aggregate nuclei, shows that increasing the deposition rate or decreasing the value of the aggregation parameter (i.e., the adatom capture cross-section) both lead to higher nuclei densities, but smaller-sized clusters.

A review of previous atomistic studies which have tried to assess the nucleation and growth of thin films prepared by thermal deposition methods can be found in

References [9] and [10]. Lewis [64] directly compared the atomistic and thermodynamic approaches to nucleation theory, concluding that in practical deposition studies, the atomistic model is preferred since the critical nucleus is seldom larger than two atoms. Atomistic theory has also been used to predict the dependence of saturation nucleus density on deposition conditions [58], and comparisons with experimental studies indicate that substrate defects may play a dominant role in the nucleation process [13]. Logan [65] derived expressions for the time required for saturation to occur when (a) atom pairs are stable and no desorption occurs, (b) atom pairs are stable but single atoms can evaporate, and (c) triplets are stable and no desorption occurs.

Studies have also tried to distinguish between the early stages of atomic clustering and the later stages when cluster coalescence is significant. Using a set of generalized Zinsmeister equations, Takeuchi and Kinosita [66,67] modeled the early growth stages of gold deposits on amorphous carbon substrates, determining that at substrate temperatures below 400°C, the film growth is surface diffusion controlled while at higher temperatures it is re-evaporation controlled. Velfe and Krohn [68] investigated the early stages by developing a nucleation theory that assumes that nearly all mobile nuclei are captured by immobile clusters. Chakraverty [69] studied the later stages of film growth with an analytical theory that takes into account both effects of direct impingement and coalescence; his results have compared favorably with experimental measurements of cluster size distributions. An atomistic theory for the later stages of the nucleation process indicates that coalescence reactions decrease the density of stable clusters present on the substrate [70]. Coalescence reactions have also been included in a kinetic rate theory used to numerically model the nucleation and growth of In clusters on GaAs [71]. In practice, multilayer film growth will occur after coalescence has

16

begun, and several studies have focused on this problem [72,73,74].

Several phenomenological models have been used to simulate the structure of thin film deposits. The solid-on-solid (SOS) model has been used to describe the dynamics of crystal growth as well as thin film formation [37,75]. In the SOS model, each site on a simple cubic lattice is either vacant or occupied by a single atom with the requirement that every occupied site be directly above another occupied site, thus excluding "overhangs". In simple terms, the SOS model describes the structure of a thin film as an array of interacting columns of varying integer heights. Growth or evaporation of the film only involves the "surface atoms" at the tops of these columns. Although the SOS model permits clusters of atoms, surface vacancies, and irregular step structures to exist, the no-overhang restriction becomes increasingly unrealistic at very high temperatures. Moreover, particle impingement effects, energy dissipation, evaporation, and atom incorporation onto the substrate lattice are all idealized in the SOS model since it represents a probabilistic picture of nucleation dynamics. These limitations make the SOS model an unreliable tool in the study of energetic atom deposition.

Structure-zone models have proven very useful in providing an overview of the relationship between the microstructure of vacuum deposited coatings and important deposition parameters. Thornton has developed an extended model [76] which depicts the microstructure of an evaporated coating as a function of T/T_m ($T =$ substrate temperature, $T_m =$ melting temperature of the deposited coating) and the argon working gas pressure used in a magnetron sputtering system. Four zones are identified, each with its own characteristic structure and physical properties, as shown in Figure 2.4. The low temperature ($T/T_m < 0.3$) zone 1 structure is columnar, consisting of tapered units defined by voided growth boundaries. The zone 2 structure ($0.3 < T/T_m < 0.5$) consists of columnar grains

17
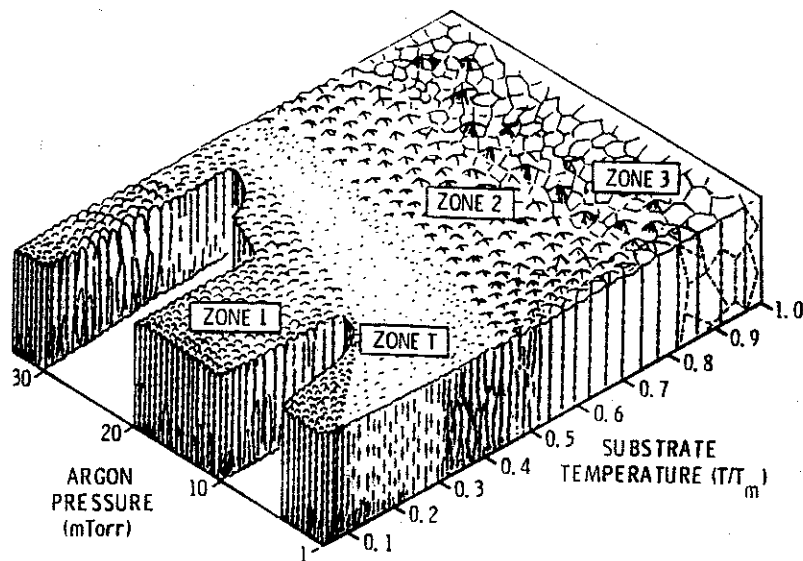
Figure 2.4. Thornton's structure-zone model for metal films deposited by magnetron sputtering. T is the substrate temperature and T_m is the coating material melting point. From Reference [83].

defined by metallurgical grain boundaries. These grains increase in width with T/T_m in accordance with activation energies typical of surface diffusion. The high temperature ($T/T_m > 0.5$) zone 3 structure consists of equiaxed grains which increase in size in accordance with activation energies typical of bulk diffusion. The fourth zone is a transition region between zones 1 and 2, consisting of a dense array of poorly defined fibrous grains.

Some relatively novel computer simulations have used interesting approaches to study thin film formation. Sedehi et al. [77] developed a real-time computer simulation of the nucleation and growth of thin films thermally deposited from the vapor phase. Using atomistic statistical theory, this simulation computes the 3-D structure of the film and provides 2-D plots at desired instants of the projection of the film on the substrate. Nucleation and growth plots for Ag and Au on NaCl

18

substrates appear to be similar to electron micrographs published in the literature. Outlaw and Heinbockel [78] have used a Monte Carlo simulation employing an atomistic potential energy scaling technique to model the initial stages of thin film nucleation and growth of Au on NaCl (100). This model considers both the surface migration of Au on NaCl, as well as the vertical migration of Au atoms to second and third layers of the growing film. Results prove to be consistent with experimental data. Adams and Jackson [79] have developed a Monte Carlo computer simulation that can be applied to the co-deposition of two different atomic species.

Bauer and Frurip [80] studied the homogeneous nucleation of metal vapors using a kinetic model based on the solution of a master equation for n-mer growth, $A_n + A_i + M \rightleftharpoons A_{n+i} + M$. Species M is a stabilizing catalyst for the interaction. Cluster growth was modeled as an accretion process in which an n-mer collides with an i-mer and the two adhere. The resulting set of stiff, non-linear, coupled differential equations which describe the system populations were solved using a GEAR integration subroutine [81]. Solutions were obtained for monomer addition only ($i = 1$) and monomer $\rightarrow$ pentamer addition inclusive ($i = 1 \rightarrow 5$), for $2 \leq n \leq 80$. Computer time on an IBM-370 was quite long [80]; in fact, limitations on computer time, both practical and monetary, prevented calculations from extending significantly past $n = 80$.

In order to avoid the computational difficulties that arise when solving such a large system of equations, Clement and Wood [82] modeled the growth of a distribution of small physical objects by using a set of discrete kinetic equations coupled to a continuum distribution. All objects were assumed to grow by the addition of one atom at a time, and no multiple additions, coalescence, or losses of atoms (i. e., evaporation) were possible. Coupled differential equations were

19

derived for the moments of the discrete distribution produced with no source term. Although solutions have been obtained for physical growth laws, this formulation does not include dissociation processes which are important in cluster nucleation and growth, causing the cluster-size distribution to disperse.

2.2 Energetic Deposition Studies

2.2.1 Energetic Deposition Experiments

In addition to assisting deposition processes, energetic particle bombardment techniques enable one to diagnose surface structures and modify surface features. Data obtained in sputtering experiments, reflection measurements, ion implantation studies, and plasma-surface interactions can be used to enhance our understanding of the physics involved in thin film formation studies. One must restrict such correlations to known particle-surface interactions of interest, avoiding extrapolations which include reactions with the bulk material target.

Penetration of the substrate lattice by incident atoms is expected to occur with energies above 1 eV [58]. These penetration sites might act as nucleation centers, substantially changing the growth behavior of a growing film. Studies of the microstructure of sputter-deposited coatings reveal that energetic particle bombardment can create dense films [83]. High energy bombardment can also cause composition changes in multicomponent materials due to differences in sputtering yields [3]. As an additional feature, energetic particles have a higher mobility and a shorter lifetime on a substrate than a thermally deposited species.

When an energetic particle strikes a solid, it may simply be reflected off the surface or if it has enough energy, it may sputter the surface or implant itself in one of the near surface layers. Sputtering yield measurements [84] depend on different

parameters such as the energy and atomic number of the incident species, angle of incidence, and the target atomic number. Crystallographic orientation is also a factor [85]. As mentioned in Chapter 1, ion scattering measurement experiments have been developed for the production of well characterized noble gas and metal ion beams over the energy range of 20 to 10,000 eV [12]. Another experiment has recently been designed to measure the particle and energy reflection coefficients of low energy (10 to 200 eV) hydrogenic ions incident on selected metal surfaces [86]. All of these experiments provide valuable information for characterizing the energetic particle deposition processes important in thin film formation studies.

Low-energy (often < 100 eV) deposition experiments have been used to control the growth kinetics and thus the physical properties of thin films, resulting in a number of interesting features. These features include film densification and increased oxidation resistance in optical films; minimization or elimination of columnar microstructure in metallization layers used in electronic devices; alteration of the state of stress, average grain size, and preferred grain orientation; increased film/substrate adhesion; enhanced conformal coverage; control of magnetic anisotropy in recording layers; epitaxial growth at lower temperatures; stimulation of surface chemical reactions; tailored film compositions; deposition of selective species; growth of metastable phases; and increased dopant incorporation probabilities (with a corresponding decrease in segregation-induced broadening of dopant profiles) in molecular beam epitaxy (MBE)-grown Si and III-V semiconductors [87,88]. Nonetheless, one desired feature may be accompanied by several deleterious features, jeopardizing the utility of a specific thin film application. Thus, in an effort to better clarify the impact of the energetic species and to assess the role of experimental parameters, the study of energetic particle bombardment during thin film formation needs to be approached at a more fundamental level.

Three excellent review articles [88,89,90] provide a summary of experimental work performed over the past 15 to 20 years on the controlled use of low-energy particle bombardment on the early stages of film growth. These studies, however, often describe basic nucleation phenomena with conflicting results. For example, the nucleation rate and density of Ge clusters have been found to increase or decrease with ion irradiation, depending upon the choice of substrate material and substrate temperature used for the deposition [91]. Substrate "hardness" and thermal conductivity arguments were used to explain these discrepancies in terms of incident particle embedding effects and enhanced adatom mobility. The influence of particle bombardment on average cluster size is also subject to debate. Studies on thermal In and partially ionized In^+ beam experiments, used to deposit In islands on amorphous Si_3N_4 substrates at room temperature in an ultra-high vacuum MBE system, report a decrease in island number densities in the presence of ion irradiation which leads to larger average island sizes [92]. The authors attribute this irradiation effect to the loss of small clusters by sputtering and ion-induced dissociation. On the other hand, studies of Ar^+ ion bombardment during room temperature growth of Ag films reveal that irradiation decreases grain size, thus indicating that energetic particle deposition promotes smaller average cluster sizes [93]. Since an understanding of fundamental nucleation kinetics leads to the ultimate control of film growth, such discrepancies need to be resolved.

The nucleation and growth of gold clusters on sodium chloride substrates has been systematically studied because of the inert properties of gold, the ease with which well-defined surfaces can be obtained by cleaving NaCl single crystals, and the excellent resolution of Au clusters under electron microscopy. Thermal deposition studies of the Au/NaCl system have been used to investigate the initial stages of nucleation and growth [23], the mobility and coalescence of Au nuclei

[14,94], as well as cluster size [95] and spatial [26] distributions. Inconsistencies in several such thermal deposition studies led to the realization that the creation of preferred surface sites, induced by low-energy electrons originating in the Au vapor source, inadvertently influenced the nucleation kinetics [96,97]. Electron bombardment of a NaCl surface, during the evaporation of Au, has also been shown to lead to increased maximum island densities [98].

Energetic Au/NaCl deposition studies have also been performed. High-energy ion-beam sputtering systems have been used to sputter Au targets onto NaCl substrates. Observed increases in the maximum number density of Au islands, compared with results for thermal evaporation, can be quantitatively described by the generation of preferred nucleation sites on the substrate during the deposition [99,100]. The nucleation kinetics also depend on the angle at which the sputtered gold atoms strike the NaCl surface; Au atoms deposited at normal incidence have been shown to produce larger island densities than atoms bombarding the substrate at angles 60° to the normal [101]. Rf-sputtering systems, which complicate matters by introducing plasma effects and the presence of a sputtering gas into the deposition environment, have also been used to study Au/NaCl nucleation phenomena. Harsdorff and Jark [102] rf-sputtered gold atoms onto NaCl substrates in a helium atmosphere, observing increased nucleation rates and island densities as compared to thermal evaporation works. Cluster size distributions were measured which appeared to be "quite similar to distributions from evaporation experiments" described by Schmeisser [95]. Magnets placed directly in front of the substrate surface were used to minimize crystal damage and heating that would occur as a result of electron and ion charged particle bombardment; however, the substrate remained open to backscattered neutral helium bombardment which could have influenced their results.

The redeposition phenomena observed in magnetic fusion systems is a unique example of thin film formation by energetic particle deposition. Plasma-wall interactions, the precursors to redeposition, are inevitable consequences of the magnetic confinement scheme used in toroidal devices. In many cases, the observed characteristics of the fusion plasma core are determined more by the plasma-surface interactions than by classical plasma physics [103]. As a result, the core plasma physics and global reactor operation are indirectly related to the redeposition phenomena via the plasma-edge conditions.

Present experimental results indicate that the most probable energy of particles emanating from the edge of a tokamak reactor plasma will be in the range of 10 to 300 eV [104]. If these energetic particles strike a plasma-interactive component, sputtering can occur; these sputtered particles can be recycled in the plasma edge and redeposited on material surfaces. The redeposited material may have properties different from those of the base material. These synergistic effects of sputtering, implantation, and redeposition will effectively determine the lifetime of plasma-interactive components in tokamak reactors, influencing reactor costs.

The PISCES facility at UCLA has been used to investigate the surface modifications of materials by continuous plasma bombardment under simultaneous erosion and redepositon conditions [5]. Under redeposition-dominated conditions, the material erosion rate due to plasma bombardment was significantly smaller (up to a factor of 10) than that expected from classical ion beam sputtering yield data. Also, the surface morphologies of redeposited materials were shown to be strongly dependent on the plasma bombardment conditions.

Since the surface characteristics of plasma-interactive components can affect the entire operation of a fusion reactor system, it should be evident that materials

24

selection is a major issue for current reactor experiments and future fusion devices. Material coatings may be necessary, and in-situ deposition techniques may be used to repair or replace these coatings in hope of mitigating plasma-surface interactions [105]. Hopefully, a better understanding of the energetic atom deposition phenomena will provide more insight into redeposition rates and coating techniques in future fusion devices.

2.2.2 Energetic Deposition Theories

Comprehensive theoretical treatments on the influence of low-energy particle-surface interactions on the initial stages of thin film formation have not yet developed to the author's knowledge. Previous kinetic rate equation formulations, though, have been developed in order to interpret the results of deposition measurements which were influenced by the presence of surface defects. Lane and Anderson [100] used ion-beam sputtering to deposit Au on NaCl, measuring island densities as a function of substrate temperature and deposition rate. They were successful in interpreting their results in terms of a kinetic model which assumed a constant density of preferred adsorption sites. Usher and Robins [97] used a rate equation approach to analyze experiments in which preferred sites were continuously generated at a rate proportional to a power of the deposition rate. Using this approach, they were able to resolve several discrepancies in previous Au/NaCl nucleation measurements. Both of these studies developed analytical solutions to the film growth problem by making rather gross, time-independent estimates for cluster mobility effects. Direct impingement phenomena and particle-surface interactions were ignored, and neither solution provided any information on the cluster size distribution. Although many variables were experimentally difficult parameters to determine, the assumptions made in developing these analytical

models are generally supported by their overall agreement with deposition measurements.

Detailed theoretical modeling of thin film formation by energetic particle deposition will have to incorporate analyses of surface defect production, cluster dissociation, sputtering, ion implantation, particle reflection, and redeposition in the study. A historical survey of different sputtering models can be found in Reference [106]. Sigmund [107] developed an ion transport theory of sputtering by solving the Boltzmann transport equation for moving atoms near the surface of a material undergoing sputtering events. A rather crude extrapolation is found necessary in the treatment of the motion of low energy atoms. Despite this shortcoming, Sigmund's theory remains one of the standard references for sputtering yield measurements. Other theories have considered the ejection of atomic particles from ion bombarded single crystals where crystallographic effects are important [108,109].

An elaborate computer program to model the erosion and redeposition behavior of materials in tokamak fusion reactors is embodied in the REDEP code [110]. REDEP models the erosion of tokamak limiter and divertor surfaces by considering only physical sputtering mechanisms. The code accepts as input the plasma parameters characteristic of the plasma-edge region. The sputtering phenomenon depends strongly on the plasma sheath potential, taken to be $e\phi = 3\,kT_e$, and on the charge state of the impinging ions. It is shown that most of the sputtered species are redeposited on the host structure. A key assumption used in this study is that the properties of the redeposited material are the same as the original surface material; however, recent studies [5,7] indicate that this assumption may not be valid. REDEP analyses on limiters coated with high-Z materials indicate that

26

self-sputtering may be a significant erosion mechanism unless plasma-edge temperatures can be kept low ($\simeq 50$ eV). Additional studies indicate that redeposition may be a mixed blessing since the redeposited coating may grow to be too thick, thus influencing limiter performance and operation [111].

Since the bombardment of fusion reactor surfaces by low energy ions and charge exchange neutrals is the dominant physical phenomenon in the plasma-edge region, several sophisticated theoretical analyses of the ion-surface reflection process have been developed [112,113,114]. The Monte Carlo simulation program, TRIM.SP [116] (a sputtering version of the original TRIM code [115]), has been used to calculate particle and energy reflection coefficients, as well as energy and angular distributions, of reflected hydrogenic species with incident energies from 0.2 to 300 eV [112]. Such analyses are applicable to the energy ranges of interest in thin film formation by energetic particle deposition.

The original TRIM code [115] simulates the slowing down and scattering of energetic ions in amorphous targets using a binary collision model (BCM). Another BCM simulation, TRIPOS, has been used to study ion transport processes in polyatomic solids [117,118,119]. The use of a BCM simulation to study low energy sputtering and reflection processes is questionable, however, because at low energies the interaction of a particle cannot be treated as an interaction with one single counterpart due to the increasing range of the particle-particle interaction with decreasing energy. The TRIM.SP code [116] compensates for this increased interaction in the low energy regime by taking more distant collisions into account. The comparison of calculated light-ion reflection coefficients with experimental data above 50 eV is reasonably good, whereas for energies below 50 eV, no experimental data exists. It is in this region where the TRIM.SP code falls under scrutiny.

TRIMCSR, another modified version of the TRIM code, introduces a simple model to describe the variation of atomic potentials between the surface and the bulk of a solid target [120]. TRIMCSR simultaneously calculates all of the resulting ion-solid interactions, namely point defect generation, sputtering yield, and replacement/relocation events. TRIMCSR has been used to calculate ion-solid interactions of Si on Si for ion energies ranging from 10 to 10,000 eV. Again, results obatined below 50 eV are to be taken with caution, since the detailed description of ion trajectories becomes increasingly difficult at these energies, as multiple collisions rather than binary collisions dominate the ion-solid interaction.

In order to establish the necessary conditions for film growth, the low energy ion transport problem is best solved using molecular dynamics (MD) techniques. Due to the disparity between the MD time step ($\simeq 10^{-14}$ sec) and typical deposition times (seconds-hours), direct MD simulations of thin film growth by energetic atom deposition are computationally impractical. Nonetheless, MD simulations can be used to study the questions related to fundamental atomic transitions, thus enabling one to determine particle reflection and sputtering coefficients, implantation parameters, atomic mixing rates, and surface defect characteristics.

The choice of a suitable interatomic potential is of considerable importance to the success of the MD simulation. In energetic atom deposition, the energies of the impinging species and substrate atoms will fall in the thermal and superthermal ranges. In the thermal energy range below 2 eV, the embedded atom method (EAM) [121,122] can be used rather than idealized pair interatomic potentials. In the superthermal energy regime above 10 eV, the empirical universal pair potential [123] can be used. Chou and Ghoniem [124] and Prinja [125] have recently developed methods to couple the EAM potential to the universal potential over the transition region of interest, enabling one to perform consistent MD simulations

28

over a continuous energy range.

Chapter 3

Problem Description

The first step in modeling thin film formation by energetic particle deposition involves identifying the various physical processes which occur when an energetic particle impinges on a host substrate material. A set of equations can be developed to describe these events and the various stages of film formation which follow. In this dissertation, an atomistic approach is used to model the deposition phenomena, particle-surface interactions, atomic clustering mechanisms, and the resulting thin film nucleation and growth. This Chapter discusses the important kinetic processes and basic temporal stages which characterize thin film formation.

3.1 Important Kinetic Processes

The nature of the deposited species depends on both the deposition method and the processing environment. Individual atoms can be thermally evaporated from an effusion cell, providing a source material that allows growth to occur under conditions near thermodynamic equilibrium. Ion-beam deposition, ion-beam sputter deposition, and ion-assisted MBE promote non-equilibrium growth conditions by subjecting the substrate to energetic particle bombardment. Energetic neutrals often accompany these techniques. Clusters of atoms can also be ionized and

accelerated toward a substrate, dissolving into individual atoms upon impact. A plasma can enhance any of these deposition techniques, accelerating chemical reactions within the deposition environment and stimulating particle-surface interactions. Regardless of the method, the net result of the deposition process is to place particles on a substrate, eventually covering the surface and forming a coating.

Direct impingement occurs when a deposited particle lands directly on an atomic cluster already present on the substrate. Direct impingement effects are usually not important until the later stages of atomic clustering, when a substantial portion of the substrate is covered with growing clusters. Cluster size and geometry, as well as the deposition rate, determine the magnitude of direct impingement interactions.

Once accomodated on the substrate, particles can participate in a variety of thermally activated events. If a particle has enough thermal energy, it may evaporate off the substrate. Single particles are more likely to evaporate than actual clusters. Particles and clusters also diffuse across the substrate surface at rates which depend on cluster size and geometry, substrate temperature, and an appropriate activation energy. During the early stages of thin film formation, two migrating clusters may aggregate into a larger entity, conserving particles in the process. In the later stages of film growth, this phenomenon is termed mobility coalescence. This should be distinguished from growth coalescence, which occurs when the substrate is so crowded with clusters that two clusters coalesce by simply growing into each other.

The above kinetic processes arise during both thermal and energetic particle deposition. Energetic deposition techniques, however, influence film growth with

a variety of synergistic effects that are absent during thermal deposition. Surface defect production, sputtering, and particle reflection events depend on the energy, mass, flux, and angle of incidence of the bombarding species, as well as the mass and orientation of the substrate target atoms. If an energetic projectile creates a collision cascade within the vicinity of a large cluster, dissociation can occur, breaking up the large cluster into a number of smaller ones. If the bombarding energy is high enough, collisional mixing and implantation may result, trapping a portion of the deposit in the substrate bulk and surface layers. These mechanisms lead to increased film/substrate adhesion. Energetic deposition also promotes local surface heating and enhanced surface diffusion, accelerating thermally activated phenomena. Finally, plasma-assisted processes can stimulate particle-surface reactions, substantially changing both the chemistry and kinetics taking place on the substrate host.

3.2   Basic Stages of Thin Film Formation

A temporal history of thin film formation includes a number of distinct stages that are easily identified in the laboratory. Figure 3.1 illustrates these stages with a schematic representation of cluster density, $n(t)$, as a function of fractional substrate surface coverage, $Z(t)$. During the first stage, the deposition species is transported through the deposition environment (e. g., vacuum, plasma, etc.) to the substrate surface, where it can participate in or be influenced by a number of physical processes. After a certain induction time, enough particles will have condensed on the substrate so that nucleation and growth can proceed. This marks the onset of the second stage, where both cluster density and size increase with time, virtually unaffected by neighboring clusters. A saturation stage arises when the cluster density has reached the maximum value (n_{max}) that the substrate

32
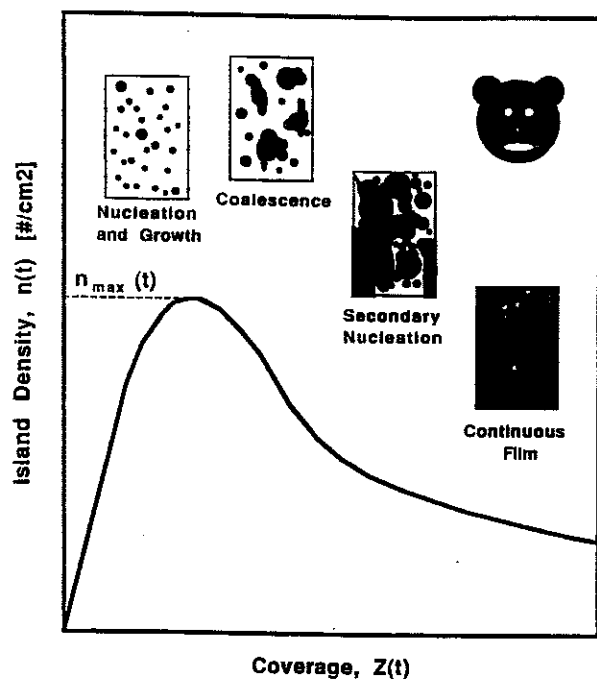
Figure 3.1. Schematic representation of cluster density, $n(t)$, as a function of fractional substrate surface coverage, $Z(t)$, during thin film formation.

can accomodate for the given deposition conditions. Clusters continue to grow in size, but now coalesce with one another, producing a rapid decrease in cluster density. The remaining channels and voids are filled by secondary nucleation, cluster growth, and coalescence events. In the final stage, a continuous film forms; this is ultimately followed by multilayer growth. In general, the saturation stage marks the transition between the early and later stages of thin film formation.

Chapter 4

Model Formulation

Developing a realistic theoretical model of a complex physical system requires an understanding of how the system evolves with respect to space and time, knowledge of the relevant components which constitute the system, and insight into the physical phenomena which govern system behavior. Mathematical equations can usually be formulated which describe the intracacies of the system; however, their solution may be intractable, depending upon the simulation details. The resourceful modeler is then faced with the arduous task of deciding which processes can be relaxed and which solution technique is most appropriate, without sacrificing the integrity of the work. This Chapter describes the assumptions, methodology, and solution techniques used to model the early stages of thin film formation under energetic particle bombardment. Unique features of this model which provide new insight into thin film nucleation and growth kinetics are also discussed.

4.1   Assumptions and Basic Definitions

In this model of thin film formation, the deposition source is assumed to produce a monoenergetic single-particle species of energy E, consisting of either charged particles or fast neutrals, which strike the substrate at a rate of q particles/unit

area/unit time. Particle-surface interactions result in the creation of surface vacancies which will be denoted as *single traps* in this work. The quantity $C_T(t)$ denotes the number of single traps present on the substrate, per unit substrate area. These defects can trap a portion of the single-atom population that is initially accomodated on the substrate. The single-atom population, $C(1,t)$, thus consists of a *bound* single-atom component, $C_b(1,t)$, bound to defect sites, and a *mobile* single-atom component, $C_{mob}(1,t)$, which can diffuse across the substrate. Nucleation and growth leads to the production of x-atom clusters, characterized by the cluster density, $C(x,t)$.

Single traps, mobile and bound single atoms, and x-atom clusters are the basic constituents of the thin film system. The evolution of these species is governed by the following physical processes and general assumptions:

1. Only monoenergetic, single particles of energy E are deposited.

2. Point defects are generated at the rate $q\,p(E)$, where $p(E)$ is the average number of vacancy-interstitial pairs produced by each deposited particle. Only surface vacancies (i. e., traps) are created. $p(E)$ depends on the collision cascade generated by charged or neutral particle bombardment. Interstitial atoms are implanted well into the substrate (at least > 5 atomic layers) and thus are not considered to influence surface atomic clustering [126].

3. If $E \geq E_{eject}$, single atoms will be sputtered off the substrate. E_{eject} is the energy required to eject a single atom off the substrate. Ballistic migration effects are not considered.

4. Cluster growth and decay proceed via single-particle transitions. Coalescence reactions are not considered, thus the model is only valid for the early growth stages where less than 15% of the substrate is covered.

5. Single traps are mobile, governed by a diffusion energy, E_d^T. They aggregate with other species on the substrate at a rate $\nu_{T,i}(t)\,C_i(t)$ [where $i = T$, m, b, or x for other traps, mobile single atoms, bound single atoms, and x-atom clusters, respectively]. The "T,b" and "T,x" reactions are assumed to only influence the single-trap population.

6. Mobile single atoms are governed by a diffusion energy, E_d. They aggregate with other species on the substrate at a rate $\nu_{m,i}(t)\,C_i(t)$.

7. Bound single atoms and larger x-atom clusters ($x \geq 2$) are immobile.

8. Thermal oscillations can evaporate mobile single atoms off the substrate. This is characterized by an adsorption energy, E_a, and residence time, $\tau_a = \nu_a^{-1}$.

9. Thermal oscillations can release bound single atoms from traps, creating mobile single atoms in the process. The activation energy, E_T, determines the bound single-atom confinement time, $\tau_T = \nu_T^{-1}$.

10. Direct impingement of the deposit on single-trap sites creates bound single atoms at the rate $\nu_{imp,T}\, C_T(t)$.

11. Direct impingement of the deposit on x-atom clusters produces ($x+1$)-atom entities at the rate $\nu_{imp}(x)\, C(x,t)$.

12. Energetic particle bombardment dissociates x-atom clusters into ($x-1$)-atom clusters and mobile single atoms at the rate $\nu_{diss}(x,E)\, C(x,t)$.

4.2 General Formulation of the Hybrid Clustering Model

In several theoretical studies of thin film formation, a kinetic formulation of hierarchical discrete rate equations has been used to describe cluster sizes [13,50, 51,61,62,75,80,127]. These rate equations are coupled, non-linear, and extremely complex. Thus, they are difficult to solve unless some simplifying physical assumptions are introduced. From a computational standpoint, these approaches must solve a large system of equations to obtain specific clustering details since the number of atoms in the largest cluster dictates the number of discrete equations that must be solved.

It will be shown in Section 4.2.1 that the model assumptions outlined in Section 4.1 can be used to derive a system of discrete kinetic rate equations which describe the early stages of thin film formation by energetic particle bombardment. If the largest cluster contains X_{max} atoms, then a set of ($X_{max} + 2$) coupled, non-linear, stiff, ordinary differential equations must be solved. Since cluster sizes increase with time, X_{max} must also increase, which dictates that more equations

36

be solved as the deposition proceeds. If one has limited computing resources (e. g., time or money), this poses quite a problem, since atomic clusters can easily contain many thousands of atoms.

To circumvent this problem, Section 4.2.2 derives a Fokker-Planck-type continuum equation for $X_c \leq x \leq X_{max}$, where x denotes the number of atoms in an x-atom cluster. A transition cluster size, X_c, is defined as the smallest size described by the continuum. Clusters containing X_c or more atoms are described by a continuum distribution function, $C_{con}(x,t)$, which depends on the following characteristics of the distribution: $C_{tot}(t)$, the total density of clusters in the continuum; $\langle x \rangle(t)$, the average size of the continuum clusters; and $M_n(t)$, the nth central moment of the continuum distribution, where $2 \leq n \leq N$ and N is the number of moments used to reconstruct the distribution function. In this manner, atomic clustering phenomena will be modeled by a set of discrete kinetic rate equations for $1 \leq x \leq (X_c - 1)$, coupled to a set of kinetic moment equations which characterize a continuum distribution for $X_c \leq x \leq X_{max}$. In Section 4.2.2, it will be shown that the early stages of film growth can be described by a hybrid system of $(X_c + N + 2)$ kinetic rate equations for the following variables of interest: single traps, $C_T(t)$; mobile single atoms, $C_{mob}(1,t)$; bound single atoms, $C_b(1,t)$; discrete x-atom clusters, $C(x,t)$ for $2 \leq x \leq (X_c - 2)$; the total density of continuum clusters, $C_{tot}(t)$; the average size of continuum clusters, $\langle x \rangle(t)$; the central moments of the continuum, $M_n(t)$ for $2 \leq n \leq N$; and the net number of particles deposited, $X_{depos}(t)$. The size of this hybrid system of equations, $(X_c + N + 2)$, can be typically several thousand times less than the size of the original discrete clustering system containing $(X_{max} + 2)$ equations, providing faster computations without loss of accuracy.

4.2.1 Discrete System of Kinetic Clustering Equations

Assuming that the largest cluster present on the substrate contains X_{max} atoms, production and loss mechanisms governing the single-trap population reveal that

$$
\begin{aligned}
\frac{\partial C_T(t)}{\partial t} = {} & q\,p(E) + \nu_{imp}(1)\,C_b(1,t)\,\Theta(E - E_{eject}) + \nu_T\,C_b(1,t) - \nu_{imp,T}\,C_T(t) \\
& - [2\,\nu_{T,T}(t)\,C_T(t) + \nu_{T,m}(t)\,C_{mob}(1,t) + \nu_{T,b}(t)\,C_b(1,t)] \\
& - \sum_{x=2}^{X_{max}} \nu_{T,x}(t)\,C(x,t)
\end{aligned}
\tag{4.1}
$$

where $\Theta(z) = 1$ for $z \geq 0$ and $\Theta(z) = 0$ for $z < 0$. Traps are produced by the collision cascade, when bound single atoms are sputtered out of traps, and when thermal oscillations release a bound single atom from a trap site. Direct impingement creates bound single atoms, removing traps in the process. As traps migrate over the substrate, they are also destroyed as they encounter other traps, mobile and bound single atoms, and larger x-atom clusters. It should be noted that $\nu_{T,T}(t)\,C_T(t)$ is the rate at which two traps *aggregate* together, however, since two traps are lost during each interaction, the total *loss rate* is $2\,\nu_{T,T}(t)\,C_T(t)$. This di-trap production rate is assumed to be negligible so that the di-trap population is insignificant compared to the single-trap density.

The mobile single-atom population is characterized by

$$
\begin{aligned}
\frac{\partial C_{mob}(1,t)}{\partial t} = {} & q + \nu_T\,C_b(1,t) \\
& + \sum_{x=2}^{X_{max}} \nu_{diss}(x,E)\,C(x,t)\,(1 + \delta_{x2}) - \nu_a\,C_{mob}(1,t) \\
& - \nu_{imp,T}\,C_T(t) - \nu_{imp}(1)\,\{C_{mob}(1,t) + C(1,t)\,[1 - \Theta(E - E_{eject})]\} \\
& - \sum_{x=2}^{X_{max}} \nu_{imp}(x)\,C(x,t)
\end{aligned}
$$

$$- \left[\nu_{m,T}(t)\, C_T(t) + 2\,\nu_{m,m}(t)\, C_{mob}(1,t) + \nu_{m,b}(t)\, C_b(1,t) \right]$$

$$- \sum_{x=2}^{X_{max}} \nu_{m,x}(t)\, C(x,t) \tag{4.2}$$

where $\delta_{ab} = 1$ if $a = b$ and zero otherwise. Mobile single atoms are produced by the deposition source, the release of bound single atoms from trap sites due to thermal oscillations, and from the dissociation of discrete x-atom clusters. The δ-function accounts for the fact that two mobile singles are produced when a two-atom cluster dissociates. Desorption, direct impingement, and aggregation processes deplete the mobile single-atom inventory. The total single-atom density is $C(1,t) = C_{mob}(1,t) + C_b(1,t)$. Similar to trap-trap aggregation in Equation 4.1, the rate at which two mobile single atoms aggregate together is $\nu_{m,m}(t)\, C_{mob}(1,t)$, however, two mobile singles are lost in the process so the total loss rate is $2\,\nu_{m,m}(t)\, C_{mob}(1,t)$.

The kinetic equation for bound single atoms is somewhat simpler:

$$\frac{\partial C_b(1,t)}{\partial t} = \left[\nu_{imp,T} + \nu_{m,T}(t) \right] C_T(t)$$

$$- \left[\nu_T + \nu_{m,b}(t) + \nu_{imp}(1) \right] C_b(1,t). \tag{4.3}$$

Bound singles are created when the deposit directly impinges on a trap or as mobile single atoms diffuse to traps. Bound singles are destroyed when thermal oscillations release a bound single from a trap site. Aggregation of mobile singles with bound singles and direct impingement of the deposit on bound singles create two-atom clusters, destroying bound single atoms in the process.

A separate kinetic equation must be written for two-atom clusters:

$$\frac{\partial C(2,t)}{\partial t} = \frac{1}{2} \left[2\,\nu_{m,m}(t)\, C_{mob}(1,t) \right] + \nu_{m,b}(t)\, C_b(1,t)$$

$$+ \nu_{imp}(1)\, C(1,t) \left[1 - \Theta(E - E_{eject}) \right]$$

$$- \left[\nu_{m,2}(t) + \nu_{diss}(2, E) + \nu_{imp}(2) \right] C(2, t)$$

$$+ \nu_{diss}(3, E) C(3, t). \tag{4.4}$$

Two-atom clusters are produced when two mobile singles aggregate together, mobile and bound singles aggregate, and when a low-energy deposit $(E < E_{eject})$ directly impinges on the single-atom population. The factor of $\frac{1}{2}$ is needed in the first term in order to avoid counting twice each encounter between two atoms from the same $C_{mob}(1, t)$ population. Aggregation, dissociation, and direct impingement reactions involving two-atom clusters, though, deplete the two-atom population. The dissociation of three-atom clusters produces two-atom clusters and mobile single atoms.

Larger discrete clusters are modeled with a general kinetic rate equation. For $3 \leq x \leq (X_{max} - 1)$,

$$\frac{\partial C(x, t)}{\partial t} = \left[\nu_{m,x-1}(t) + \nu_{imp}(x - 1) \right] C(x - 1, t)$$

$$- \left[\nu_{m,x}(t) + \nu_{diss}(x, E) + \nu_{imp}(x) \right] C(x, t)$$

$$+ \nu_{diss}(x + 1, E) C(x + 1, t) \tag{4.5}$$

where cluster growth and decay proceed via single-particle transitions.

The final kinetic rate equation used in the discrete system model describes the net number of particles deposited on the substrate, $X_{depos}(t)$, where

$$X_{depos}(t) = \sum_{x=1}^{X_{max}} x \, C(x, t). \tag{4.6}$$

Taking the time derivative of Equation 4.6 and extending Equation 4.5 to $x = X_{max}$, one can use a linear combination of Equations 4.2 – 4.5 to obtain

$$\frac{\partial X_{depos}(t)}{\partial t} = q - \nu_a C_{mob}(1, t) - \nu_{imp}(1) C(1, t) \Theta(E - E_{eject})$$

40

$$+ X_{max}\, \nu_{diss}(X_{max} + 1, E)\, C(X_{max} + 1, t)$$

$$- (X_{max} + 1)\left[\nu_{m, X_{max}}(t) + \nu_{imp}(X_{max})\right] C(X_{max}, t). \quad (4.7)$$

From a physical standpoint, the net number of particles deposited on the substrate should be a balance between the deposition rate and losses due to evaporation and sputtering. The two additional terms involving the discrete cluster densities $C(X_{max}, t)$ and $C(X_{max} + 1, t)$ arise because of the assumption that the largest discrete cluster contains X_{max} atoms. With this in mind, X_{max} is assumed to be so large that the density $C(X_{max} + 1, t)$ does not exist, and may be taken to be zero.

Equations 4.1−4.7 represent $(X_{max} + 2)$ equations in the $(X_{max} + 2)$ unknowns $C_T(t)$, $C_{mob}(1, t)$, $C_b(1, t)$, $C(x, t)$ for $2 \leq x \leq (X_{max} - 1)$, and $X_{depos}(t)$. Solving a kinetic equation for $X_{depos}(t)$ allows one to determine the unknown discrete cluster density $C(X_{max}, t)$ as

$$C(X_{max}, t) \;=\; \left(\frac{1}{X_{max}}\right)\left[X_{depos}(t) - \sum_{x=1}^{X_{max}-1} x\, C(x, t)\right] \qquad (4.8)$$

ensuring particle conservation in the model. Solving this discrete system of $(X_{max} + 2)$ kinetic clustering equations allows one to model the early stages of thin film formation by energetic particle bombardment for clusters containing up to X_{max} atoms.

4.2.2 Hybrid System of Kinetic Clustering Equations

The basic limitation of the method outlined in Section 4.2.1 is that the number of equations which must be solved depends on the maximum size cluster present on the substrate (# of eqns $= X_{max} + 2$). If the largest cluster contains 1000 atoms, for instance, then 1002 coupled, non-linear, stiff differential equations must be solved. Since cluster size increases with time, X_{max} increases, which dictates that

41

more and more equations be solved as the deposition proceeds. If one has limited computing resources, then this can pose quite a dilemma.

To circumvent this problem, Equation 4.5 is used to obtain a continuum equation for cluster sizes $3 \leq x \leq X_{max}$. To derive this continuum equation, the aggregation rate $\nu_{m,x-1}(t) \, C(x-1, t)$, the direct impingement rate $\nu_{imp}(x-1) \, C(x-1, t)$, and the dissociation rate $\nu_{diss}(x+1, E) \, C(x+1, t)$ are each expanded in a second order Taylor series about the cluster size, x. Substituting these expansions into Equation 4.5, then truncating to second order, yields the following continuum equation approximation for single-atom transitions over $3 \leq x \leq X_{max}$:

$$\frac{\partial C_{con}(x, t)}{\partial t} \simeq -\frac{\partial \mathcal{J}(x, t)}{\partial x} \tag{4.9}$$

where $C_{con}(x, t)$ denotes the continuum-cluster distribution function. The nucleation current, $\mathcal{J}(x, t)$, is defined to be

$$\mathcal{J}(x, t) = \mathcal{F}(x, t) \, C_{con}(x, t) - \frac{\partial}{\partial x} [\mathcal{D}(x, t) \, C_{con}(x, t)] \tag{4.10}$$

where the drift and dispersion frequencies, $\mathcal{F}(x, t)$ and $\mathcal{D}(x, t)$, are

$$\mathcal{F}(x, t) = \nu_{m,x}(t) - \nu_{diss}(x, E) + \nu_{imp}(x) \tag{4.11}$$

$$\mathcal{D}(x, t) = \frac{1}{2} [\nu_{m,x}(t) + \nu_{diss}(x, E) + \nu_{imp}(x)]. \tag{4.12}$$

Equation 4.9 is a Fokker-Planck-type equation, consisting of systematic drift and random dispersion terms, which describes the evolution of the cluster size distribution for $x \geq 3$. It has the form of a generalized diffusion equation in which the cluster size, x, plays the role of a spatial coordinate. The use of a Fokker-Planck formalism as an approximate method of treating the kinetics of single-particle transitions is not new, having been initiated by Becker and Döring [56]

42

and brought into its modern form by Frenkel [128]. This technique has been used to study the kinetics of particle growth in colloidal systems [129], the nucleation of voids and dislocation loops in irradiated microstructures [130,131,132], and in the author's previous studies of thin film formation [133,134,135].

It should be noted that both the continuum equation, Equation 4.9, and the general discrete kinetic equation, Equation 4.5, are both valid for $3 \leq x \leq X_{max}$. In order to couple the discrete equations to the continuum, a transition cluster size, X_c, will be defined as the smallest cluster size represented in the continuum. Thus, atomic clustering will be described by a set of discrete kinetic rate equations for $1 \leq x \leq (X_c - 1)$ and by a continuum equation for $X_c \leq x \leq X_{max}$.

Kinetic central moment equations will be used to describe the characteristics of the continuum-cluster distribution function, $C_{con}(x,t)$, over the range $X_c \leq x \leq X_{max}$. The nth truncated central moment, $M_n(t)$, of the continuum-cluster size distribution, is defined as

$$M_n(t) = \left(\frac{1}{C_{tot}(t)} \right) \int_{X_c}^{X_{max}} [x - \langle x \rangle(t)]^n \, C_{con}(x,t) \, dx \qquad (4.13)$$

where $C_{tot}(t)$ is the total density of continuum clusters,

$$C_{tot}(t) = \int_{X_c}^{X_{max}} C_{con}(x,t) \, dx \qquad (4.14)$$

and $\langle x \rangle(t)$ is the average cluster size in the continuum distribution,

$$\langle x \rangle(t) = \left(\frac{1}{C_{tot}(t)} \right) \int_{X_c}^{X_{max}} x \, C_{con}(x,t) \, dx \qquad (4.15)$$

Coupling the set of discrete kinetic rate equations to the continuum requires that terms (i. e., summations which appear in Equations 4.1 and 4.2) which extend into the continuum be appropriately averaged over the continuum distribution. For a general function $g(x,t) \, C(x,t)$,

$$\sum_{x=2}^{X_{max}} g(x,t) \, C(x,t) = \sum_{x=2}^{X_c-1} g(x,t) \, C(x,t) + \int_{X_c}^{X_{max}} g(x,t) \, C_{con}(x,t) \, dx$$

43

$$= \sum_{x=2}^{X_c-1} g(x,t)\, C(x,t) + \langle g(x,t) \rangle\, C_{tot}(t). \tag{4.16}$$

Averages over the unknown continuum-cluster distribution function will be determined from the central moments using

$$\langle g(x,t) \rangle = \left[g(x,t) + \sum_{n=2}^{N} \frac{M_n(t)}{n!} \frac{\partial^n g(x,t)}{\partial x^n} \right]_{@x=\langle x \rangle(t)} \tag{4.17}$$

where N is the total number of central moments used to describe the continuum distribution.

Coupling the discrete kinetic rate equations to the kinetic central moment equations results in the following hybrid system of $(X_c + N + 2)$ kinetic rate equations:

$$\frac{\partial C_T(t)}{\partial t} = q\, p(E) + \nu_{imp}(1)\, C_b(1,t)\, \Theta(E - E_{eject}) + \nu_T\, C_b(1,t) - \nu_{imp,T}\, C_T(t)$$

$$- \left[2\, \nu_{T,T}(t)\, C_T(t) + \nu_{T,m}(t)\, C_{mob}(1,t) + \nu_{T,b}(t)\, C_b(1,t) \right]$$

$$- \left[\sum_{x=2}^{X_c-1} \nu_{T,x}(t)\, C(x,t) + \langle \nu_{T,x}(t) \rangle\, C_{tot}(t) \right] \tag{4.18}$$

$$\frac{\partial C_{mob}(1,t)}{\partial t} = q + \nu_T\, C_b(1,t)$$

$$+ \left[\sum_{x=2}^{X_c-1} \nu_{diss}(x,E)\, C(x,t)\, (1 + \delta_{x2}) + \langle \nu_{diss}(x,E) \rangle\, C_{tot}(t) \right] - \nu_a\, C_{mob}(1,t)$$

$$- \nu_{imp,T}\, C_T(t) - \nu_{imp}(1) \left\{ C_{mob}(1,t) + C(1,t)\, [1 - \Theta(E - E_{eject})] \right\}$$

$$- \left[\sum_{x=2}^{X_c-1} \nu_{imp}(x)\, C(x,t) + \langle \nu_{imp}(x) \rangle\, C_{tot}(t) \right]$$

$$- \left[\nu_{m,T}(t)\, C_T(t) + 2\, \nu_{m,m}(t)\, C_{mob}(1,t) + \nu_{m,b}(t)\, C_b(1,t) \right]$$

$$- \left[\sum_{x=2}^{X_c-1} \nu_{m,x}(t)\, C(x,t) + \langle \nu_{m,x}(t) \rangle\, C_{tot}(t) \right] \tag{4.19}$$

44

$$\frac{\partial C_b(1,t)}{\partial t} \;=\; [\nu_{imp,T} + \nu_{m,T}(t)]\, C_T(t)$$

$$-\,[\nu_T + \nu_{m,b}(t) + \nu_{imp}(1)]\, C_b(1,t) \qquad (4.20)$$

$$\frac{\partial C(2,t)}{\partial t} \;=\; \frac{1}{2}\,[2\,\nu_{m,m}(t)\, C_{mob}(1,t)] + \nu_{m,b}(t)\, C_b(1,t)$$

$$+\,\nu_{imp}(1)\, C(1,t)\, [1 - \Theta(E - E_{eject})]$$

$$-\,[\nu_{m,2}(t) + \nu_{diss}(2,E) + \nu_{imp}(2)]\, C(2,t)$$

$$+\,\nu_{diss}(3,E)\, C(3,t) \qquad (4.21)$$

$$\frac{\partial C(x,t)}{\partial t} \;=\; [\nu_{m,x-1}(t) + \nu_{imp}(x-1)]\, C(x-1,t)$$

$$-\,[\nu_{m,x}(t) + \nu_{diss}(x,E) + \nu_{imp}(x)]\, C(x,t)$$

$$+\,\nu_{diss}(x+1,E)\, C(x+1,t) \quad \dots \quad 3 \le x \le (X_c - 2) \quad (4.22)$$

$$\frac{\partial C_{tot}(t)}{\partial t} \;=\; \mathcal{J}(X_c,t) \qquad (4.23)$$

$$\frac{\partial \langle x \rangle(t)}{\partial t} \;=\; \xi_1(t) + \langle \mathcal{F}(x,t) \rangle \qquad (4.24)$$

$$\frac{\partial M_n(t)}{\partial t} \;=\; \xi_n(t) + \phi_n(t) + \psi_n(t) \qquad \dots \quad 2 \le n \le N \qquad (4.25)$$

45

where the nucleation current going into the continuum, $\mathcal{J}(X_c, t)$, is defined by the expression

$$\mathcal{J}(X_c, t) = [\nu_{m,X_c-1}(t) + \nu_{imp}(X_c - 1)] \, C(X_c - 1, t)$$

$$- \nu_{diss}(X_c, E) \, C(X_c, t) \tag{4.26}$$

while the drift and dispersion frequency functions at $x = X_c$, $\mathcal{F}(X_c, t)$ and $\mathcal{D}(X_c, t)$, are

$$\mathcal{F}(X_c, t) = \nu_{m,X_c}(t) - \nu_{diss}(X_c, E) + \nu_{imp}(X_c) \tag{4.27}$$

$$\mathcal{D}(X_c, t) = \frac{1}{2} [\nu_{m,X_c}(t) + \nu_{diss}(X_c, E) + \nu_{imp}(X_c)]. \tag{4.28}$$

The special nucleation frequency function, $\xi_1(t)$, is

$$\xi_1(t) = \frac{[X_c - \langle x \rangle(t)] \, \mathcal{J}(X_c, t) + \mathcal{D}(X_c, t) \, C(X_c, t)}{C_{tot}(t)} \tag{4.29}$$

while the general nucleation [$\xi_n(t)$], drift [$\phi_n(t)$], and dispersion [$\psi_n(t)$] frequency functions for $2 \leq n \leq N$ are

$$\xi_n(t) = \frac{\{[X_c - \langle x \rangle(t)]^n - M_n(t) - n \, M_{n-1}(t) \, [X_c - \langle x \rangle(t)]\} \, \mathcal{J}(X_c, t)}{C_{tot}(t)}$$

$$+ \frac{n \, \mathcal{D}(X_c, t) \, C(X_c, t) \left\{ [X_c - \langle x \rangle(t)]^{n-1} - M_{n-1}(t) \right\}}{C_{tot}(t)} \tag{4.30}$$

$$\phi_n(t) = n \left\{ \left\langle \mathcal{F}(x, t) \, [x - \langle x \rangle(t)]^{n-1} \right\rangle - M_{n-1}(t) \, \langle \mathcal{F}(x, t) \rangle \right\} \tag{4.31}$$

$$\psi_n(t) = n \, (n-1) \left\langle \mathcal{D}(x, t) \, [x - \langle x \rangle(t)]^{n-2} \right\rangle. \tag{4.32}$$

The boundary conditions $C(X_{max}, t) = 0$ and $\mathcal{J}(X_{max}, t) = 0$ have been used in deriving Equations 4.23−4.25. These assumptions are justified if one assumes that

46

the upper range of the continuum is so large that no clusters exist which contain X_{max} atoms.

The final kinetic rate equation used in the hybrid model describes the net number of particles deposited on the substrate, $X_{depos}(t)$, where

$$X_{depos}(t) = \sum_{x=1}^{X_c-1} x\, C(x,t) + \langle x \rangle(t)\, C_{tot}(t). \qquad (4.33)$$

Taking the time derivative of Equation 4.33 and extending Equation 4.22 to $x = (X_c - 1)$, one can use a linear combination of Equations 4.19 – 4.24 to obtain

$$\frac{\partial X_{depos}(t)}{\partial t} = q - \nu_a\, C_{mob}(1,t) - \nu_{imp}(1)\, C(1,t)\, \Theta(E - E_{eject})$$
$$+ \frac{1}{2}\, \mathcal{F}(X_c,t)\, C(X_c,t). \qquad (4.34)$$

From a physical standpoint, the net number of particles deposited on the substrate should be a balance between the deposition rate and losses due to evaporation and sputtering. An additional term arises, however, because of the hybrid coupling at $x = X_c$.

Equations 4.18 – 4.34 represent $(X_c + N + 2)$ equations in the $(X_c + N + 2)$ unknowns $C_T(t)$, $C_{mob}(1,t)$, $C_b(1,t)$, $C(x,t)$ for $2 \leq x \leq (X_c - 2)$, $C_{tot}(t)$, $\langle x \rangle(t)$, $M_n(t)$ for $2 \leq n \leq N$, and $X_{depos}(t)$. Solving a kinetic equation for $X_{depos}(t)$ allows one to determine the unknown discrete cluster density $C(X_c - 1, t)$ as

$$C(X_c - 1, t) = \left(\frac{1}{X_c - 1} \right) \left[X_{depos}(t) - \sum_{x=1}^{X_c-2} x\, C(x,t) - \langle x \rangle(t)\, C_{tot}(t) \right] (4.35)$$

ensuring particle conservation in the hybrid model. These equations represent a hybrid system of kinetic rate equations which model the early stages of thin film formation by energetic particle bombardment. From a computational viewpoint, this scheme is not limited by the maximum cluster size.

4.3 Characteristic Clustering Frequencies

Additional functions and definitions are needed in order to solve either the discrete (Section 4.2.1) or hybrid (Section 4.2.2) systems of kinetic clustering equations. Physical processes are modeled with a number of characteristic clustering frequencies. The frequencies at which mobile single atoms $[\nu_{m,i}(t)]$ and single traps $[\nu_{T,i}(t)]$ aggregate with other species on the substrate [where $i = T$, m, b, or x as described in Section 4.1] are

$$\nu_{m,i}(t) = \frac{1}{4} a_\circ a(1) \nu_1 \exp\left(-\frac{E_d}{kT}\right) C_{mob}(1,t) \, (1 + \beta_{m,i}) \, (1 + \gamma_{m,i}) \quad (4.36)$$

$$\nu_{T,i}(t) = \frac{1}{4} a_\circ a_T \nu_1 \exp\left(-\frac{E_d^T}{kT}\right) C_T(t) \, (1 + \beta_{T,i}) \, (1 + \gamma_{T,i}) \quad (4.37)$$

where the diameters $a_\circ$, $a(1)$, and a_T characterize the size of the substrate atoms, deposit species, and single traps; ν_1 is an average vibrational frequency for both mobile single-atom and single-trap diffusive "hops" in *all* directions on the substrate; and kT is the substrate temperature. The β's and γ's are size and motion factors for a particular interaction, as shown in Table 4.1.

The frequencies at which the deposit directly impinges on x-atom clusters and single traps are

$$\nu_{imp}(x) = q\frac{\pi a^2(x)}{4} \quad (4.38)$$

$$\nu_{imp,T} = q\frac{\pi a_T^2}{4}. \quad (4.39)$$

The diameter of an x-atom cluster, $a(x)$, is

$$a(x) = a(1) x^r \quad (4.40)$$

Table 4.1. Size (β's) and Motion (γ's) Factors

i	$\beta_{m,i}$	$\beta_{T,i}$	$\gamma_{m,i}$	$\gamma_{T,i}$
T	$\frac{a_T}{a(1)}$	1	$\exp\left(\frac{E_d - E_d^T}{kT}\right)$	1
m	1	$\frac{a(1)}{a_T}$	1	$\exp\left(\frac{E_d^T - E_d}{kT}\right)$
b	1	$\frac{a(1)}{a_T}$	0	0
x	x^r	$\frac{a(1)}{a_T}x^r$	0	0

where r is the growth exponent, defined over $0 \le r < 1$. A specific value for r dictates cluster geometry; for example, $r = \frac{1}{2}$ describes 2-D discs, while $r = \frac{1}{3}$ describes 3-D spheres.

Thermal oscillations can cause mobile single atoms to desorb off the substrate, as well as release bound single atoms from traps. The associated frequencies for these effects are

$$\nu_a = \nu_o \exp\left(-\frac{E_a}{kT}\right) \tag{4.41}$$

$$\nu_T = \nu_2 \exp\left(-\frac{E_T}{kT}\right) \tag{4.42}$$

where ν_o and ν_2 are characteristic vibrational frequencies.

The frequency at which x-atom clusters dissociate into $(x-1)$-atom clusters and mobile single atoms depends on the cluster size, $a(x)$, as follows:

$$\nu_{diss}(x,E) = q\frac{\pi}{4}\left[a(x) + 2\lambda(E)\right]^2 \qquad \text{for} \quad a(x) < 2\lambda(E) \tag{4.43}$$

49

$$\nu_{diss}(x, E) = 2\pi q \lambda(E) a(x) \qquad \text{for} \quad a(x) \geq 2\lambda(E). \qquad (4.44)$$

The parameter $\lambda(E)$ is defined as the *mean free path for single-atom re-solution.* Cluster dissociation occurs when an energetic particle impinges within a distance $\lambda(E)$ from the edge of a cluster. It should be noted that the dissociation of small clusters does not require a direct impact if the cluster is within the collision cascade regime [126]. The outside edges of larger clusters can also be "chipped" off. Thus, a length of $\lambda(E)$ extends both inside and outside a cluster, as shown in Figure 4.1.
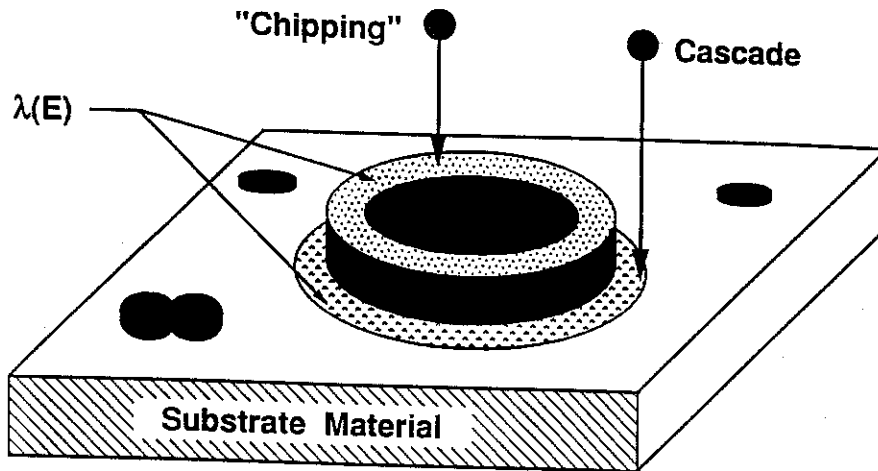

Figure 4.1. $\lambda(E)$, the mean free path for single-atom re-solution, characterizes cluster dissociation.

4.4 Reconstructing the Continuum-Cluster Size Distribution

In order to close the hybrid system of kinetic clustering equations described in Section 4.2.2, the continuum-cluster density at X_c, $C_{con}(X_c, t)$, must be specified.

Up to this point, however, the continuum-cluster distribution function remains unknown. This Section describes the method used to determine $C_{con}(x, t)$.

It is a well-known property of a statistical distribution that if its moments are known, then the distribution itself is often completely determined. Orthogonal polynomials can be used to expand such distributions in terms of their moments. The most suitable and natural set of polynomials for this problem is the set of associated Laguerre polynomials, for these are defined over the entire positive, real axis, x. In this study, however, the continuum distribution function will be expanded in a series of Chebyshev-Hermite polynomials. Such expansions are known in statistics as a Gram-Charlier series [136]. They have the disadvantage that they are only asymptotically convergent in the region x and t both large, the basic reason being that the natural range of the Chebyshev-Hermite polynomials is the entire real axis, x, while the nucleation and growth process is defined only for x positive. For x and $\langle x \rangle(t)$ both large, though, the Gram-Charlier series becomes increasingly accurate [137]. A numerical example, demonstrating the worth of the Laguerre and Chebyshev-Hermite polynomial expansion techniques to the problem of the pure growth process, has been published [138].

Using a series of Chebyshev-Hermite polynomials, the continuum-cluster distribution function for $x \geq X_c$ is

$$C_{con}(x, t) = C_{Norm}(x, t) \left\{ 1 + \sum_{j=2}^{N} \mathcal{A}_j(t) \, \mathcal{H}_j \left[\rho(x, t) \right] \right\} \qquad (4.45)$$

based on using a total of N moments for the reconstruction. The normal distribution, $C_{Norm}(x, t)$, is

$$C_{Norm}(x, t) = \frac{C_{tot}(t)}{\sqrt{2 \pi M_2(t)}} \exp \left[-\frac{\rho^2(x, t)}{2} \right] \qquad (4.46)$$

where

$$\rho(x,t) = \frac{x - \langle x \rangle(t)}{\sqrt{M_2(t)}}.$$ (4.47)

The Chebyshev-Hermite polynomials, $\mathcal{H}_j(z)$, are

$$\mathcal{H}_0(z) = 1$$
$$\mathcal{H}_1(z) = z$$ (4.48)
$$\mathcal{H}_j(z) = z\,\mathcal{H}_{j-1}(z) - (j-1)\,\mathcal{H}_{j-2}(z) \qquad \dots \quad j \geq 2.$$

The expansion coefficients, $\mathcal{A}_j(t)$, are

$$\mathcal{A}_j(t) = \theta(j,t) + \sum_{n=1}^{n_{max}} \frac{(-1)^n\,\theta(j-2n,t)}{2^n\,n!}$$ (4.49)

where $n_{max} = \frac{j}{2}$ for j-even, $j \geq 2$, or $n_{max} = \left(\frac{j-1}{2}\right)$ for j-odd, $j \geq 3$. The moment ratio functions, $\theta(j,t)$, are given by

$$\theta(j,t) = \frac{M_j(t)}{j!\left[\sqrt{M_2(t)}\right]^j}.$$ (4.50)

This hybrid system of kinetic clustering equations is completely closed by specifying

$$C(X_c,t) = C_{con}(X_c,t).$$ (4.51)

One may standardize the distribution by expressing it in terms of the reduced variable, $\rho(x,t)$. The distribution in standard measure is given by

$$C_{sm}[\rho(x,t),t] = \sqrt{M_2(t)}\,C_{con}(x,t)$$ (4.52)

and has zero mean and unit variance. Two distributions in standard measure can be readily compared in regard to form, skewness, and other qualities, but not with respect to mean or variance.

4.5 Solving the Hybrid System of Kinetic Clustering Equations

The hybrid system of $(X_c + N + 2)$ kinetic rate equations described in Section 4.2.2 is an initial value problem whose solution depends upon the initial starting values of $C_T(t)$, $C_{mob}(1,t)$, $C_b(1,t)$, $C(x,t)$ for $2 \leq x \leq (X_c - 2)$, $C_{tot}(t)$, $\langle x \rangle(t)$, $M_n(t)$ for $2 \leq n \leq N$, and $X_{depos}(t)$ at some initial time $t = t_o$. A problem exists with this formulation when one wishes to simulate a deposition event on an initially bare, defect-free substrate. Although one can readily set $C_T(t_o) = C_{mob}(1,t_o) = C_b(1,t_o) = C(x,t_o)$ [for $2 \leq x \leq (X_c - 2)$] $= X_{depos}(t_o) = 0$, the continuum characteristics $C_{tot}(t_o)$, $\langle x \rangle(t_o)$, and $M_n(t_o)$ for $2 \leq n \leq N$ remain completely undetermined. The hybrid problem is ill-posed because one cannot specify initial conditions for the unknown continuum distribution.

To circumvent this problem, the discrete system of kinetic clustering equations described in Section 4.2.1 is used to generate initial values for the hybrid system of equations. The deposition event dictates the initial values of the $(X_{max} + 2)$ discrete unknowns $C_T(t)$, $C_{mob}(1,t)$, $C_b(1,t)$, $C(x,t)$ for $2 \leq x \leq (X_{max} - 1)$, and $X_{depos}(t)$ at time $t = t_o$. Solving the discrete system of kinetic clustering equations at a later time t^* (i.e., $t^* > t_o$) enables one to determine the X_{max} discrete cluster densities. Moments of this discrete system distribution can be determined as follows:

$$C_{tot}(t^*) = \sum_{x=X_c}^{X_{max}} C(x, t^*) \tag{4.53}$$

$$\langle x \rangle(t^*) = \left(\frac{1}{C_{tot}(t^*)} \right) \sum_{x=X_c}^{X_{max}} x\, C(x, t^*) \tag{4.54}$$

$$M_n(t^*) = \left(\frac{1}{C_{tot}(t^*)} \right) \sum_{x=X_c}^{X_{max}} [x - \langle x \rangle(t^*)]^n\, C(x, t^*) \quad \ldots \; 2 \leq n \leq N. \tag{4.55}$$

53

One can now use these discrete system solutions at time t^* as initial starting values for the hybrid system of clustering equations, formulating a well-posed hybrid problem that begins at time t^*. The value of t^* must be small enough and X_{max} must be large enough so that the density $C(X_{max}, t^*) \simeq 0$, yet some realistic discrete system distribution still exists.

4.6 Unique Features of the Hybrid Clustering Model

The kinetic rate equations outlined in this Chapter can be numerically solved on a computer to obtain information about the nucleation kinetics and cluster size distribution characterizing the early stages of thin film formation by energetic particle bombardment. Surface defect production, sputtering, and cluster dissociation phenomena are modeled for an energetic deposition process, thus supplementing the aggregation and direct impingement reactions present in thermal deposition. The usefulness of this approach to nucleation and growth studies awaits experimental verification.

The continuum-cluster size distribution provides an indication of which physical processes are most responsible for dispersion and asymmetries in observed film structures. Such information might be used to identify deposition conditions which promote tailored film microstructures. Simulations of continuous nucleation and growth can be used to characterize many standard deposition techniques, while flux interruption effects (particularly important in MBE systems) can also be interpreted.

Simultaneously incorporating surface defect production, cluster dissociation, and sputtering phenomena into the model enables one to study the influence of energetic particle bombardment on the initial stages of nucleation and growth.

These energetic effects can be studied as separate mechanisms or as synergistic factors, and their influence on the cluster size distribution readily seen. In particular, it would be interesting to compare trapping simulations to the case of accelerated ion doping during MBE experiments, where the ion flux is low, trapping is the desired effect, and sputtering of the growing film is not significant [88]. Thermal deposition studies performed in conjunction with such energetic simulations may resolve some of the discrepancies in the current literature.

Since this dissertation is based on a computational study of the thin film formation problem, gross approximations and time-independent estimates are not needed as in previous analytical treatments. The early stages of film growth can be studied over a continuous range of time, without having to resort to restricted time-regional solutions. The influence of cluster geometry and different material systems can also be easily examined.

Chapter 5

Sensitivity Analysis of the Proposed Model

The model outlined in Chapter 4 represents a computational study of thin film formation under low-energy particle bombardment. As such, a number of model parameters are needed in order to perform a computer simulation. Many of these parameters can be judiciously estimated depending upon the deposition process and materials' system under study. Other parameters are not so easily specified. This Chapter studies the influence that several of these variables have on the thin film nucleation and growth kinetics. These parameters are grouped according to the mathematical or physical impact that each imposes on the computational results.

5.1 A Set of Reference Simulation Conditions

In order to perform a sensitivity analysis of the proposed model, a set of reference simulation conditions must first be established as a standard. These conditions consist of the following:

1. For each simulation, deposition begins on a bare, defect-free substrate at time $t = 0$. The substrate is at room temperature, 300 K.

2. Focusing on the early stages of the deposition process enables one to neglect direct impingement reactions on traps and clusters.

3. Sputtering is neglected.

4. The vibrational frequencies ν_o, ν_1, and ν_2 are fundamental material constants of the order 10^{12} sec^{-1}.

5. Basing material-dependent parameters on the Au/NaCl system, one uses $a(1) = 2.9 \times 10^{-8}$ cm as the diameter of the Au deposit and $a_o = 2.8 \times 10^{-8}$ cm for the NaCl substrate.

6. Surface defects are features of the substrate, thus $a_T = a_o$. In reality, the substrate atoms can relax around a trap, decreasing a_T, but this effect is ignored.

7. Activation energies for the Au/NaCl system are taken to be $E_d = 0.16$ eV and $E_a = 0.48$ eV, based upon a consistent set of nucleation measurements for substrate temperatures between 123 and 448 K [94].

8. E_d^T is equivalent to an activation energy for surface-vacancy diffusion, taken to be 0.50 eV for this study.

9. E_T is estimated to be $2\,E_a = 0.96$ eV, indicative of the increased binding provided by defect sites.

10. The deposition rate is chosen to be $q = 10^{13}$ atoms/cm^2/sec.

11. Since Au nucleates as 3-D entities on NaCl, $r = \frac{1}{3}$ [50].

12. The effects of surface defect production and cluster dissociation are modeled with $p(E) = 10^{-3}$ and $\lambda(E) = 1.5 \times 10^{-8}$ cm, respectively.

13. For the continuum-cluster size distribution, $X_c = 5$ and $N = 4$. A four-moment reconstruction allows one to model dispersion, skewness, and kurtosis in the distribution, features readily compared with experimental observations.

Changes in any of the above conditions will impact the nucleation and growth behavior of thin films. In order to systematically limit and characterize such influences, the following kinetic variables will be analyzed:

- $C_{tot}(t)$, the total density of continuum clusters [#/cm^2]

- $\mathcal{J}(X_c, t)$, the nucleation current going into the continuum [#/cm^2/sec]

- $\langle x \rangle(t)$, the average size of continuum clusters [atoms]

- $M_2(t)$, the second central moment (i. e., variance) of the continuum-cluster size distribution [dimensionless]

- $C_{con}(x,t)$, the continuum-cluster size distribution [#/cm²]

The response of these kinetic variables to proposed changes in the reference simulation conditions forms the basis of the sensitivity analysis. The strength of the model can thus be understood in terms of its sensitivity to the fundamental mathematical and physical parmeters.

5.2 Mathematical Sensitivity Analysis

In order to demonstrate the mathematical sensitivity of the computational results, five model characteristics are investigated. These features consist of:

- The influence of the transition cluster size for $X_c = 5$, 50, and 100.

- The influence of the number of moments used for reconstructing the continuum-cluster size distribution for $N = 2$, 4, 6, 8, and 10.

- The influence of the growth exponent for $r = 0$, $\frac{1}{3}$, and $\frac{1}{2}$.

- The effect of changes in the Hybrid System initial conditions.

- The validity of replacing a discrete-size distribution function with a continuum-size distribution for large x-atom clusters.

The influence of X_c on the nucleation kinetics is illustrated in Figures 5.1 − 5.4. Since X_c is simply a marker which divides the cluster-size distribution into discrete $[1 \leq x \leq (X_c - 1)]$ and continuum $(x > X_c)$ regions, meaningful X_c-studies must include both regions during analysis. For clarity of presentation, the fractional substrate surface coverage, $Z(t)$, is defined as $X_{depos}(t) \frac{\pi a^2(1)}{4}$. Figures 5.1 − 5.3 indicate that X_c does not influence the total cluster density, nucleation rate, and average cluster size of the complete distribution (which includes both discrete and continuum clusters; i. e., $x \geq 1$). These results demonstrate that X_c is simply a
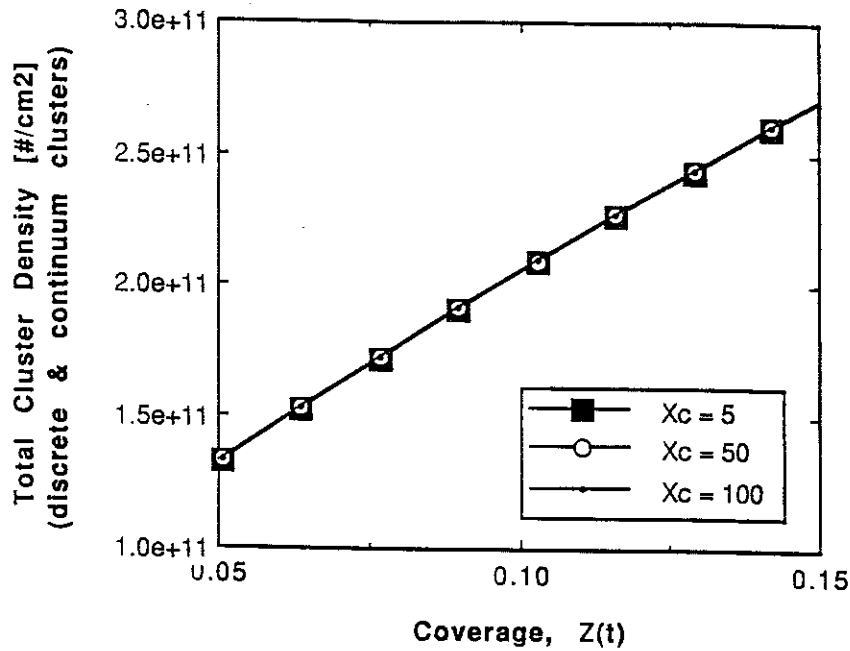
Figure 5.1. Influence of the transition cluster size, X_c, on the total cluster density for the complete distribution.

mathematical variable which has no impact on the atomic clustering physics. In Figure 5.4, however, larger values of X_c decrease the second moment, reducing dispersion in the distribution. This phenomenon might be an artifact of the continuum portion of the distribution. As X_c is increased, the range of the continuum decreases, creating a narrower continuum distribution. Since Figure 5.4 indicates that the width of the complete distribution also decreases, this may indicate that the nucleation kinetics are more sensitive to its continuum properties, rather than its discrete characteristics.

Since no true distribution is available for the energetic deposition conditions presented in Section 5.1, a more detailed discussion of the influence of N will have to wait until Chapter 6. A four-moment reconstruction was selected for the reference conditions because it allows one to model dispersion, skewness, and kurtosis in the distribution, features readily compared with experimental measurements.
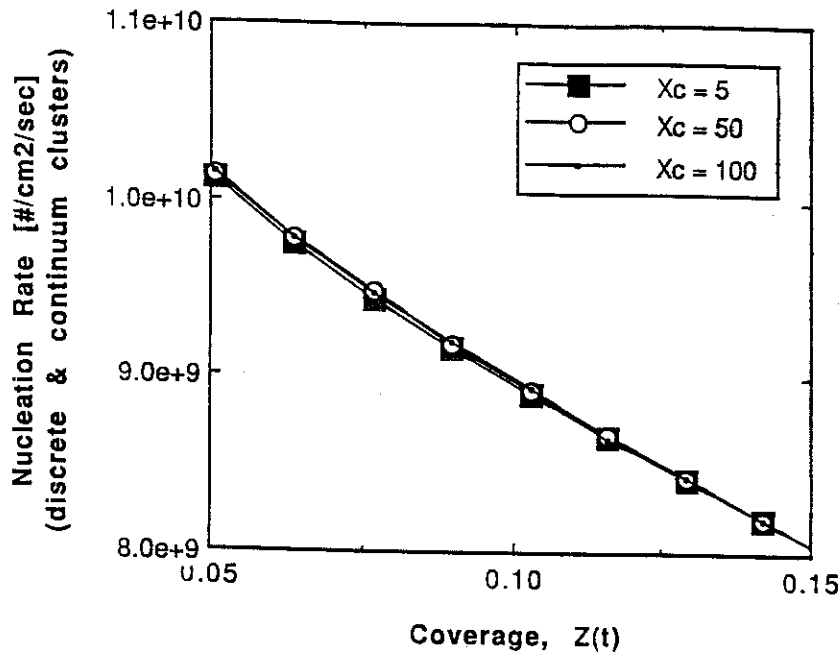
59

Figure 5.2. Influence of the transition cluster size, X_c, on the cluster nucleation rate for the complete distribution.

In practice, numerical moments of order higher than the fourth are rarely used, being so sensitive to sampling fluctuations that values computed from moderate numbers of observations are subject to a large margin of error [139]. The reconstruction scheme discussed in Section 4.4 may be subject to such fluctuations, leading to oscillations in the reconstructed distribution. Section 6.2 compares a thermal particle deposition study to a known analytical solution, indicating that the reconstruction *technique* as well as the number of moments used for the reconstruction are both crucial to obtaining a realistic size distribution.

The influence of the growth exponent, r, on the thin film nucleation kinetics is studied for $r = 0, \frac{1}{3}$, and $\frac{1}{2}$. When cluster dissociation is not considered [134], continuous nucleation occurs which promotes an increase in the values of $C_{tot}(t)$, $\langle x \rangle(t)$, and $M_2(t)$ with time. Calculations also indicate that $\langle x \rangle(t)$ and $M_2(t)$,
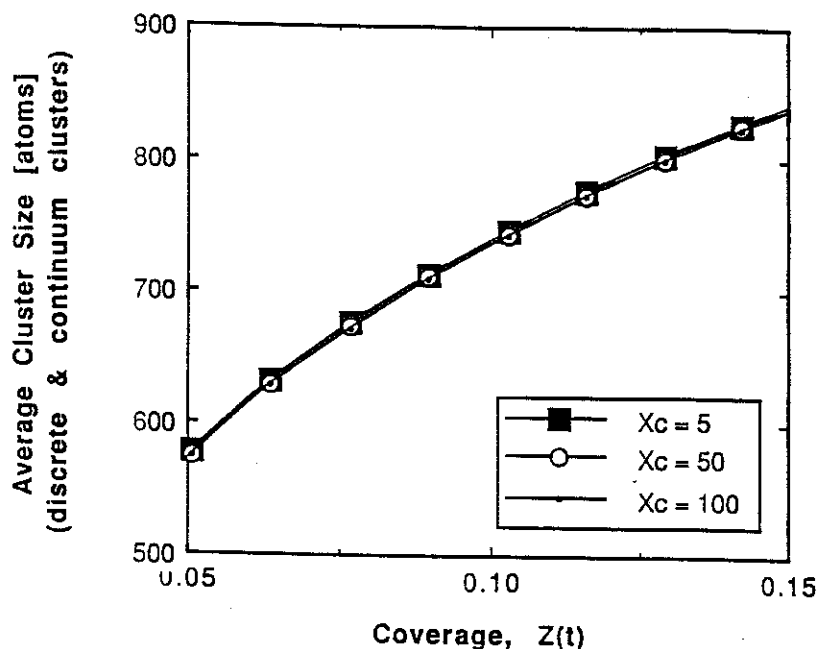
60

Figure 5.3. Influence of the transition cluster size, X_c, on the average cluster size for the complete distribution.

as well as $\frac{\partial (x)(t)}{\partial t}$ and $\frac{\partial M_2(t)}{\partial t}$, all increase with r over all deposition times. Consequently, at a specific time, 2-D clusters will not only be larger than 3-D clusters, but they will grow at a much faster rate. Additionally, at the same time, the 2-D cluster distribution function will have a broader range of cluster sizes than the 3-D cluster distribution, as well as dispersing more quickly. All of these results, where dissociation is not considered, can be attributed to enhanced aggregation which is characteristic of a larger growth exponent.

Figure 5.5 shows how the continuum-cluster size distribution varies over time for $r = 0, \frac{1}{3}$, and $\frac{1}{2}$ when cluster dissociation occurs. Notice that for a specific value of r, the total density, average size, and the second moment (i. e., the area, mean, and width of the distribution) all increase as time progresses from $t = 1.0$ to 10.0 seconds. Although dissociation reactions strictly prohibit continuous nucleation, thermally activated aggregation processes at 300 K dominate over dissociation
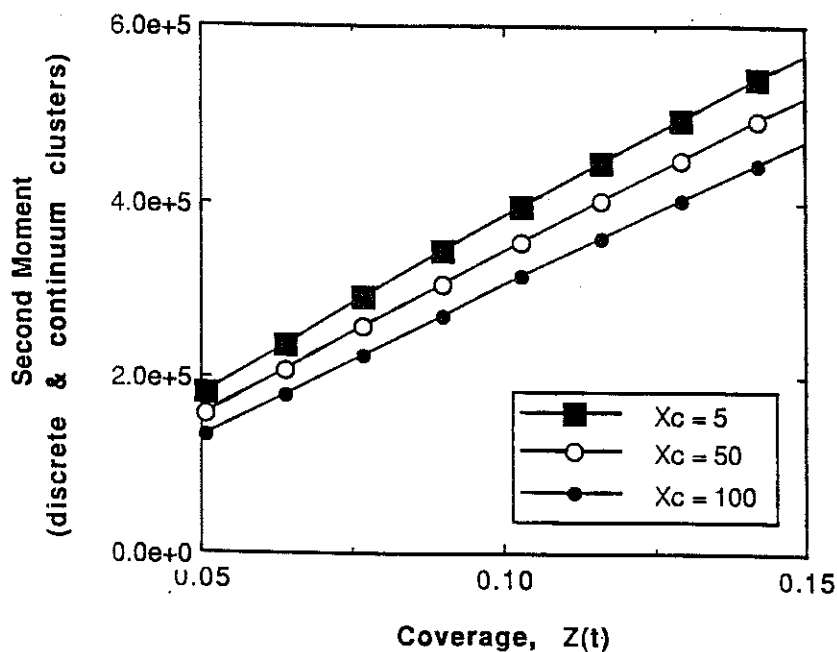
61

Figure 5.4. Influence of the transition cluster size, X_c, on the second moment (i.e., variance) of the complete cluster size distribution.

events, resulting in what appears to be continuous nucleation. At a specific time, though, Figure 5.5 indicates that a larger growth exponent promotes a larger average size and a more disperse distribution, in accordance with the purely continuous nucleation results of Reference [134]. As will be shown in Chapter 7, cluster dissociation plays a more significant role when thermally activated processes are not dominant. In the meantime, enhanced aggregation is found to promote a shift and a broadening in the calculated size distributions.

As discussed in Section 4.5, one must use Discrete System solutions as initial starting values for the Hybrid System of clustering equations in order to formulate a well-posed problem that begins at time t^*. If the discrete code generates the values of $C_{tot}(t^*)$, $\langle x \rangle(t^*)$, and $M_2(t^*)$, how do the Hybrid System kinetics depend on these initial values? Figures 5.6 – 5.9 address this question by plotting the temporal values of $C_{tot}(t)$, $\mathcal{J}(X_c, t)$, $\langle x \rangle(t)$, and $M_2(t)$ for $\pm 5\%$ variations in the
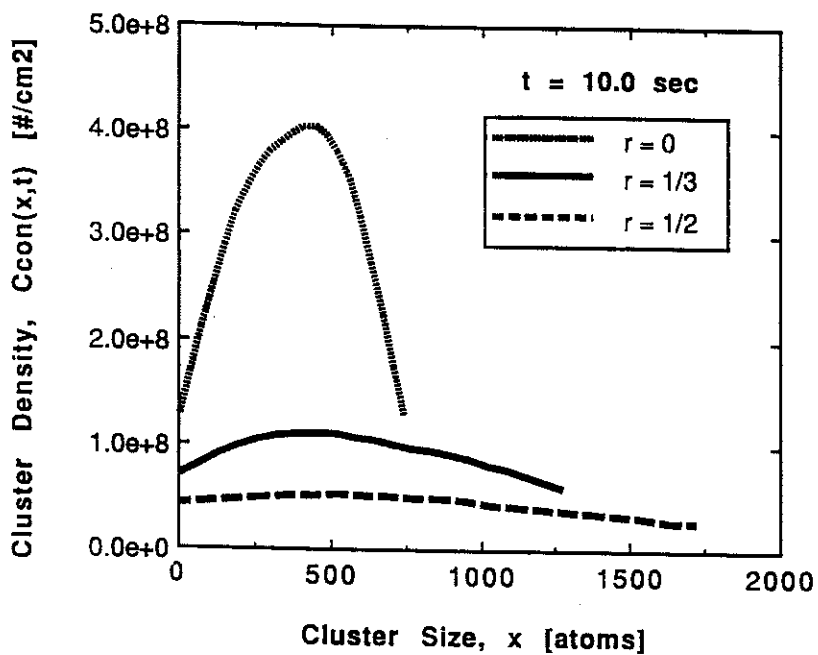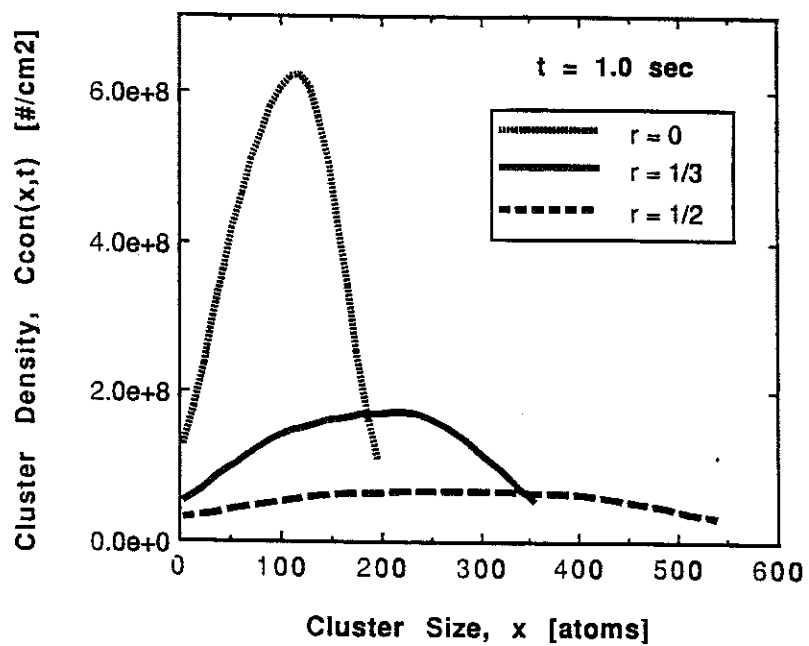
62

Figure 5.5. Continuum-cluster size distributions at times (a) $t = 1.0$ sec, and (b) $t = 10.0$ sec, for various values of the growth exponent, r.

initial values of $C_{tot}(t^*)$, $\langle x \rangle(t^*)$, and $M_2(t^*)$.   Each Figure contains seven curves.
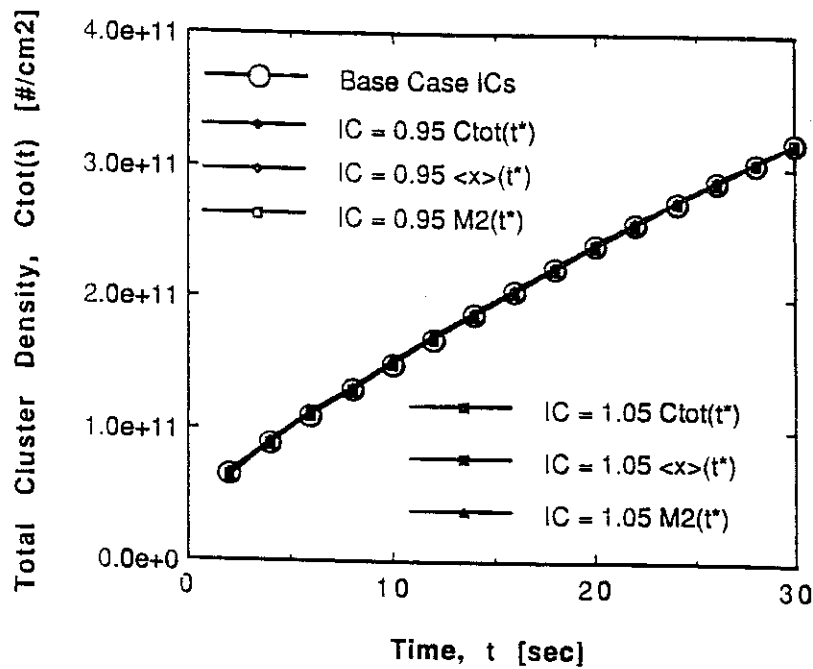

Figure 5.6.   Effects of changes in the Hybrid System initial conditions on the total cluster density.

The "Base Case ICs" curve represents the temporal behavior of the specified nucleation variable subject to no perturbations in any of the initial values at t^*. The other six curves illustrate the temporal behavior of the nucleation variable due to a perturbation in the indicated initial condition. For instance, in Figure 5.6, the curve labeled "IC = $0.95 \langle x \rangle(t^*)$ " represents the temporal behavior of the total cluster density during a simulation which uses the values of $C_{tot}(t^*)$, $0.95 \langle x \rangle(t^*)$, and $M_2(t^*)$ as the initial conditions for the Hybrid System kinetic variables $C_{tot}(t)$, $\langle x \rangle(t)$, and $M_2(t)$.

Using $t^* = 7.5 \times 10^{-2}$ sec, Figures 5.6 – 5.8 illustrate that $\pm 5\%$ variations in the initial values of $C_{tot}(t^*)$, $\langle x \rangle(t^*)$, and $M_2(t^*)$ have no influence on the total cluster density, nucleation rate, and average cluster size. In Figure 5.9, variations in $M_2(t^*)$ do not influence the temporal character of the second moment; however,
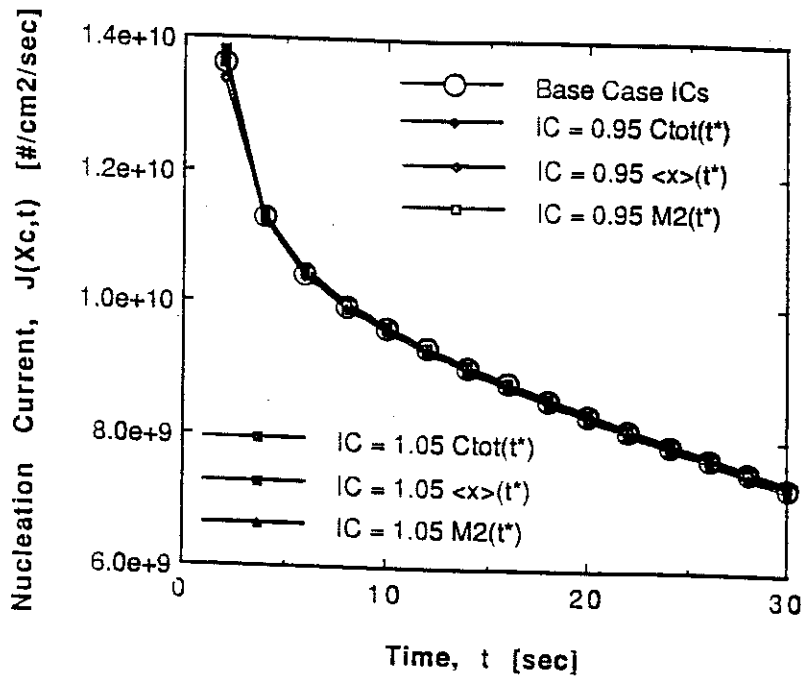
Figure 5.7. Effects of changes in the Hybrid System initial conditions on the cluster nucleation rate.

after 5 seconds of deposition, -5% variations in $C_{tot}(t^*)$ and $\langle x \rangle(t^*)$ reduce $M_2(t)$ slightly, while $+5\%$ perturbations in $C_{tot}(t^*)$ and $\langle x \rangle(t^*)$ increase $M_2(t)$. After 30 seconds, these changes have not caused $M_2(t)$ to deviate more than 4.5% from the "Base Case ICs" value. Such disparities are not expected to significantly influence the early stages of thin film formation.

The final mathematical sensitivity issue to be addressed concerns how well a continuum-size distribution function replaces a discrete-size distribution function for $x \geq X_c$. Using the reference simulation conditions of Section 5.1, Figure 5.10 plots the cluster size distributions that are obtained by solving the Discrete System of kinetic clustering equations outlined in Section 4.2.1, as well as the Hybrid System of kinetic clustering equations described in Section 4.2.2. The Discrete System distribution is determined with $X_{max} = 100$, thus solving $(X_{max}+2) = 102$ equations for its solution. The Hybrid System distribution, using $X_c = 5$ and
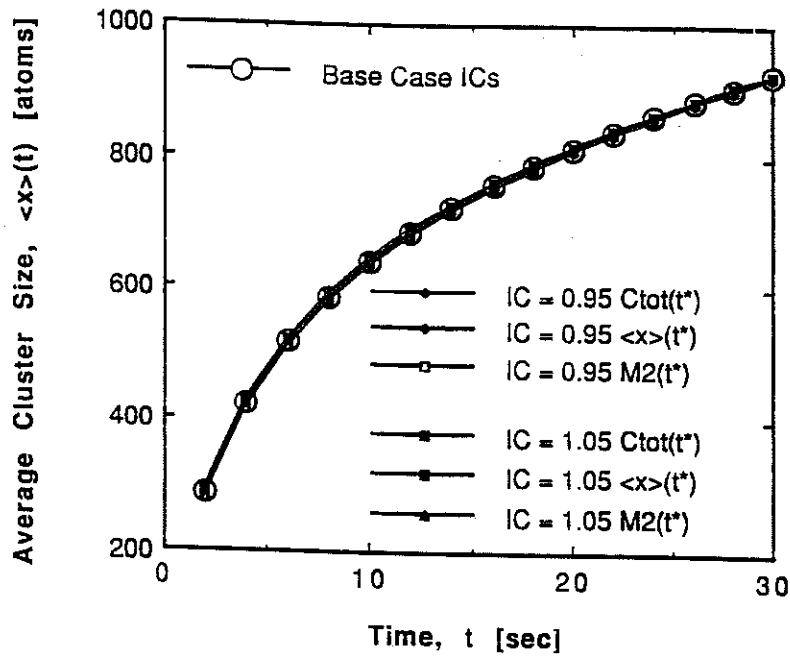
65

Figure 5.8. Effects of changes in the Hybrid System initial conditions on the average cluster size.

$N = 4$, only solves $(X_c + N + 2) = 11$ equations. The most obvious problem with Figure 5.10 is that the Hybrid System exhibits a poor discrete-to-continuum coupling at the transition cluster size, X_c. This is undoubtedly due to the nature of the Chebyshev-Hermite polynomials used to reconstruct the continuum portion of the Hybrid System distribution; as discussed in Section 4.4, the natural range of the Chebyshev-Hermite polynomials is the entire real axis, x, while the cluster nucleation and growth process is defined only for x positive. In Figure 5.10 (a), which corresponds to a fractional substrate surface coverage of $Z(t) \simeq 2.0 \times 10^{-5}$, the computations reveal that both the Discrete and Hybrid distributions possess the same total cluster density and average cluster size; however, the Discrete System distribution has a variance of $M_2(t) = 6.8$, compared to $M_2(t) = 4.4$ for the Hybrid System. As the deposition proceeds to $t = 7.5 \times 10^{-2}$ seconds [corresponding to $Z(t) \simeq 3.4 \times 10^{-4}$] in Figure 5.10 (b), both the Discrete and Hybrid
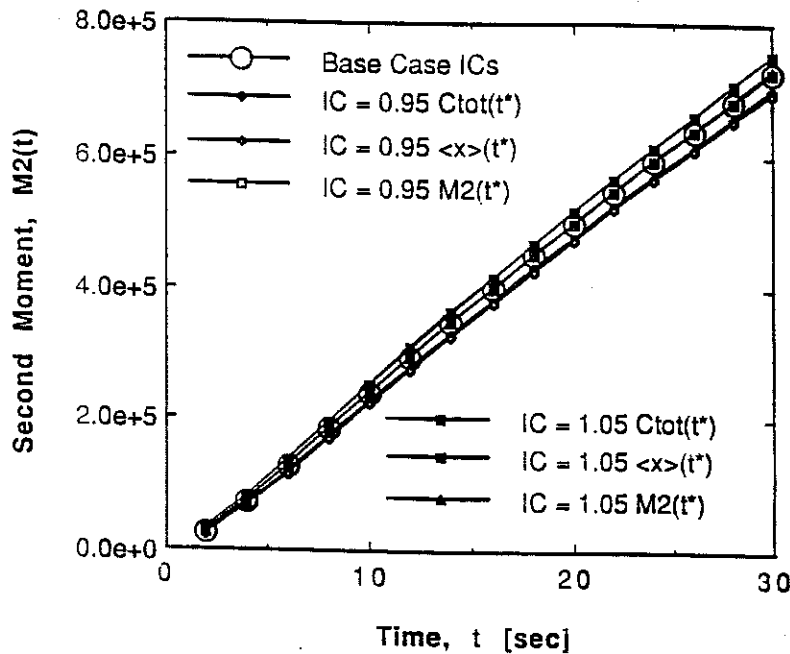
66

Figure 5.9. Effects of changes in the Hybrid System initial conditions on the second moment (i. e., variance) of the cluster size distribution.

distributions have the same total cluster density, average size, and second moment. As discussed in Section 4.4, the Hybrid System reconstructs the continuum distribution with a technique that becomes increasingly accurate for x and $\langle x \rangle (t)$ both large. This is shown quite well in Figure 5.10 (b) for $x > 25$.

In summary, the mathematical parameters X_c, N, and r must self-consistently be determined at any particular time if one wishes to compare this model with experimental measurements. A four-moment reconstruction should be adequate for initial studies, allowing one to model dispersion, skewness, and kurtosis in the distribution, features which can be readily compared with experimental observations. Nonetheless, a new reconstruction *technique* should be investigated, since the current scheme employing Chebyshev-Hermite polynomials has problems coupling the discrete distribution to the continuum at $x = X_c$. The Hybrid System model is not sensitive to small fluctuations in the initial conditions, and agrees
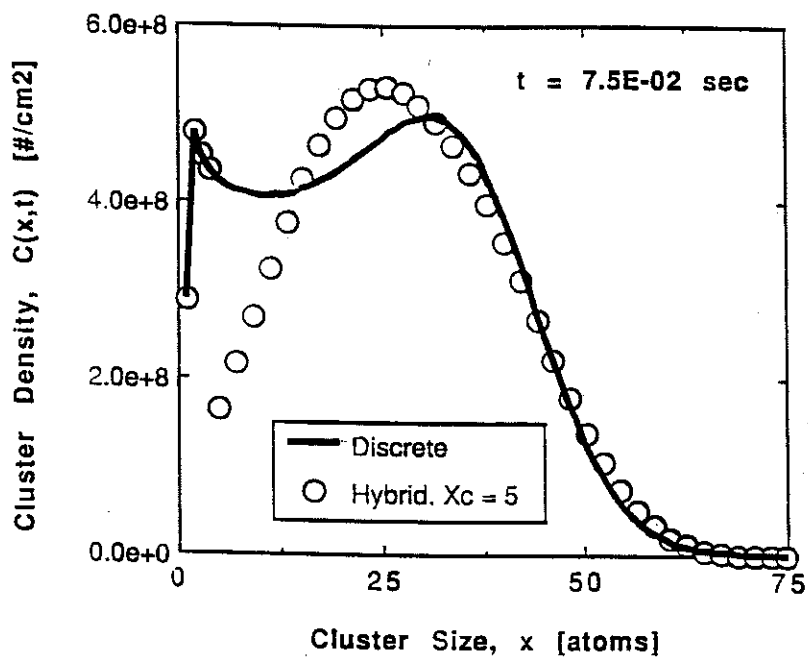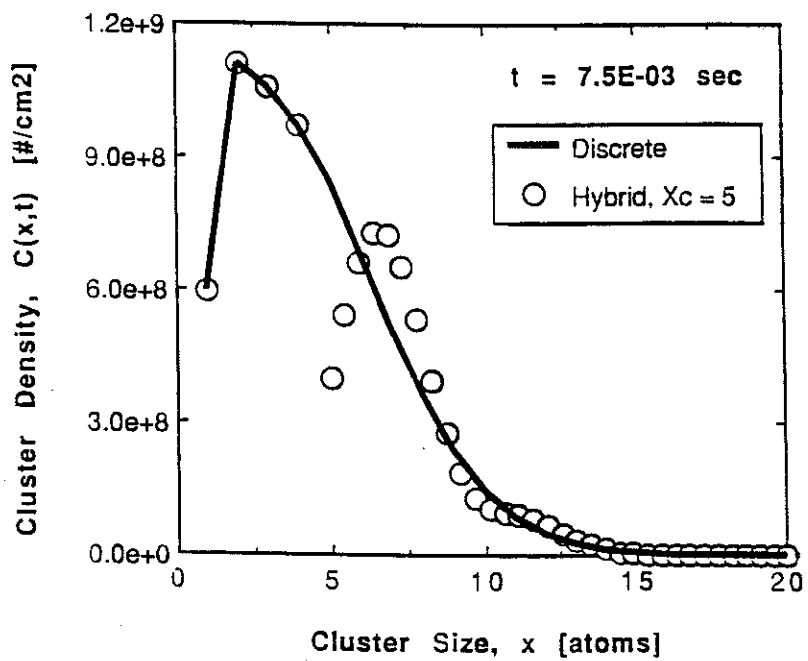
Figure 5.10. Comparison of the Discrete System and Hybrid System cluster size distributions at times (a) $t = 7.5 \times 10^{-3}$ sec, and (b) $t = 7.5 \times 10^{-2}$ sec. The Discrete System solves 102 equations, while the Hybrid System only solves 11.

very well with the Discrete System for large cluster sizes (e. g., $x > \langle x \rangle (t)$). This agreement improves as the deposition proceeds in time.

5.3 Physical Sensitivity Analysis

Atomistic kinetic rate theory models of cluster nucleation and growth are known to be sensitive to activation energies [10,13]. In this study, the sensitivity of the computational results to physical material parameters is studied via $\pm 10\%$ variations in the following activation energies:

- E_d, the activation energy for mobile single-atom diffusion across the substrate
- E_d^T, the activation energy for surface defect (i. e., single trap) diffusion on the substrate
- E_a, the activation energy for mobile single-atom desorption off the substrate
- E_T, the activation energy for releasing bound single atoms from trap sites

Before discussing these results, a description of the graphical notation used in Figures 5.11 − 5.14 is needed.

The abscissa is used to specify the value of an activation energy, E_i (where E_i denotes either E_d, E_d^T, E_a, or E_T). This parameter is expressed as a fraction of the reference condition value, $E_{i\,Base}$. Section 5.1 designates $E_{d\,Base} = 0.16$ eV, $E_{d\,Base}^T = 0.50$ eV, $E_{a\,Base} = 0.48$ eV, and $E_{T\,Base} = 0.96$ eV. An "Activation Energy Ratio, $E_i / E_{i\,Base}$" of 1.05 thus indicates that $E_d = 0.168$ eV, $E_d^T = 0.525$ eV, $E_a = 0.504$ eV, or $E_T = 1.008$ eV. The ordinate is used to specify the ratio of a particular kinetic variable to its reference condition value.

As an example, refer to Figure 5.11 (a) where the total cluster density ratio, $C_{tot}(t) / C_{tot}(t)_{Base}$, is plotted as a function of the four activation energy ratios.

Now set $E_d^T = E_{d\,Base}^T$, $E_a = E_{a\,Base}$, and $E_T = E_{T\,Base}$. When $E_d = E_{d\,Base}$, the reference conditions are obtained and the total cluster density, $C_{tot}(t)$, equals $C_{tot}(t)_{Base}$. Consequently, $C_{tot}(t)/C_{tot}(t)_{Base} = 1.0$, and a solid square symbol appears at the point (1.00, 1.0). If the energies E_d^T, E_a, and E_T remain constant, but the diffusion energy E_d is increased to $E_d = 1.05\,E_{d\,Base}$, then the total cluster density increases to $1.09\,C_{tot}(t)_{Base}$ and a solid square appears at the point (1.05, 1.09). One can thus deduce that a 5% increase in the mobile single atom diffusion energy, E_d, produces a 9% increase in the total cluster density when all other parameters remain unchanged from the reference simulation conditions. The remaining solid square symbols are obtained by holding the other activation energies at $E_i = E_{i\,Base}$ and varying only E_d. A similar procedure is done for each individual energy.

With all this notation in mind, Figure 5.11 demonstrates the influence of E_d, E_d^T, E_a, and E_T on the total cluster density, $C_{tot}(t)$. Increases in E_d and E_a both promote larger values of $C_{tot}(t)$. Increasing E_d reduces the rate at which mobile single atoms aggregate with other species on the substrate, producing a large population of small-sized clusters. Increasing E_a lengthens the time that a mobile single atom stays on the substrate before evaporating; this effectively increases the mobile single-atom population, leading to larger values of $C_{tot}(t)$.

In Figure 5.11 (b), the cluster density also increases with E_d^T, indicative of enhanced nucleation on surface defect sites. Figure 5.11 (a) does not exhibit this feature because the surface defect density has not yet reached a high enough level to significantly influence the clustering kinetics. E_T does not alter the total cluster density in either Figure.

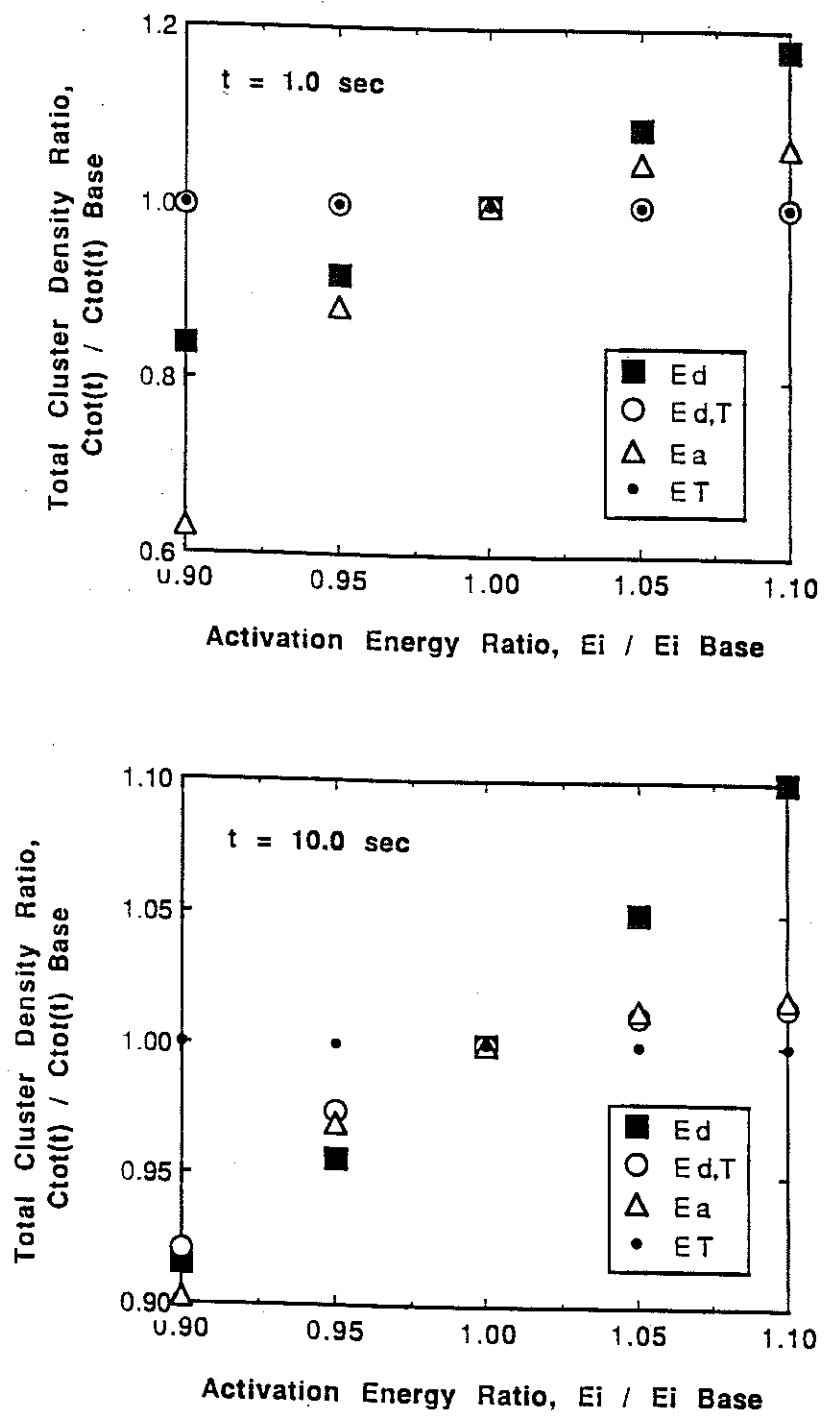Figure 5.12 shows the nucleation rate dependency on activation energies. At

Figure 5.11. Influence of the activation energies E_d, E_d^T, E_a, and E_T on the total cluster density at times (a) $t = 1.0$ sec, and (b) $t = 10.0$ sec.
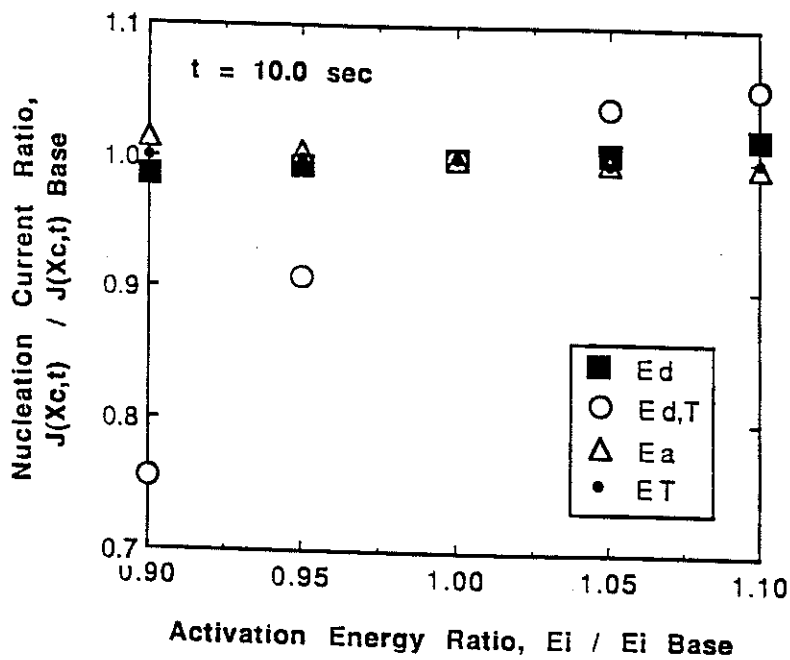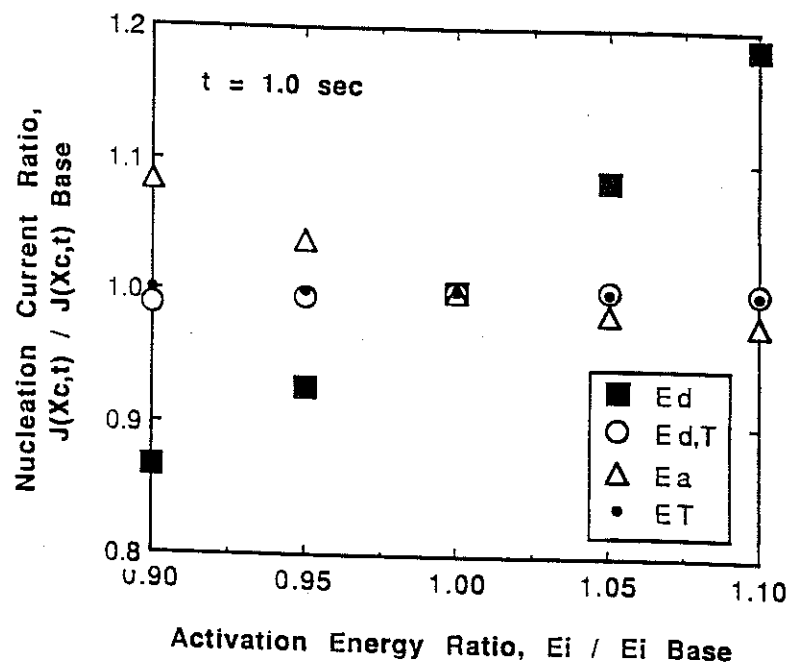
Figure 5.12. Influence of the activation energies E_d, E_d^T, E_a, and E_T on the cluster nucleation rate at times (a) $t = 1.0$ sec, and (b) $t = 10.0$ sec.

72

$t = 1.0$ sec, the E_d^T and E_T values indicate that surface defects have not yet influenced the nucleation current. Increasing E_d slows down single-atom diffusion, decreasing aggregation rates, and providing for a larger mobile single-atom population. This larger single-atom density provides a source of nucleation centers on the substrate, thus increasing the nucleation rate. The trend predicted by the E_a variation will increase the mobile single-atom population, which should provide a source term to increase the nucleation current.

Figure 5.12 (b) demonstrates that after 10.0 sec of deposition, the nucleation current is essentially unaffected by changes in E_d, E_a, or E_T. The surface defect density has now risen to a significant level so that preferred nucleation occurs on trap sites, increasing the nucleation rate. This is indicated by the enhancement of $\mathcal{J}(Xc, t)$ with E_d^T in the Figure.

Since increases in the surface diffusion energy, E_d, decrease cluster aggregation rates, one would expect smaller-sized clusters to be favored. This feature is clearly demonstrated in Figure 5.13. Increasing E_a increases the mobile single-atom density, boosting the overall aggregation rate, and promoting a distribution of larger-sized clusters. At $t = 10.0$ sec, the single-trap population is large enough so that surface defect influences are noticeable. Figure 5.13 (b) shows that increasing E_d^T enhances the trapping ability of defect sites, reducing the average cluster size as expected. E_T again has no impact on the nucleation kinetics.

Enhancing the aggregation rate by decreasing E_d results in higher values of $M_2(t)$, as exemplified in Figure 5.14. As one decreases E_a, increasing the evaporation rate of single atoms, the single-atom population decreases, providing for a less disperse distribution. Surface defect energies do not appear to impact the second moment of the distribution.
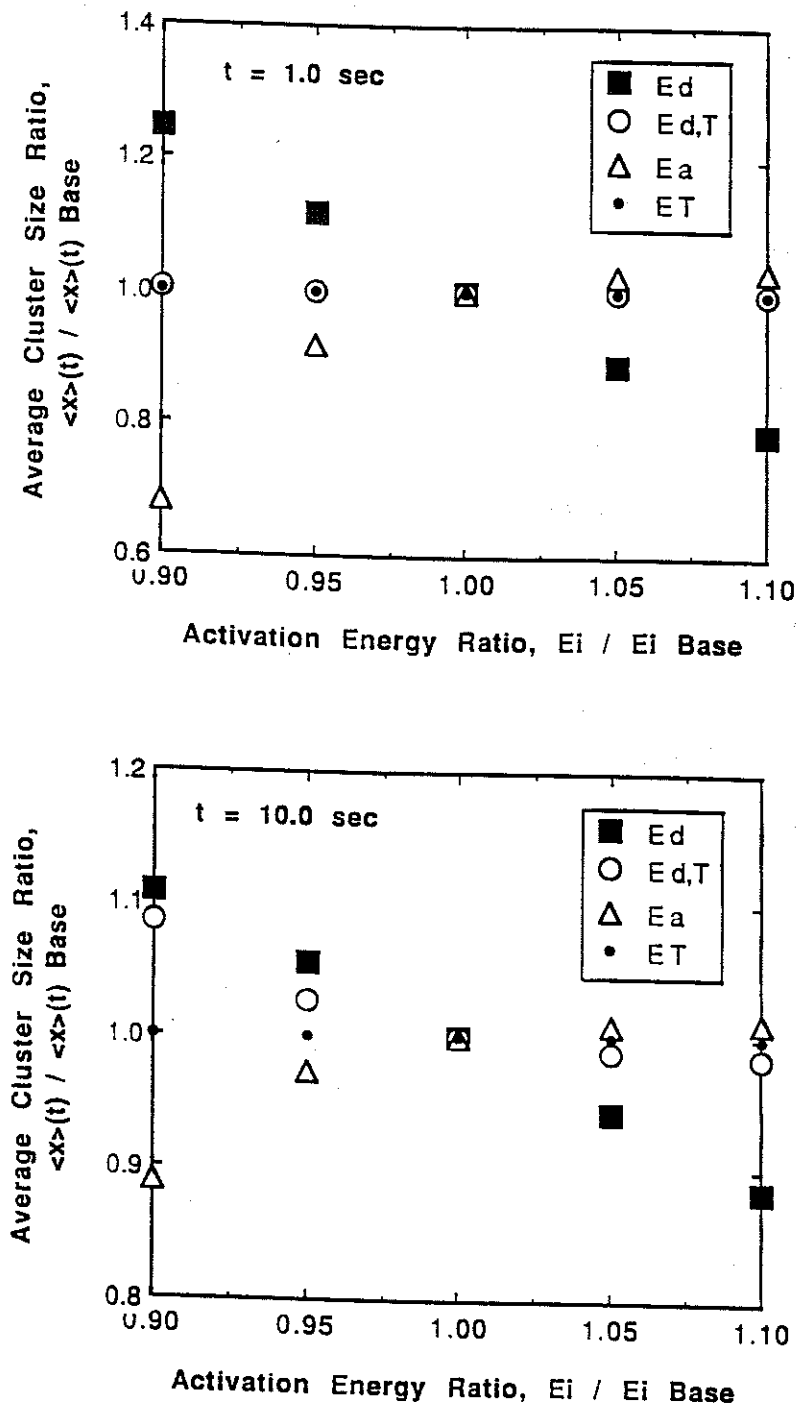
Figure 5.13. Influence of the activation energies E_d, E_d^T, E_a, and E_T on the average cluster size at times (a) $t = 1.0$ sec, and (b) $t = 10.0$ sec.
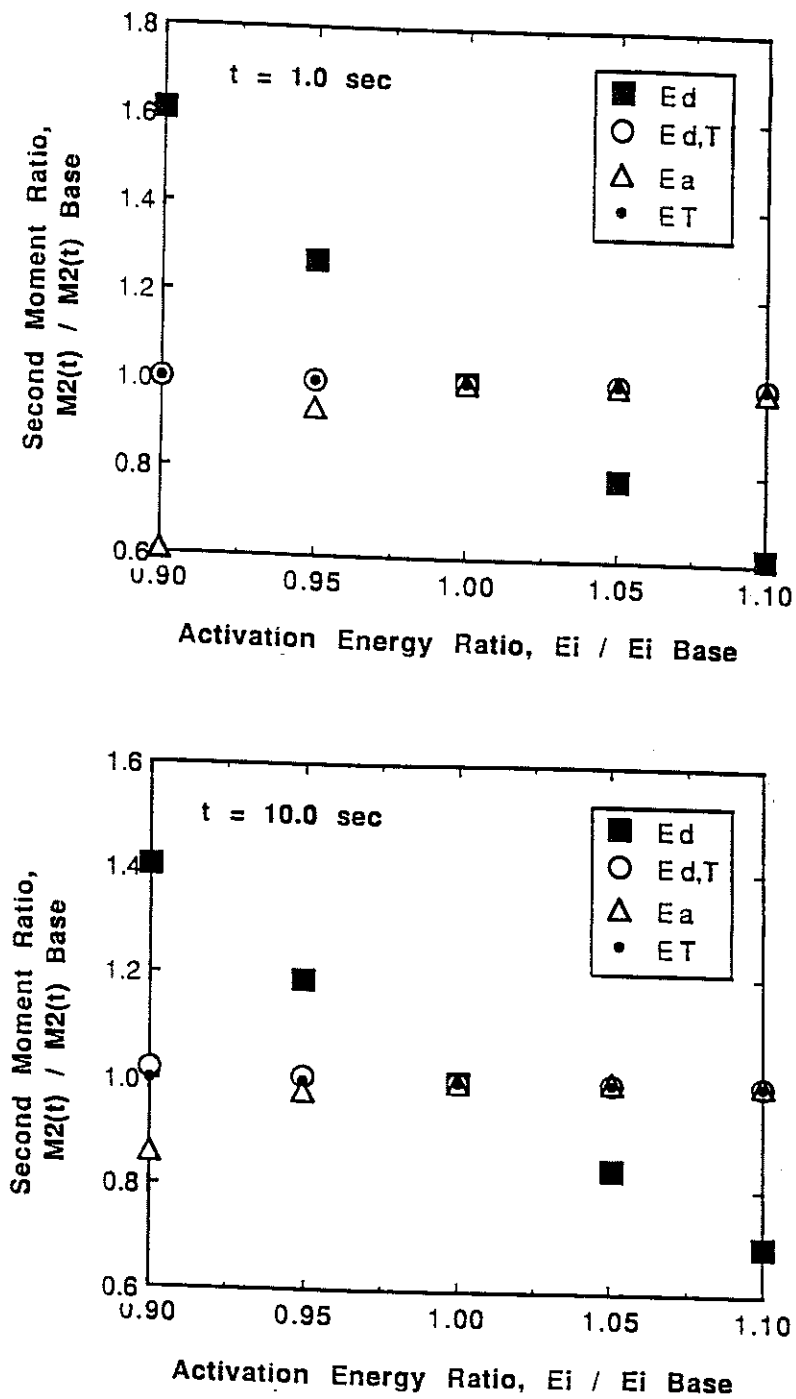
Figure 5.14. Influence of the activation energies E_d, E_d^T, E_a, and E_T on the second moment (i. e., variance) of the cluster size distribution at times (a) $t = 1.0$ sec, and (b) $t = 10.0$ sec.

In summary, the activation energies for mobile single-atom diffusion (E_d) and desorption (E_a) influence the single-atom population and cluster aggregation rates, which in turn impact the nucleation kinetics. Increasing E_d decreases the cluster aggregation frequency, $\nu_{m,i}(t)$, whereas decreasing E_a decreases the mobile single-atom density, $C_{mob}(1,t)$. Both of these features reduce the overall cluster aggregation rate, which promotes a faster nucleation rate, a smaller average cluster size, and a less disperse distribution. Since the total cluster density is proportional to the single-atom population, increases in both E_d and E_a promote larger cluster densities.

If a significant number of defects exist on the substrate, then preferred nucleation influences the clustering kinetics. Increasing E_d^T reduces the overall rate at which surface traps interact with other species on the substrate, accelerating particle-cluster kinetics. This promotes a larger cluster density, enhanced nucleation, and a smaller average cluster size. The nucleation kinetics are more sensitive to surface defect diffusion than to defect trapping phenomena, as demonstrated in these results.

Chapter 6

Thermal Particle Deposition Studies

Thermal particle deposition processes are quite a bit easier to characterize than energetic particle depositions since surface defect production, cluster dissociation, sputtering mechanisms, particle reflection, and atomic mixing effects are absent. As a result, the comprehensive kinetic clustering model presented in Chapter 4 can be simplified when studying thermal deposition phenomena. In some cases, analytical solutions can be obtained; Section 6.1 discusses one in detail. Another analytical solution for thermal particle deposition is used in Section 6.2 to demonstrate that a numerical reconstruction of the cluster size distribution depends on both the reconstruction technique and the number of moments used to perform the reconstruction. The latter Sections of this Chapter compare model results to thermal deposition experiments and also study the role of pre-existing surface defects on the nucleation kinetics during thermal particle deposition.

6.1   A Three-Region Analytical Solution

An analytical solution of the comprehensive kinetic clustering equations outlined in Chapter 4 can be obtained for thermal deposition studies. Assuming that

thermal deposition begins on a bare, defect-free substrate at time $t = 0$, and that only the early stages are considered when direct impingement reactions are negligible, the Discrete System Equations 4.2, 4.4, and 4.5 become

$$\frac{\partial C_{mob}(1,t)}{\partial t} = q - \nu_a\,C_{mob}(1,t) - 2\,\nu_{m,m}(t)\,C_{mob}(1,t)$$

$$-\frac{1}{2}\,\nu_{m,m}(t)\sum_{x=2}^{\infty} C(x,t) \tag{6.1}$$

$$\frac{\partial C(2,t)}{\partial t} = \nu_{m,m}(t)\,C_{mob}(1,t) - \nu_{m,2}(t)\,C(2,t) \tag{6.2}$$

$$\frac{\partial C(x,t)}{\partial t} = \nu_{m,x-1}(t)\,C(x-1,t) - \nu_{m,x}(t)\,C(x,t) \quad \ldots \quad x \geq 3 \tag{6.3}$$

To derive the above equations, the growth exponent is assumed to be $r = 0$. This is certainly a reasonable simplification, since the early nucleation and growth stages are primarily determined by the change with time of the mobile single atom population, $C_{mob}(1,t)$. Making an allowance for size-dependent growth (i.e., $r \neq 0$) results only in a quantitative change in the results.

Equation 6.1 reads as follows: The change with time of the density of mobile single atoms is equal to the number q arriving, less the number $\nu_a\,C_{mob}(1,t)$ of atoms that evaporate from the substrate, due to their limited residence time. Mobile single atoms then disappear as a result of dimer formation and as a result of aggregation with other clusters on the substrate. For Equation 6.2, the change with time of the concentration of dimers is equal to the difference between the rate of dimer formation and the rate at which they are converted into trimers. The equations for x-atom clusters of $x \geq 3$ are analogous.

The analytical solution for this thermal deposition problem provides insight into the temporal behavior of the following two quantities:

78

- $C_{mob}(1, t)$, the mobile single atom density [$\#/cm^2$]

- $C_{agg}(t) = \sum_{x=2}^{\infty} C(x, t)$, the aggregate cluster density [$\#/cm^2$]

Since defect sites do not exist in this study, no bound single atoms are present and $C(1, t) = C_{mob}(1, t)$; i.e., all single atoms are mobile. The aggregate cluster density is the variable that can be compared with experimental results, since it is very difficult to measure single-atom densities and small-cluster populations on a surface. The fact that electron microscopy can only resolve clusters containing as few as 5 to 15 atoms has no influence, since at the normal observation periods of $t \geq 1$ sec, the proportion of unobservable clusters can be neglected [62].

The aggregate cluster density is obtained by first summing up all of the kinetic rate equations described by Equations 6.2 and 6.3:

$$\sum_{x=2}^{\infty} \frac{\partial C(x, t)}{\partial t} = \nu_{m,m}(t) \, C_{mob}(1, t) = \Gamma \, C_{mob}^2(1, t) \tag{6.4}$$

where the diffusion coefficient, Γ, is

$$\Gamma = a_o \, a(1) \, \nu_1 \, \exp\left(-\frac{E_d}{kT}\right). \tag{6.5}$$

Taking the time integral of Equation 6.4 yields

$$C_{agg}(t) = \sum_{x=2}^{\infty} C(x, t) = \Gamma \int_0^t C_{mob}^2(1, t') \, dt'. \tag{6.6}$$

Substituting Equation 6.4 into Equation 6.1, and using the definition of Γ, a new kinetic equation can be obtained for $C_{mob}(1, t)$:

$$\frac{\partial C_{mob}(1, t)}{\partial t} = q - \nu_a \, C_{mob}(1, t) - 2 \, \Gamma \, C_{mob}^2(1, t)$$

$$-\frac{1}{2} \Gamma^2 \, C_{mob}(1, t) \int_0^t C_{mob}^2(1, t') \, dt'. \tag{6.7}$$

Equation 6.7 is a non-linear, integro-differential equation for the density of mobile single atoms. This equation cannot be solved in closed form, thus numerical methods must be used for its evaluation.

79

Numerical solutions of these kinetic rate equations show that the change with time of the mobile single atom density $C_{mob}(1,t)$ can be divided into three regions. Region I encompasses the very short times when $C_{mob}(1,t)$ is so small that all of the expressions on the RHS of Equation 6.7 can be neglected with the exception of q. As a result, $C_{mob}(1,t) = qt$.

In Region II, the substrate temperature is high and the desorption frequency ν_a is so large that evaporation dominates. Consequently, $\partial C_{mob}(1,t)/\partial t = q - \nu_a C_{mob}(1,t)$ and $C_{mob}(1,t) = q\tau_a [1 - \exp(-t/\tau_a)]$ where $\tau_a = \nu_a^{-1}$. For times $t \geq 5\tau_a$, one has $C_{mob}(1,t) \simeq q\tau_a$.

Region III occurs at longer times, after numerous clusters have been formed. The density of mobile single atoms drops, since they are consumed by aggregation with larger clusters. Evaporation and dimer formation can also be neglected. Essentially, all the atoms q arriving at the substrate are consumed by addition to the aggregates. Instead of Equation 6.7, the following condition holds:

$$q = \frac{1}{2}\Gamma^2 C_{mob}(1,t) \int_0^t C_{mob}^2(1,t')\, dt'. \tag{6.8}$$

Dividing both sides of Equation 6.8 by $C_{mob}(1,t)$ and differentiating yields

$$-\frac{d\,C_{mob}(1,t)}{C_{mob}^4(1,t)} = \left(\frac{\Gamma^2}{2\,q}\right) dt. \tag{6.9}$$

Integrating Equation 6.9 gives $C_{mob}(1,t)$ in Region III as

$$C_{mob}(1,t) = \left(\frac{2\,q}{3\,\Gamma^2}\right)^{1/3} t^{-1/3}. \tag{6.10}$$

The aggregate cluster density, $C_{agg}(t)$, can be determined for each of the three regions by substituting the appropriate expression for $C_{mob}(1,t)$ into Equation 6.6 and performing the indicated integration. Table 6.1 shows the results for each region.

Table 6.1. Three-Region Analytical Solutions for Thermal Deposition

Region	Equation 6.7 Simplifies To:	$C_{mob}(1,t)$	$C_{agg}(t)$
I	$\frac{\partial C_{mob}(1,t)}{\partial t} = q$	$q\,t$	$\left(\frac{\Gamma q^2}{3}\right) t^3$
II	$\frac{\partial C_{mob}(1,t)}{\partial t} = q - \nu_a\, C_{mob}(1,t)$	$q\,\tau_a$ for $t \geq 5\,\tau_a$	$\left(\Gamma\, q^2\, \tau_a^2\right) t$
III	$q = \frac{1}{2}\,\Gamma^2\, C_{mob}(1,t) \int_0^t C_{mob}^2(1,t')\, dt'$	$\left(\frac{2q}{3\,\Gamma^2}\right)^{1/3} t^{-1/3}$	$\left(\frac{12 q^2}{\Gamma}\right)^{1/3} t^{1/3}$

Figures 6.1 and 6.2 compare numerical solutions of $C_{mob}(1,t)$ and $C_{agg}(t)$ with the analytical results in Table 6.1. The numerical curves are based on the standard reference conditions listed in Section 5.1, but for thermal deposition conditions and $r = 0$. These curves show that the approximate analytic solutions agree very well with the numerically calculated solutions, with of course the exception of the transitions between the different regions. The analytic solutions in Region II overestimate the numerical results, indicating that aggregation reactions are significant and should probably be considered in the Region II kinetic equation for $C_{mob}(1,t)$. The overall agreement, however, lends credence to the kinetic clustering model presented in Chapter 4.

6.2 Influence of the Reconstruction Technique

The Hybrid System model discussed in Chapter 4 uses a set of Chebyshev-Hermite polynomials to reconstruct the continuum-cluster size distribution, $C_{con}(x,t)$, from
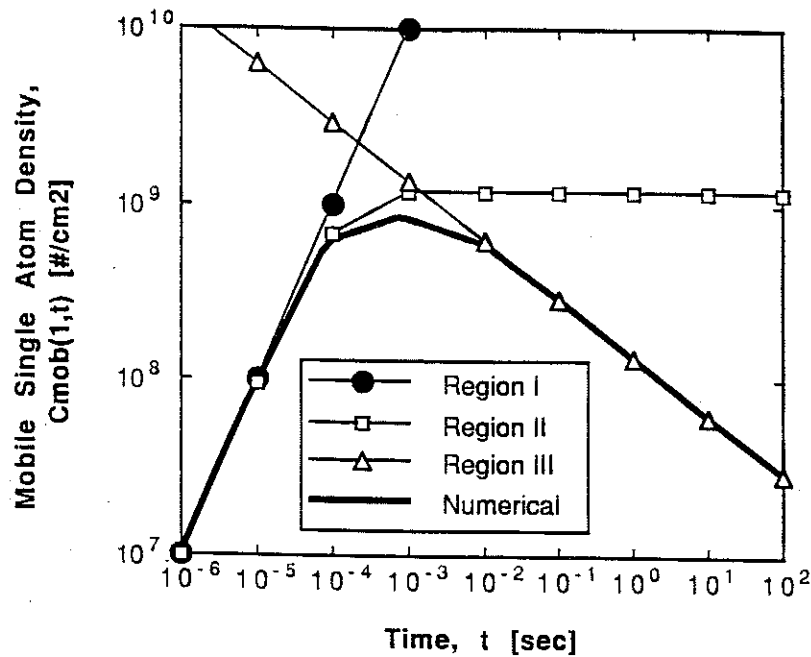
81

Figure 6.1. Comparing a numerical solution of the mobile single atom density with a three-region analytical approximation for a thermal deposition study.

the N calculated moments, $M_n(t)$. In this Section, an analytical solution of a thermal deposition problem is used to demonstrate that the reconstruction *technique* as well as the number of moments used to perform the reconstruction are both crucial to obtaining realistic size distributions.

The general problem of reconstructing a distribution function from its moments is well established in various areas of physics (e. g., ion implantation studies [140]). It is clear, however, that the information obtained from a *finite* set of N moments cannot be sufficient to *uniquely* determine the unknown function. The problem is therefore to find, among the class of functions all having the same prescribed N moments, the most reasonable distribution in some sense.

A number of reconstruction schemes are available which might be technically
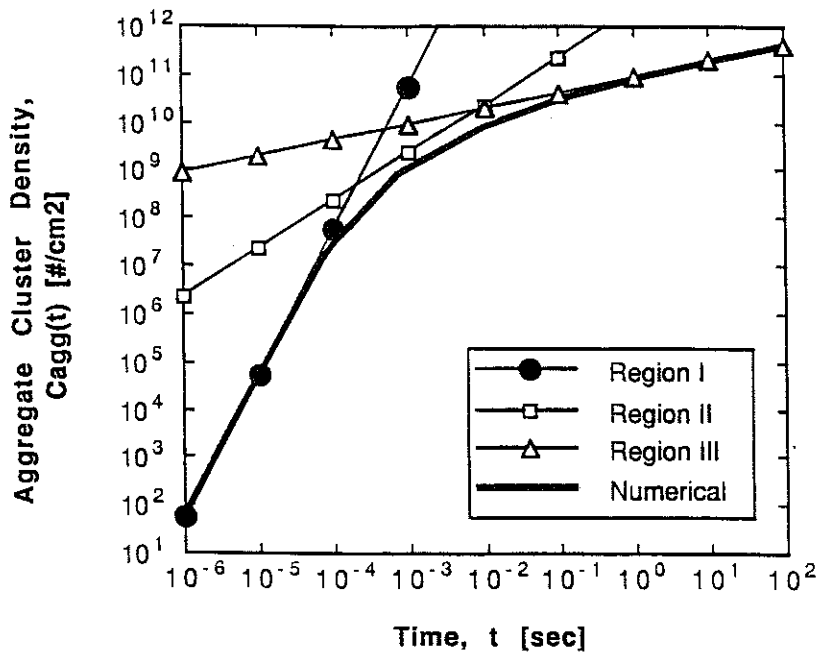
Figure 6.2. Comparing a numerical solution of the aggregate cluster density with a three-region analytical approximation for a thermal deposition study.

classified as linear or non-linear in character. In a linear reconstruction, the function is expanded in a set of orthogonal functions where the expansion coefficients are determined by the moment constraints. Making use of the orthogonality relations, the result is obtained in closed form. For functions close to a normal distribution, this method gives quite satisfactory results [140]. It completely fails, however, for highly skewed functions, as will be shown in Section 6.2.1. One severe problem inherent in all linear schemes is that the reconstructed distribution may assume negative values which are physically impossible for the true distribution.

Non-linear reconstruction techniques assume a certain form for the unknown distribution. Adjustable free parameters are used to give the correct moments. This method is especially powerful, for instance, if theoretical considerations suggest some specific functional form. Certainly the reconstructed function can be

83

forced to be non-negative. Nonetheless, since these methods are essentially non-linear, existence and uniqueness of a solution might pose a serious problem in some cases.

Zinsmeister [63] has obtained an analytical solution for the cluster size distribution in a thermal deposition study for the case of complete condensation (i.e., evaporation is negligible and all deposited particles are accomodated on the substrate). In this Section, linear and non-linear reconstruction methods are used to compare numerical distributions with Zinsmeister's true solution. These results indicate that the computed size distribution depends upon the reconstruction technique, and also provide an indication of the influence of the number of moments used during a reconstruction.

6.2.1 Linear Reconstruction Methods

The simplest possible approach to the undetermined finite moment problem is to expand the unknown distribution function in an orthogonal series and make the solution unique by truncation of the higher Fourier terms. To determine the unknown distribution function, $f(x)$, consider the set of orthogonal polynomials, $P_m(x)$, where

$$P_m(x) = \sum_{n=0}^{m} c_{mn} x^n \tag{6.11}$$

in the sense that their scalar product is

$$\int_{\mathcal{R}} P_m(x) P_n(x) w(x) dx = \delta_{m,n} \tag{6.12}$$

where the region of integration $\mathcal{R}$ may be finite or infinite, $w(x)$ is an appropriate weight function, and $\delta_{m,n} = 1$ for $m = n$ but zero otherwise. Let $f(x)$ be a function whose moments

$$\mathcal{M}_n = \int_{\mathcal{R}} x^n f(x) dx \tag{6.13}$$

84

are known. Now expand $f(x)$ in a generalized Fourier series,

$$f(x) = \sum_{m=0}^{\infty} a_m P_m(x) w(x). \tag{6.14}$$

Using the orthogonality relation of Equation 6.12, the coefficients a_m are

$$a_m = \int_{\mathcal{R}} P_m(x) f(x) dx. \tag{6.15}$$

Inserting Equation 6.11 for $P_m(x)$ into Equation 6.15 yields

$$a_m = \sum_{n=0}^{m} c_{mn} \mathcal{M}_n. \tag{6.16}$$

Substituting this result into Equation 6.14 gives the unknown distribution function, $f(x)$, in terms of the known moments, $\mathcal{M}_n$, and orthogonal polynomials, $P_m(x)$:

$$f(x) = \sum_{m=0}^{\infty} \left[\sum_{n=0}^{m} c_{mn} \mathcal{M}_n \right] P_m(x) w(x). \tag{6.17}$$

For $w(x) = e^{-x^2/2\sigma^2}$, the $P_m(x)$ are the Hermite polynomials and Equation 6.17 is identical to the Gram-Charlier series [136] with x replaced by $x - \langle x \rangle$ and $\sigma^2 = \langle x^2 \rangle - \langle x \rangle^2$. Likewise, for $w(x) = e^{-\alpha x}$, the $P_m(x)$ are the Laguerre polynomials. In this case, there is some ambiguity in choosing an appropriate parameter α.

Figure 6.3 shows a set of distribution functions in which a Gram-Charlier series reconstruction [141] is compared to the true solution for the complete condensation problem studied by Zinsmeister [63]. Numerical solutions using 2, 4, 6, 8, and 10-moment reconstructions are presented. None of these curves approximates the true distribution satisfactorily. Convergence is slow, and if the exact solution was not known, the behavior could be quite misleading. For example, by only looking at the curves for 2 and 4 moments, one might be tempted to conclude that the 4-moment reconstruction must already be close to the true solution since
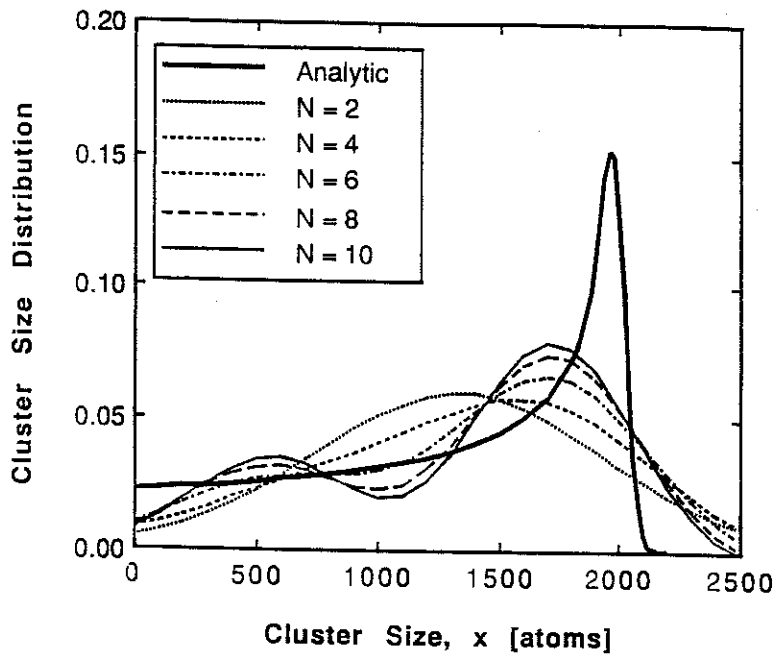
85

Figure 6.3. Analytical and numerical size distributions for a thermal atom deposition study. The numerical distributions are based on an N-moment Gram-Charlier reconstruction technique.

it deviates from the 2-moment solution by very little. Clearly, this is not so. Even worse, going to higher moments does not improve matters very much but creates rather pronounced oscillations, suggesting a bimodal distribution. These oscillations become more severe as the number of moments increases.

6.2.2 Non-Linear Reconstruction Methods

Non-linear reconstruction techniques can circumvent many of the problems associated with linear schemes (e.g., negative values, slow convergence, and violent oscillations) by assuming a certain form for the unknown function with adjustable free parameters to give the correct moments. One such method, called the Maximum Entropy Principle (MEP) [142,143] has gained much interest in recent years [144,145]. Its main drawback is that the distribution function is not explicitly given, thus one has to solve a system of non-linear simultaneous equations.

86

Among the infinite number of distribution functions $\tilde{f}(x)$ that satisfy Equation 6.13 for $n = 0, 1, \ldots, N$ moments, the MEP technique chooses the one with the highest entropy, S, where

$$S = -\int_{\mathcal{R}} \tilde{f}(x) \ln \frac{\tilde{f}(x)}{p(x)} \, dx. \tag{6.18}$$

The function $p(x)$ is an appropriate measure or prior probability [146]. This technique is recognized as a variational principle whose solution is obtained by the well-known method of Lagrange multipliers. The entropy, S, is maximized subject to the moment constraints of Equation 6.13; that is, the Lagrange multipliers λ_k have to be determined from the conditions that $\tilde{f}(x)$ has its first N moments fixed,

$$\int_{\mathcal{R}} \exp\left(-\sum_{k=0}^{N} \lambda_k \, x^k\right) x^n \, dx = \mathcal{M}_n, \qquad n = 0, 1, \ldots, N. \tag{6.19}$$

This gives the result

$$\tilde{f}(x) = p(x) \exp\left(-\sum_{k=0}^{N} \lambda_k \, x^k\right). \tag{6.20}$$

Equation 6.19 represents a set of non-linear simultaneous equations. A numerical treatment involves numerical integration and some sort of root-finding algorithm.

The MEP technique has been used to compare numerical solutions [141] of the distribution function to the true analytical solution for the complete condensation problem investigated by Zinsmeister [63]. Figure 6.4 shows these results. The curve using 2 moments is the same curve as in Figure 6.3, since in this case Equation 6.19 produces a normal distribution. Convergence to the true solution is much faster than in Figure 6.3. There are also oscillations here, but unlike in Figure 6.3, they decrease with an increasing number of moments.

Although the MEP technique gives a better reconstruction of the distribution (as compared to the Gram-Charlier series), it systematically underestimates the
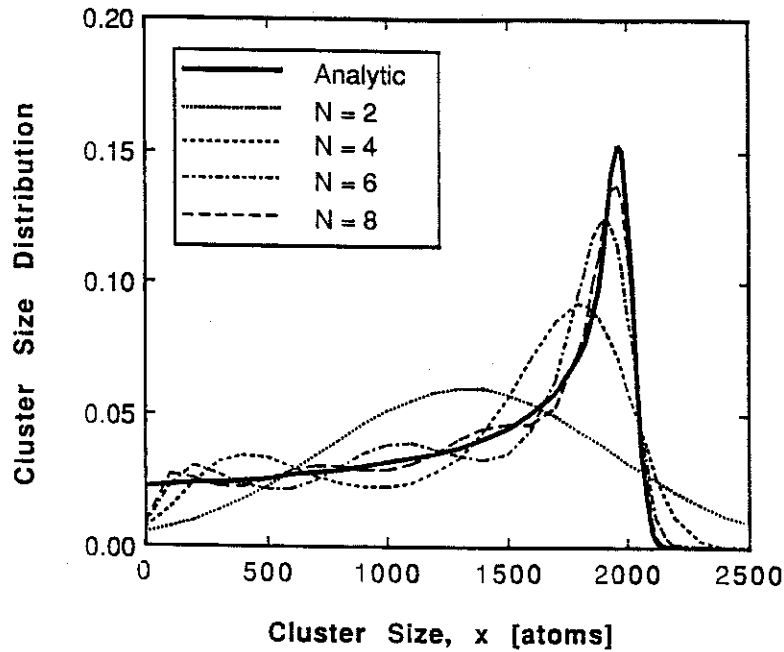
Figure 6.4. Analytical and numerical size distributions for a thermal atom deposition study. The numerical distributions are based on an N-moment Pure MEP reconstruction technique.

distribution for small clusters. To solve this problem, a constrained MEP technique is used in which the Nth moment constraint in Equation 6.19 is replaced by the boundary constraint

$$\tilde{f}(x_s) \;=\; p(x_s)\,\exp\left(-\sum_{k=0}^{N}\lambda_k\,x_s^k\right) \tag{6.21}$$

where x_s is the smallest cluster size and $\tilde{f}(x_s)$ is its prescribed value. The resulting function $\tilde{f}(x)$ will *not* be the one with maximum entropy, but will give a better approximation for small clusters.

Figure 6.5 shows results for a constrained MEP reconstruction with $x_s = 1$ [141] with Zinsmeister's [63] true analytical solution. Compared to the curves in Figure 6.4, this constrained approximation is better for small clusters where there are fewer oscillations in the reconstruction. The reproduction of the sharp peak at large cluster sizes is no worse than for the pure MEP reconstruction.
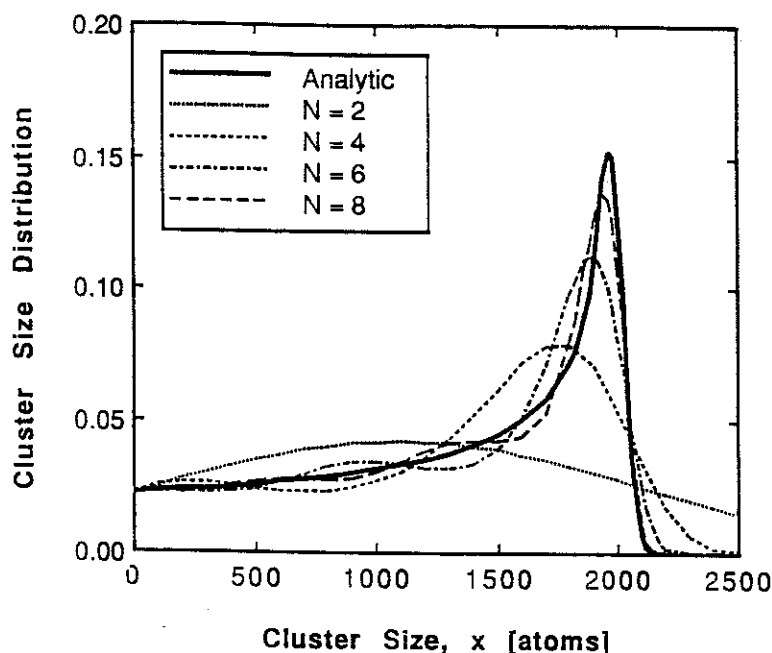
Figure 6.5. Analytical and numerical size distributions for a thermal atom deposition study. The numerical distributions are based on an N-moment Constrained MEP reconstruction technique.

6.2.3 Comparison of Linear and Non-Linear Reconstructions

In order to compare the relative merits of the Gram-Charlier, pure MEP, and constrained MEP reconstruction techniques, Figure 6.6 illustrates a quantitative measure of convergence according to the L_2-norm, where the relative error is

$$\text{Relative Error} = \left\{ \frac{\int_{\mathcal{R}} \left[f(x) - \tilde{f}(x) \right]^2 \, dx}{\int_{\mathcal{R}} f^2(x) \, dx} \right\}^{1/2} \tag{6.22}$$

where $f(x)$ denotes the exact distribution and $\tilde{f}(x)$ its approximation. As the number of moments used increases, the Gram-Charlier series converges very weakly to the true solution, whereas the pure and constrained MEP schemes converge relatively quickly. Notice that the global error according to Equation 6.22 is less for
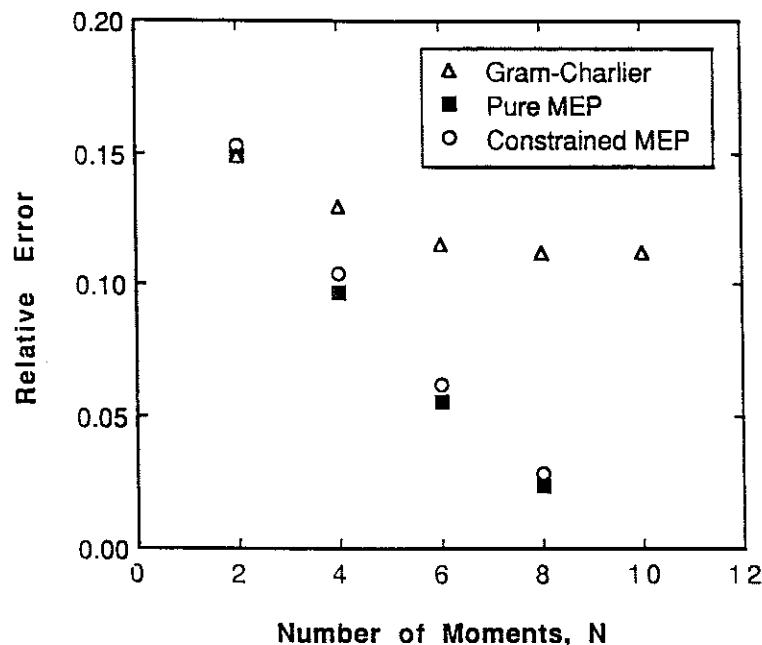
Figure 6.6. Convergence of various reconstruction techniques based on the L_2-norm.

the pure MEP method than for the constained MEP technique, although the latter displays much better behavior for small clusters. These results demonstrate that accurate reproduction of the cluster size distribution depends on both the reconstruction technique employed and the number of moments used.

6.3 Comparing the Model to Thermal Deposition Experiments

The purpose of this dissertation is to develop a comprehensive theoretical model to investigate the initial stages of thin film nucleation and growth under low-energy particle bombardment. Consequently, one may wonder how well the model "agrees" with experimental results in order to assess its reliability. There are several problems with such a comparison. First of all, tractable theories are usually

developed which only model a finite set of observable or well-known physical phenomena. These features are often measured during experiments. Nonetheless, extraneous factors, ones which the experimentalist is not aware of and the theoretician fails to consider, can subtly influence such measurements. Additionally, past theoretical studies have faltered primarily because of a scarcity of comprehensive experimental data which would have served to better guide theoretical efforts as well as to confirm or deny specific theoretical descriptions. Experimental work has also suffered from misguided theories.

Theory and experiment both have a number of variables which can be controlled during an investigation. In the realm of thin film formation, it is relatively easy to obtain agreement between data of the kind collected in nucleation and growth kinetic studies and a range of possible models. The difficult part is identifying the *physical processes* responsible for the observed behavior. Therefore, the first task in confirming the validity of a theoretical model is to establish confidence in attributing physical significance to the processes under study. In so doing, a theory should be consistent with itself, even if it does not necessarily agree with experiment [147].

This Section begins with a general investigation of how the deposition rate and substrate temperature influence a thermal deposition experiment. Using the reference conditions of Section 5.1, deposition rates of $q = 10^{13}$, 10^{14}, and 10^{15} particles/cm^2/sec are studied, as well as substrate temperatures of $kT = 100, 200,$ and 300 K. Figures 6.7 – 6.10 illustrate the effects of higher particle flux.

As the deposition rate is increased, more particles are available which drive the nucleation kinetics forward. The total cluster density and nucleation rate both increase simply because more particles and nucleation centers exist on the substrate. The average size subsequently increases, followed by a wider range of
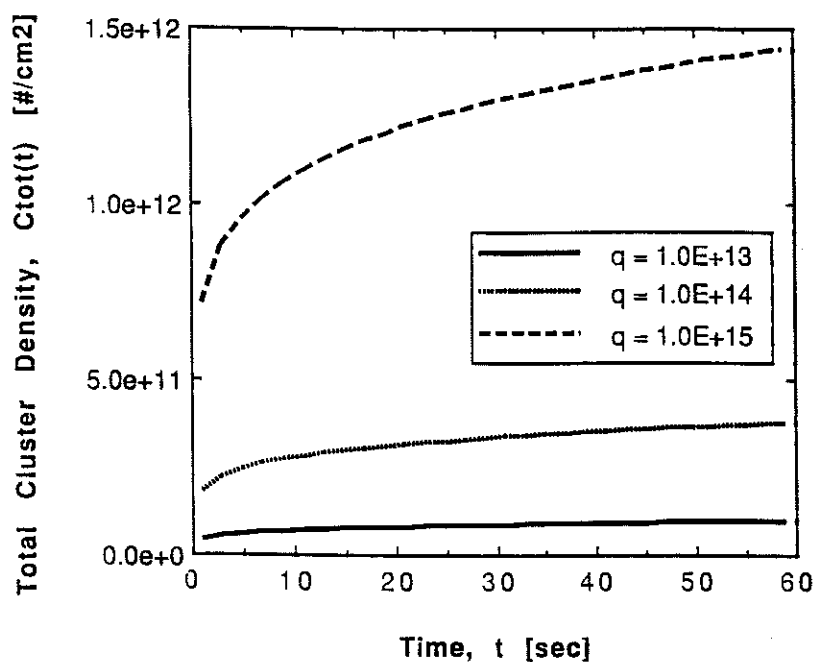
Figure 6.7. Influence of deposition rate, q [#/cm^2/sec], on the total cluster density for a thermal deposition study.

cluster sizes (i. e., more dispersion) in the deposit.

Temperature effects manifest themselves through the thermally activated processes of diffusion and desorption. At higher substrate temperatures, enhanced diffusion increases the rate at which mobile single atoms aggregate with other species on the substrate, producing a small population of large-sized clusters. Higher temperatures also increase the evaporation rate of mobile single atoms, reducing the $C_{mob}(1,t)$ population, leading to smaller values of $C_{tot}(t)$. This is shown in Figure 6.11. At lower temperatures, the higher single-atom densities increase the number of nucleation centers on the substrate, increasing the nucleation rate as shown in Figure 6.12. Figures 6.13 and 6.14 demonstrate that increased aggregation and single-atom desorption losses at higher temperatures naturally produce a wider distribution of larger clusters.

The above dependence of the nucleation kinetics on the deposition rate and
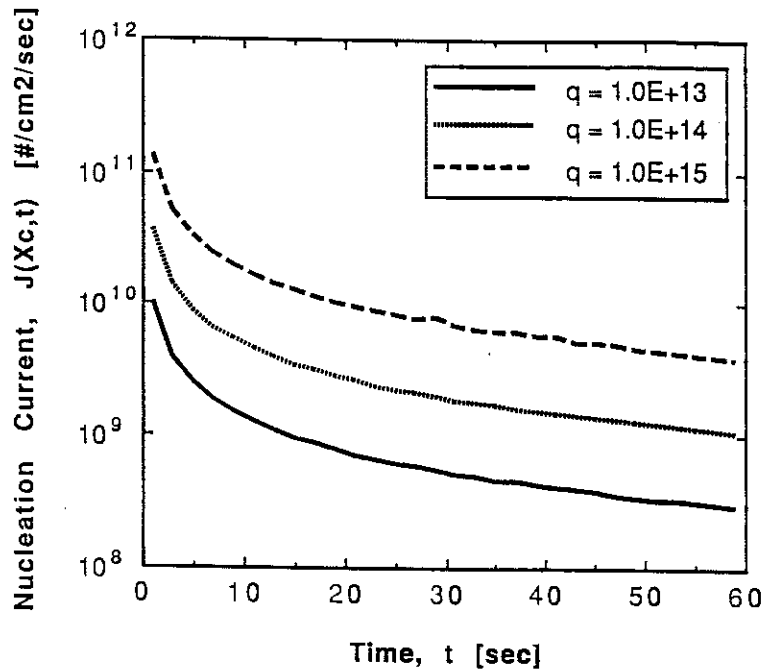
92

Figure 6.8. Influence of deposition rate, q [$\#/cm^2/sec$], on the cluster nucleation rate for a thermal deposition study.

substrate temperature have been well documented in the literature for a variety of deposit/substrate systems [10,13]. In particular, one of the most extensively studied systems is that of gold films vapor deposited onto sodium chloride single crystals. Presumably the reason for this is that gold represents a relatively inert, high atomic number deposit that is easily vaporized and readily accomodated on atomically flat regions of NaCl. In addition, the NaCl substrate is readily dissolved away in water to leave the deposited gold, usually supported in an overlayer of carbon, to be examined by transmission electron microscopy where it exhibits excellent resolution.

Since a wealth of experimental data characterizes the Au/NaCl system, it would appear to be a logical candidate to compare with theory. However, to judiciously apply the model presented in Chapter 4 to any nucleation system, one must realize that the model only considers single atoms to be mobile; larger
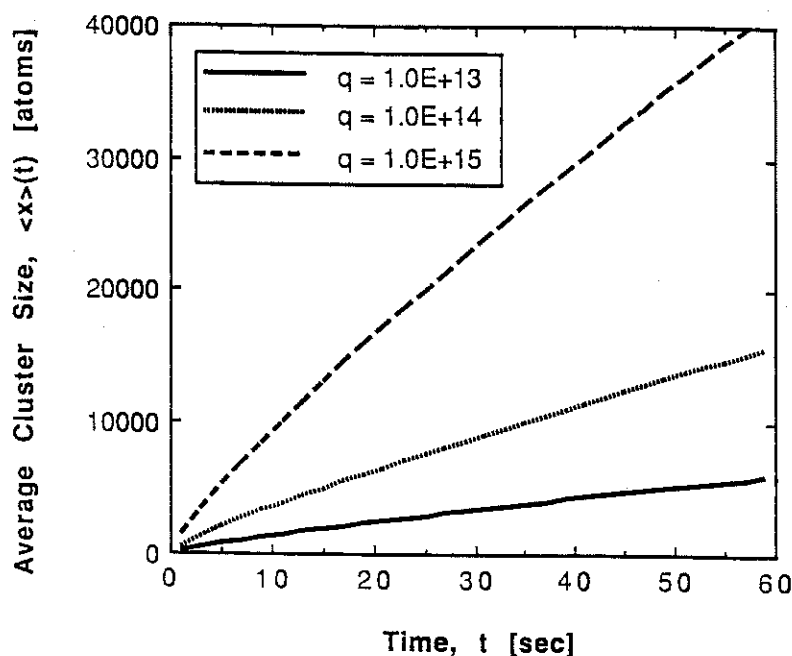
Figure 6.9. Influence of deposition rate, q $[\#/cm^2/sec]$, on the average cluster size for a thermal deposition study.

x-atom clusters cannot migrate on the substrate. Thus, consistent comparisons can only be made with experimental data which is known not to be influenced by cluster mobility effects. Fortunately, the Au/NaCl system is one of the few thin film systems that affords one this advantage.

A collection of experimental data indicates that Au clusters are mobile on NaCl substrates at temperatures as low as 133 K [94,148]. Taking this into account leaves only a paucity of data available to the theorist, this being in the form of cluster density measurements at 123 and 128 K during thermal deposition experiments. Using the reference conditions in Section 5.1, which are based on the Au/NaCl system, Figure 6.15 compares calculated cluster density curves at 123 and 128 K with the experimental data at these temperatures. To compare with these experiments, the numerical solution uses $E_d = 0.136$ eV, which is just outside the range of the currently accepted value of $E_d = 0.155 \pm 0.015$ eV [149].
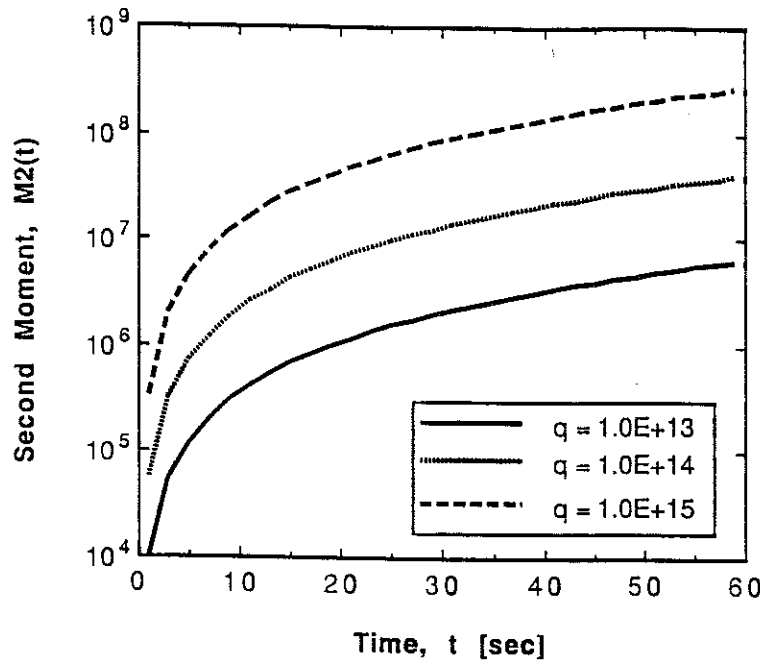
94

Figure 6.10.   Influence of deposition rate, q [$\#/cm^2/sec$], on the second moment (i.e., variance) of the cluster size distribution for a thermal deposition study.

Considering the number of unknowns involved, this agreement lends additional testament to the model.

6.4   Role of Pre-Existing Defects

Although surface defects are not generated during thermal particle deposition, a substrate may contain imperfections, debris, or other irregularities which can influence cluster nucleation and growth. In this Section, the role of pre-existing surface defects is examined (also known as "the dirty substrate problem"). Using the standard reference conditions of Section 5.1, a thermal particle deposition study is performed with the assumption that deposition begins on a *defect-covered* substrate at time $t = 0$. Initially, atomic clusters do not exist, however, surface traps are assumed to uniformly populate the substrate with a density $C_T(t = 0) =$
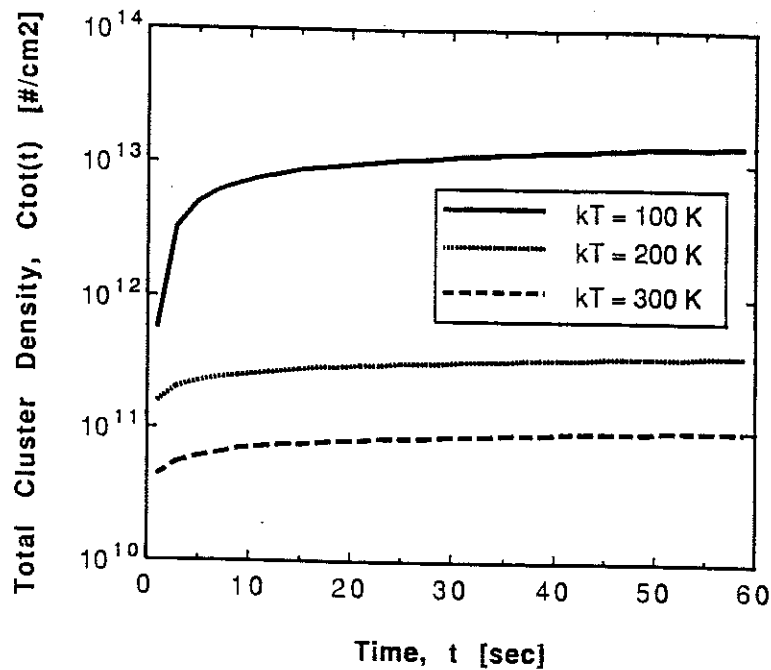
Figure 6.11.   Influence of substrate temperature, kT, on the total cluster density for a thermal deposition study.

C_T^o.

Since the substrate lattice parameter is a_o, the number of available substrate lattice sites is approximately $N_{sites} = a_o^{-2} \simeq 1.3 \times 10^{15}$ sites/cm². Three values of C_T^o are chosen in order to investigate the role of pre-existing defects: $C_T^o = 0$ describes a bare, defect-free substrate, while $C_T^o = 0.1\%\ N_{sites}$ describes a lightly-defected surface. A heavily-defected substrate is studied with $C_T^o = 1.0\%\ N_{sites}$.

Figures 6.16 – 6.19 illustrate the role of pre-existing defects on the nucleation kinetics. Defects trap a significant portion of the single atom population, converting mobile singles into bound single atoms.   Figure 6.16 shows that higher defect concentrations provide more trapping sites, significantly decreasing the mobile single atom density. Since defects increase the number of bound single atoms, preferred nucleation occurs which increases the total cluster density as demonstrated in Figure 6.17. Nonetheless, Figures 6.18 and 6.19 show that the average

96
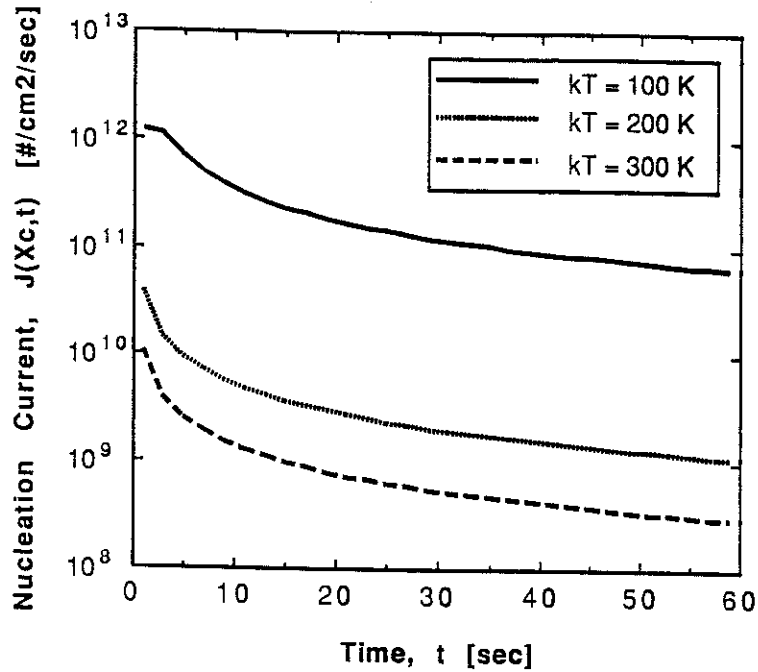
Figure 6.12. Influence of substrate temperature, kT, on the cluster nucleation rate for a thermal deposition study.

cluster size and second moment both decrease with increasing defect concentrations; this is due to the fact that the nucleation and growth kinetics are dictated by the mobile single atom population which has decreased due to trapping effects. Similar trends have been exhibited in thermal deposition experiments in which surface defects were known to exist on the substrate before deposition [150].
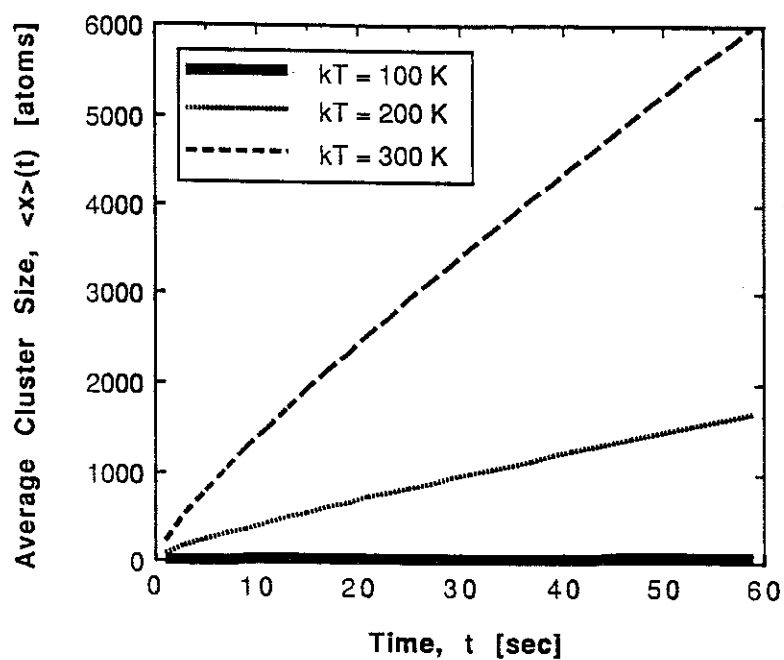
Figure 6.13. Influence of substrate temperature, kT, on the average cluster size for a thermal deposition study.
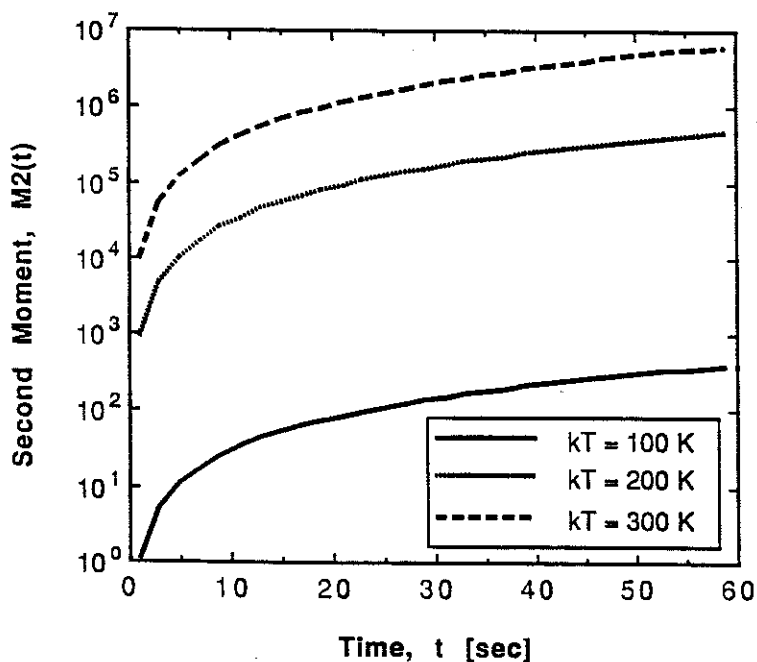
Figure 6.14. Influence of substrate temperature, kT, on the second moment (i. e., variance) of the cluster size distribution for a thermal deposition study.
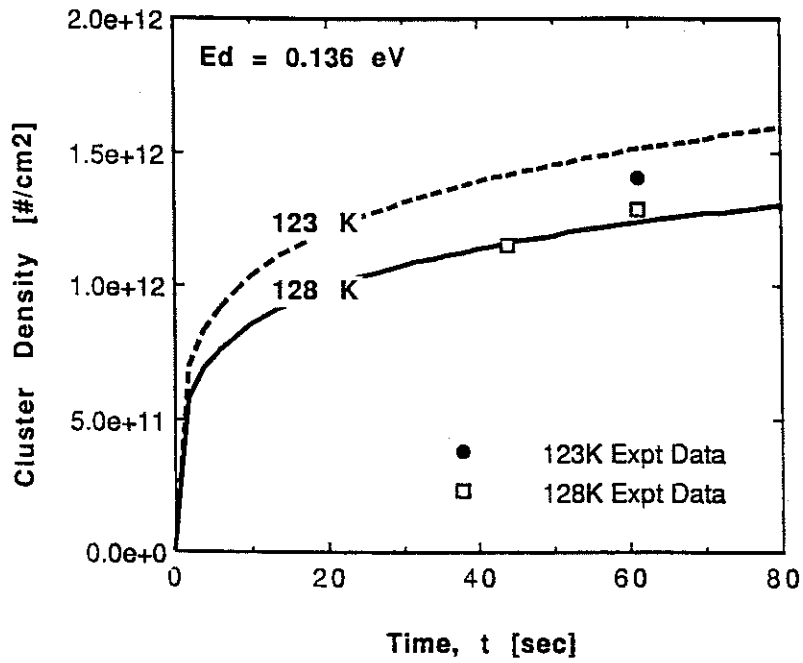
Figure 6.15. Numerically calculated cluster density curves and experimental measurements. The comparison is based on a Au/NaCl thermal deposition study in which only single atoms are mobile.

Figure 6.16. Role of pre-existing defects on the mobile single atom density for a thermal deposition study.

Figure 6.17. Role of pre-existing defects on the total cluster density for a thermal deposition study.
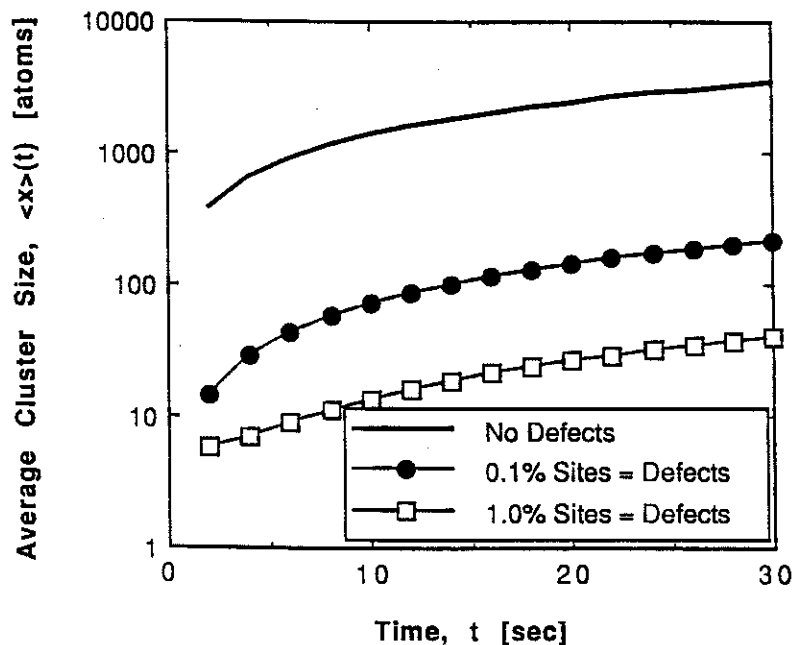
Figure 6.18. Role of pre-existing defects on the average cluster size for a thermal deposition study.
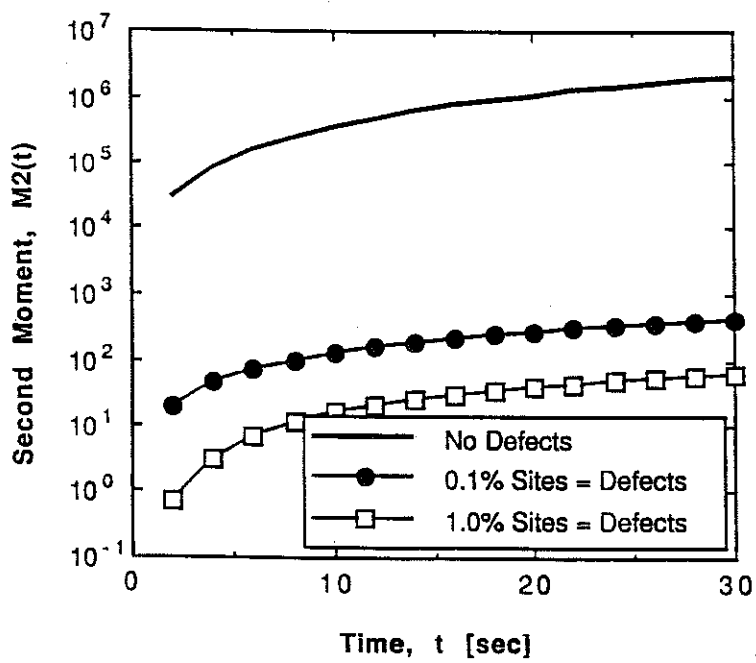
Figure 6.19. Role of pre-existing defects on the second moment (i. e., variance) of the cluster size distribution for a thermal deposition study.

Chapter 7

Energetic Particle Deposition Studies
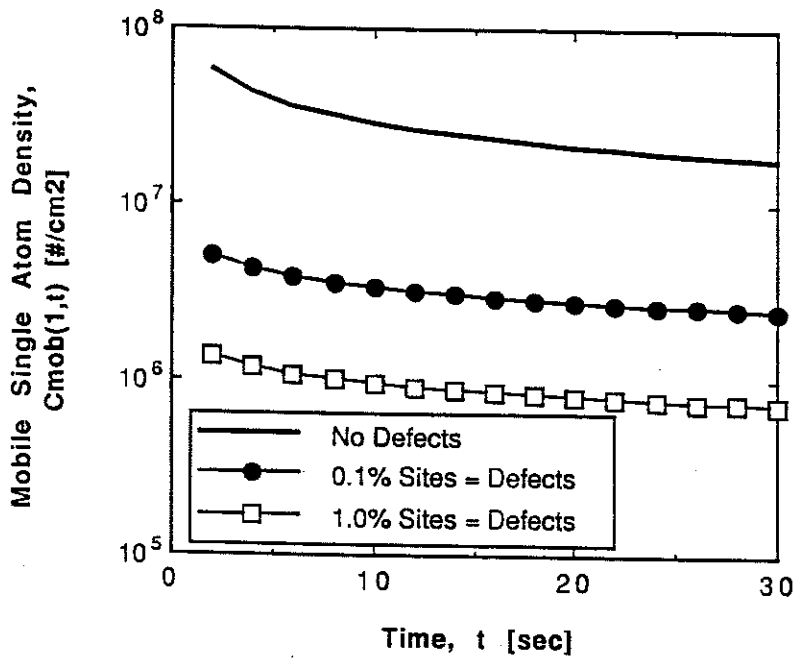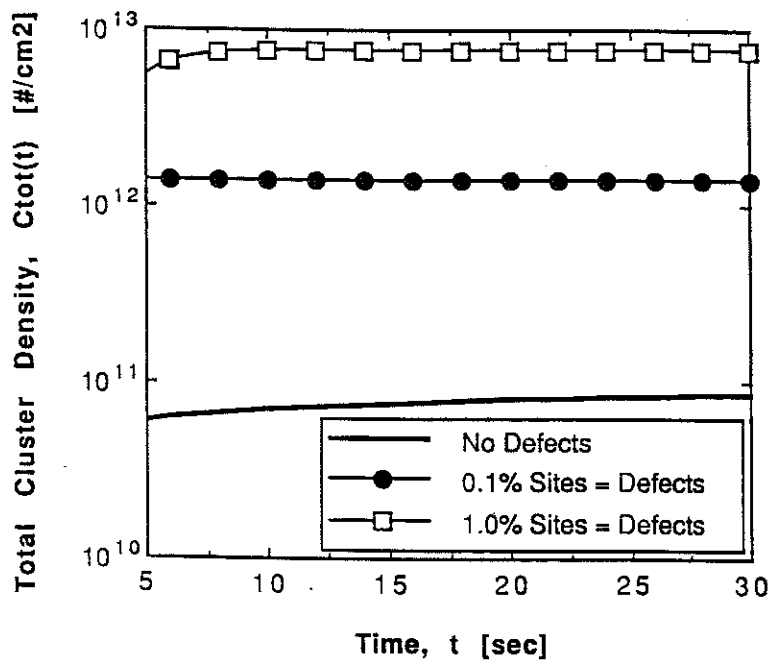
Low-energy particle-surface interactions can affect nucleation kinetics through the creation of preferred adsorption sites, cluster dissociation, and surface sputtering. This Chapter investigates the individual roles that surface defect production and cluster dissociation play during the early stages of thin film formation. Analysis of these results provides an additional understanding of the nature, rather than the detail, of the nucleation phenomena.

7.1   Influence of Surface Defect Production

The reference simulation conditions of Section 5.1 are used to study the effects of surface defect production on cluster nucleation kinetics under the assumption of no cluster dissociation, i.e., $\lambda(E) = 0$. Trap production is modeled with three values of $p(E)$ indicative of thermal $[p(E) = 0]$, low-energy $[p(E) = 10^{-4}]$, and high-energy $[p(E) = 10^{-3}]$ particle bombardment, where $p(E)$ is the average number of surface defects produced by each deposited particle. Figure 7.1 demonstrates that surface defect production enhances the nucleation rate for coverages $Z(t) > 10^{-3}$. This promotes an increase in the total cluster density, as shown in Figure 7.2. It
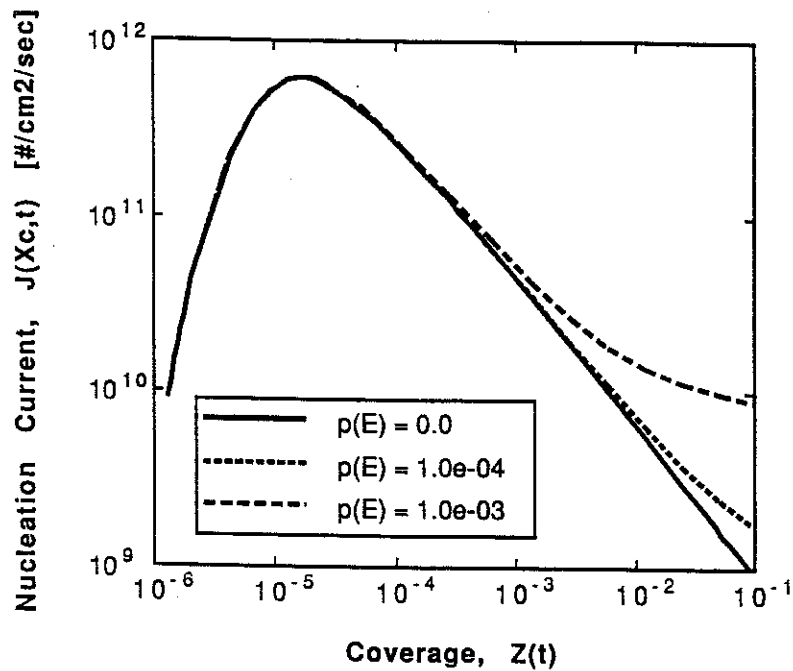
Figure 7.1. Influence of the surface defect production parameter, $p(E)$, on the cluster nucleation rate.

should be recognized that a certain incubation time is required, however, before changes in the nucleation phenomena are evident. This is clearly supported by Figure 7.3, where cluster size distributions at deposition times of $t = 0.01$ sec $[Z(t) \simeq 3 \times 10^{-5}]$ and $t = 20.0$ sec $[Z(t) \simeq 0.13]$ are displayed. In Figure 7.3 (a), one cannot distinguish any differences in the calculated size distributions. As the deposition proceeds and traps have a chance to influence the kinetics, Figure 7.3 (b) illustrates that defect production reduces both the average cluster size and the range of cluster sizes present on the substrate.

In summary, surface defect production creates preferred nucleation sites on a substrate, increasing the cluster nucleation rate, leading to larger nuclei densities and smaller cluster sizes. Films produced in this manner possess narrower size distributions, indicating that energetic particle bombardment can produce a more uniform distribution of cluster sizes during the early growth stages. It would be

103
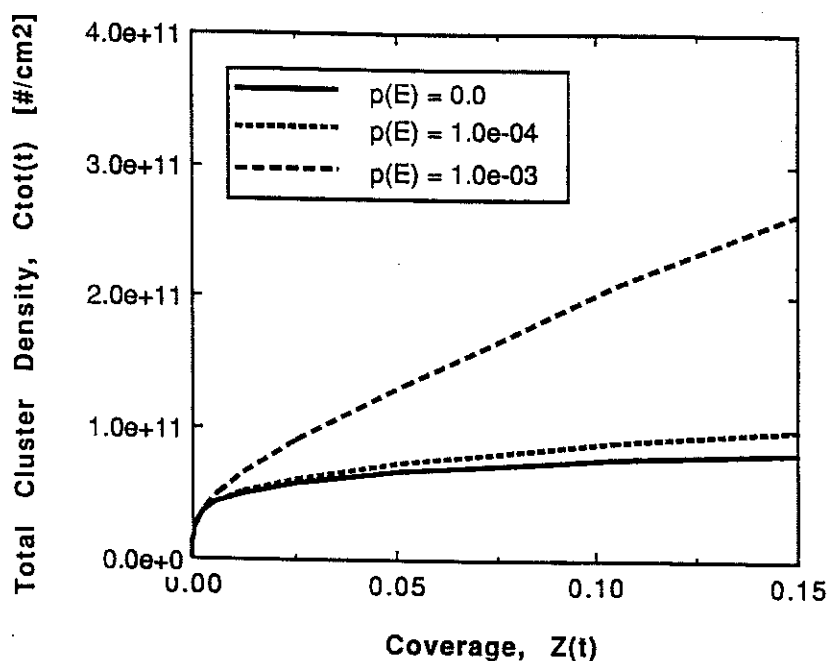
Figure 7.2. Influence of the surface defect production parameter, $p(E)$, on the total cluster density.

interesting to compare these trapping simulations to the case of accelerated ion doping during MBE experiments, where the ion flux is low, trapping is the desired effect, and sputtering of the growing film is not significant [88].

7.2 Influence of Cluster Dissociation

Cluster dissociation effects on thin film growth kinetics are studied with the reference simulation conditions of Section 5.1, but under the assumption of no surface defect production, i.e., $p(E) = 0$. Dissociation is modeled with two values of $\lambda(E)$ to simulate both thermal $[\lambda(E) = 0]$ and energetic $[\lambda(E) = 1.5 \times 10^{-8} \text{ cm}]$ particle bombardment. It should be recognized that in this study, the dissociation mechanism competes with thermally activated processes, namely single-atom desorption and aggregation. Any observed effect that cluster dissociation has on the nucleation kinetics will thus be dependent upon the particular temperature

104
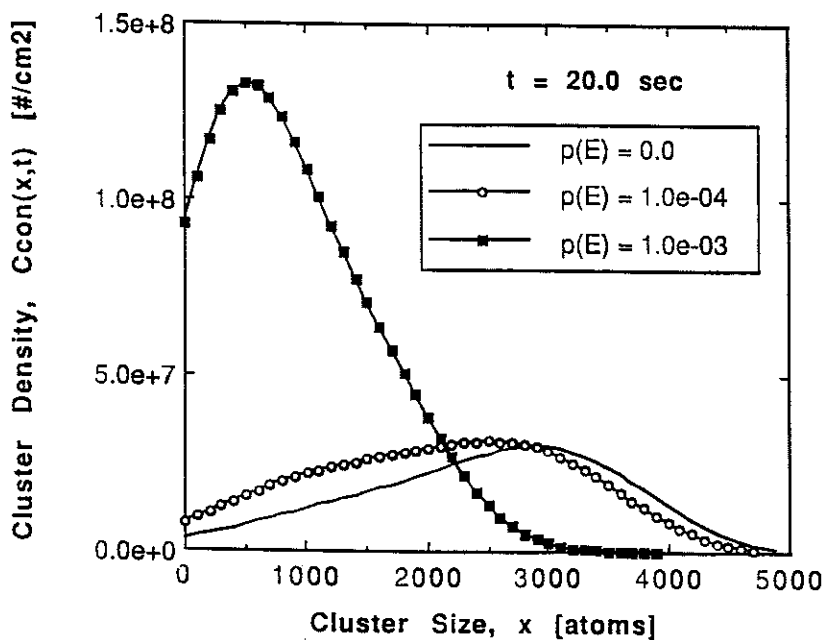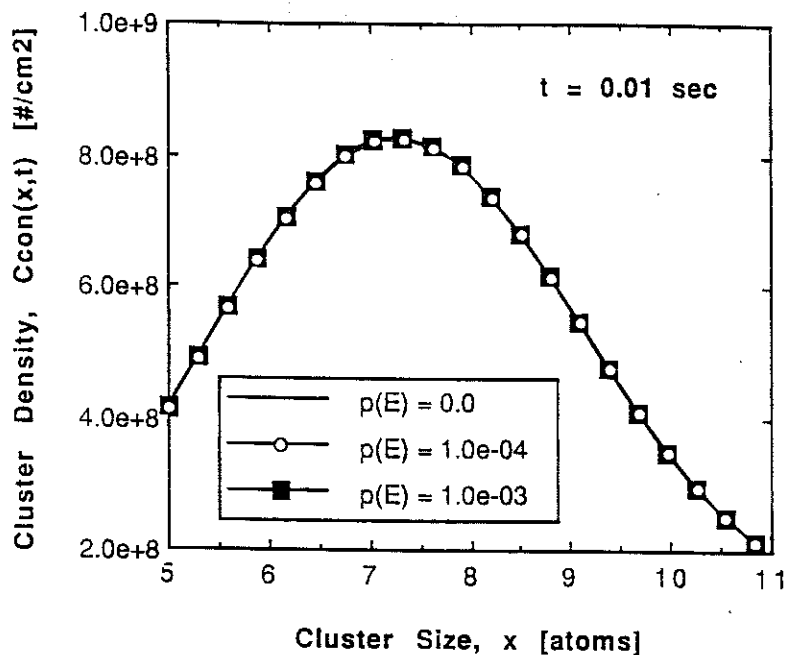
Figure 7.3. Continuum-cluster size distributions at times (a) $t = 0.01$ sec, and (b) $t = 20.0$ sec, for various values of the surface defect production parameter, $p(E)$.

used in the study. For the Au/NaCl system, experiments reveal that cluster mobility is a dominant process even down to a temperature of 133 K; dimers and larger clusters can only be considered immobile at temperatures below 128 K [94]. Since the current model considers that only single atoms are mobile (see Assumptions 6 and 7 in Section 4.1), these dissociation studies are restricted to substrate temperatures of 75, 100, and 125 K in order to be consistent with experimental observations.

During the early growth stages (e. g., less than 15% coverage) at the low substrate temperature of 75 K, dissociation promotes a decrease in the nucleation rate, leading to somewhat smaller cluster densities, as shown in Figures 7.4 and 7.5. The destructive nature of the dissociation process also produces a *smaller*

Figure 7.4. Influence of cluster dissociation on the cluster nucleation rate. The thermal case corresponds to $\lambda(E) = 0$, while the energetic case has $\lambda(E) = 1.5 \times 10^{-8}$ cm.

106
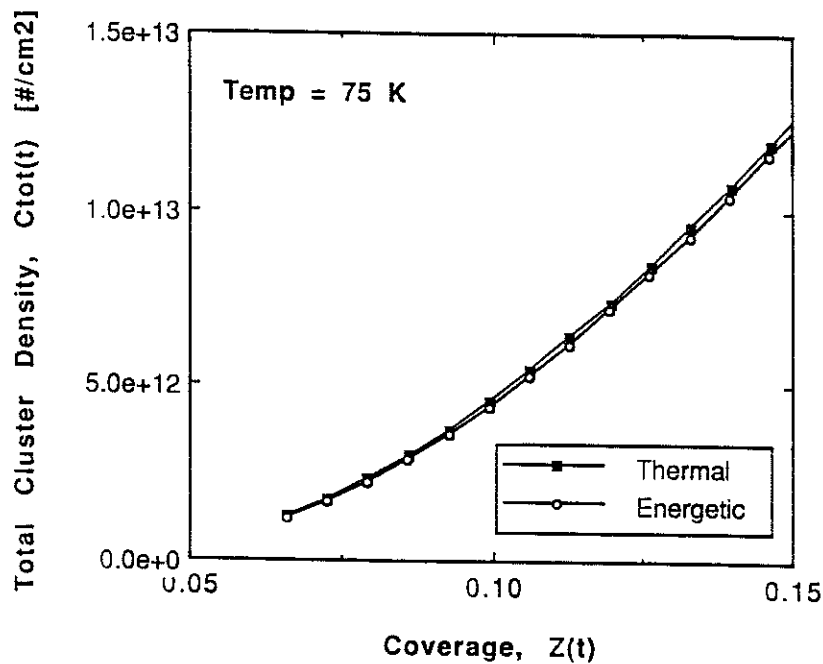
Figure 7.5. Influence of cluster dissociation on the total cluster density. The thermal case corresponds to $\lambda(E) = 0$, while the energetic case has $\lambda(E) = 1.5 \times 10^{-8}$ cm.

average cluster size, as well as a more disperse size distribution, as shown in Figures 7.6 and 7.7. At the higher substrate temperatures of 100 and 125 K, the thermally activated desorption and aggregation reactions become more prevalent. The calculations indicate that cluster dissociation does not influence the nucleation kinetics at these higher temperatures.

Previous experiments studying the effects of ion bombardment on thin film growth have reported a decrease in the nucleation rate, leading to larger average cluster sizes [92,151]. These larger island sizes were attributed to a combination of ion bombardment effects which included enhanced adatom surface diffusion, sputtering, and the dissociation of small islands and clusters. The low-temperature dissociation results presented in this Section, which do not consider enhanced adatom surface diffusion or sputtering, indicate that cluster dissociation
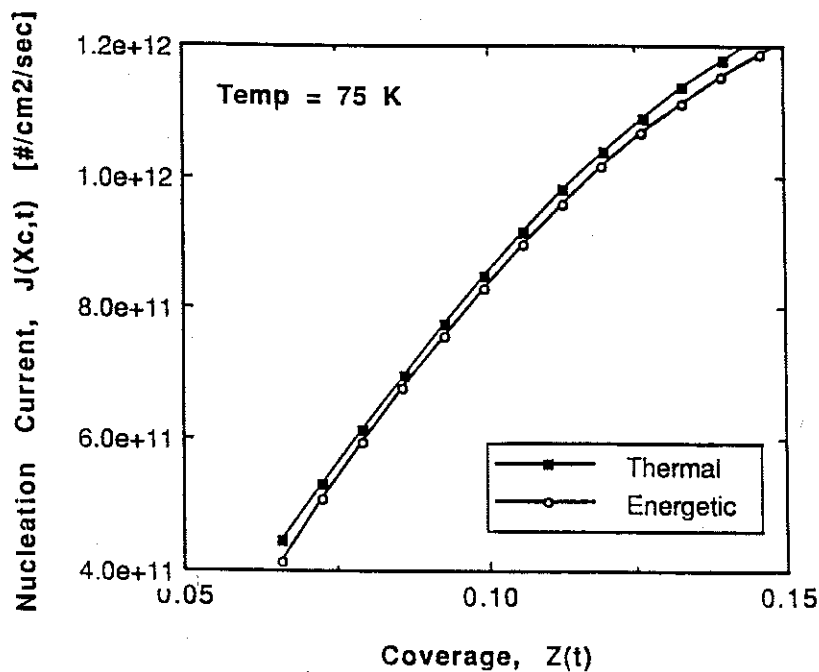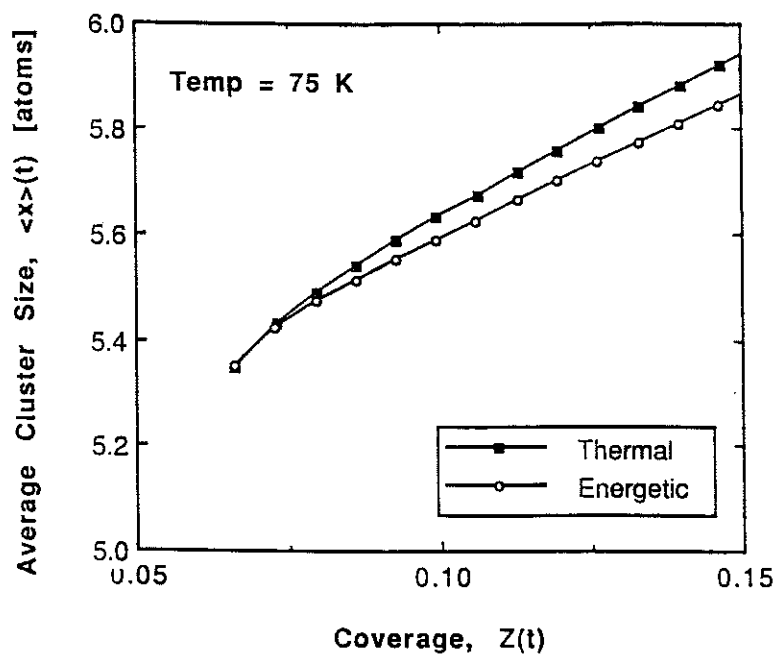
Figure 7.6. Influence of cluster dissociation on the average cluster size. The thermal case corresponds to $\lambda(E) = 0$, while the energetic case has $\lambda(E) = 1.5 \times 10^{-8}$ cm.

decreases the nucleation rate (in agreement with the quoted experiments), but *decreases* the average cluster size. This discrepancy may be due to the fact that the model assumes that any x-atom cluster can dissociate, thus attributing too much importance to dissociation. Other ion bombardment experiments [93], however, agree with the model calculations. Such differences require further investigation.

7.3 Additional Remarks

One should realize that the selected values chosen for the dissociation and trapping parameters, $\lambda(E)$ and $p(E)$, remain open to scrutiny. Molecular dynamics simulations for low-energy ion irradiation studies could possibly be designed to provide actual estimates of $\lambda(E)$ and $p(E)$ as functions of bombardment energy, E. Recent computer simulations indicate that $\lambda(E) \simeq 3 - 5 \times 10^{-8}$ cm for 100
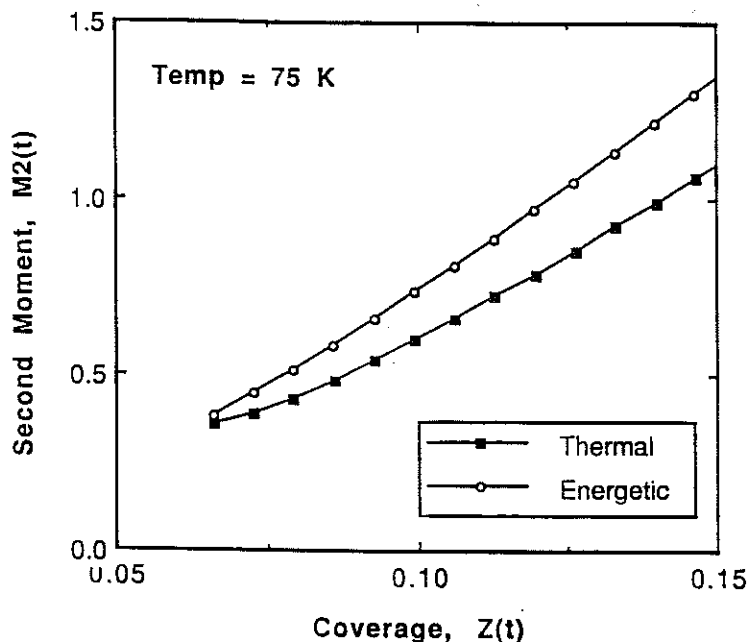
Figure 7.7. Influence of cluster dissociation on the second moment (i. e., variance) of the cluster size distribution. The thermal case corresponds to $\lambda(E) = 0$, while the energetic case has $\lambda(E) = 1.5 \times 10^{-8}$ cm.

eV Cu neutrals incident on a (100) Cu surface [126]. Choosing $\lambda(E) = 1.5 \times 10^{-8}$ cm enables one to model dissociation in the Au/NaCl system with Equation 4.44, greatly simplifying one aspect of the computations. Again, by selecting a range of $\lambda(E)$ and $p(E)$ values, one is able to study the effects of cluster dissociation and surface defect production, but not the details.

The activation energies E_d^T and E_T must also be accurately determined for more quantitative studies. Assuming that E_d^T is equivalent to an activation energy for surface-vacancy diffusion is probably not a bad approximation. Nonetheless, the manner in which traps or other defects influence the nucleation kinetics may be more complicated than currently modeled. Modulated-beam mass spectrometry and thermally stimulated desorption measurements have been used to determine the binding energy of preferred adsorption sites produced by ion irradiation [152,

153], thus promising better estimates of E_T.

Chapter 8

Recommendations and Conclusions

The initial stages of thin film nucleation and growth under low-energy particle bombardment have been investigated with a comprehensive hybrid model that couples a set of discrete kinetic rate equations to a Fokker-Planck-type continuum. As a result, only a few equations are needed to model simple atomic clustering, the total number not being dictated by the size of the largest cluster.

A sensitivity analysis of the model reveals that the transition cluster size, X_c, is simply a mathematical variable which does not influence the atomic clustering physics. The problem of coupling the set of discrete kinetic equations to the continuum at $x = X_c$ seems to be an artifact of the technique used to reconstruct the continuum-cluster size distribution from a finite set of moments. Various reconstruction schemes were considered and indicate that a non-linear method may resolve the discrete-to-continuum coupling problem if one uses enough moments. Although the current model employs a linear reconstruction technique based on a set of Hermite polynomials, the Hybrid System model is not sensitive to small fluctuations in the initial conditions and agrees very well with the Discrete System for large cluster sizes (e. g., $x > \langle x \rangle (t)$).

Atomistic kinetic rate theory models of cluster nucleation and growth are known to be sensitive to activation energies. The activation energies for mobile single-atom diffusion (E_d) and desorption (E_a) influence the single-atom population and cluster aggregation rates, which in turn impact the nucleation kinetics. Increasing E_d decreases the cluster aggregation frequency, $\nu_{m,i}(t)$, whereas decreasing E_a decreases the mobile single-atom density, $C_{mob}(1,t)$. Both of these features reduce the overall cluster aggregation rate, which promotes a faster nucleation rate, a smaller average cluster size, and a less disperse distribution. Since the total cluster density is proportional to the single-atom population, increases in both E_d and E_a promote larger cluster densities.

If a significant number of defects exist on the substrate, then preferred nucleation influences the clustering kinetics. Increasing E_d^T reduces the overall rate at which surface traps interact with other species on the substrate, accelerating particle-cluster kinetics. This promotes a larger cluster density, enhanced nucleation, and a smaller average cluster size. The nucleation kinetics appear to be more sensitive to surface defect diffusion than to defect trapping phenomena.

Thermal particle deposition studies indicate that the computational model compares favorably with an approximate analytical solution and general experimental observations. Although the modeling approach is restricted in the sense that it only considers single-atom mobility, favorable comparisons with the appropriate experimental measurements lend support to the theory. Thermal deposition experiments can be influenced by pre-existing defects on the substrate; numerical studies incorporating this phenomena corroborate experimentally observed trends.

Since a variety of synergistic effects manifest themselves during an energetic particle deposition process, it is not surprising that some discrepancies exist in

the experimental literature. The computational model described in this dissertation attempts to identify the separate influences of surface defect production and cluster dissociation reactions. Surface defect production increases the nucleation rate, leading to larger nuclei densities, smaller average sizes, and a narrower size distribution. At low substrate temperatures, where thermally activated processes are not dominant, cluster dissociation is found to decrease the nucleation rate, promoting smaller island densities. The destructive nature of the dissociation process, however, leads to smaller average sizes and a more disperse size distribution. At higher temperatures, dissociation is found not to influence the nucleation kinetics.

Although energetic particle bombardment may enhance adatom diffusivities, the dissociation results imply that such a phenomenon might become a secondary effect at higher substrate temperatures. The influence of low-energy particle-surface interactions on the later stages of thin film formation could also be significantly different from the early stages, since cluster growth and mobility coalescence reactions must be considered. Energetic particle deposition is remarkably different from thermal particle deposition as exemplified by the differences in calculated cluster size distributions and nucleation kinetics.

One of the novel features of this type of modeling approach is that it provides unique information about the cluster size distribution that has yet to be taken advantage of. For the initial studies presented in this dissertation, a four-moment reconstruction technique is used which allows one to model dispersion, skewness, and kurtosis in the distribution. These features can be readily compared with experimental measurements. If higher moments are needed in order to accurately reproduce a distribution, these characteristics might help experimentalists measure new kinetic parameters (e. g., coalescence rates, dissociation rates,

113

size-dependent features, etc.).

During the later stages of thin film formation, cluster coalescence and multilayer growth will occur. With some modifications, a new hybrid model can incorporate these effects. In the meantime, fundamental insight into the kinetics of cluster nucleation should be pursued. From this foundation, one can develop a better understanding of atomic clustering methods and their role in nucleation and growth phenomena.

Bibliography

[1] D. M. Mattox, *The Application of Plasmas to Thin Film Deposition Processes*, in **Plasma-Surface Interactions and Processing of Materials**, edited by O. Auciello, A. Gras-Marti, J. A. Valles-Abarca, and D. L. Flamm (Kluwer Academic Publishers, The Netherlands, 1990), p. 377.

[2] G. Gautherin, D. Bouchier, and C. Schwebel, *High-Vacuum Deposition Methods Involving Superthermal Free Particles*, in **Thin Films from Free Atoms and Particles**, edited by K. J. Klabunde (Academic Press, Inc., Orlando, FL, 1985), p. 203.

[3] J. M. E. Harper, J. J. Cuomo, R. J. Gambino, and H. R. Kaufman, *Modification of Thin Film Properties by Ion Bombardment During Deposition*, in **Ion Bombardment Modification of Surfaces: Fundamentals and Applications**, edited by O. Auciello and R. Kelly (Elsevier, Amsterdam, 1984), p. 127.

[4] T. Sugano, *Introduction: Importance of Plasma Processes in Semiconductor Fabrication*, in **Applications of Plasma Processes to VLSI Technology**, edited by T. Sugano (John Wiley & Sons, Inc., New York, NY, 1985), p. 1.

[5] Y. Hirooka, D. M. Goebel, R. W. Conn, G. A. Campbell, W. K. Leung, K. L. Wilson, W. Bauer, R. A. Causey, D. H. Morse, and J. Bohdansky, *Materials Surface Modification by Plasma Bombardment Under Simultaneous Erosion and Redeposition Conditions*, Nucl. Instrum. Methods **B23**, 458 (1987).

[6] D. M. Goebel, Y. Hirooka, R. W. Conn, W. K. Leung, G. A. Campbell, J. Bohdansky, K. L. Wilson, W. Bauer, R. A. Causey, A. E. Pontau, A. R. Krauss, D. M. Gruen, and M. H. Mendelsohn, *Erosion and Redeposition Experiments in the PISCES Facility*, J. Nucl. Mater. **145-147**, 61 (1987).

[7] Y. Hirooka, D. M. Goebel, R. W. Conn, W. K. Leung, and G. A. Campbell, *Materials Erosion and Redeposition Studies at the PISCES Facility – Net Erosion Under Redeposition*, J. Nucl. Mater. **141-143**, 193 (1986).

[8] P. Sioshansi, *Ion Beam Modification of Materials for Industry*, Thin Solid Films **118**, 61 (1984).

[9] J. A. Venables and G. L. Price, *Nucleation of Thin Films*, in **Epitaxial Growth**, edited by J. W. Matthews (Academic Press, Inc., New York, NY, 1975), p. 381.

[10] B. Lewis and J. C. Anderson, **Nucleation and Growth of Thin Films** (Academic Press, Inc., New York, NY, 1978).

[11] Panel Discussion, *Impact of Recent Computer Compatibility Growth on Optical Coating Models*, in **Modeling of Optical Thin Films**, edited by M. R. Jacobson (Proc. SPIE 821, Bellingham, WA, 1987), p. 142.

[12] D. L. Adler and B. H. Cooper, *Design and Performance of an UHV Beamline to Produce Low and Hyperthermal Energy Ion Beams*, Rev. Sci. Instrum. **59**, 137 (1988).

[13] D. R. Frankl and J. A. Venables, *Nucleation on Substrates from the Vapour Phase*, Advan. Phys. **19**, 409 (1970).

[14] A. J. Donohoe and J. L. Robins, *Mobility and Coalescence of Nuclei in Metal Vapour Deposition on Alkali Halide Substrates*, J. Cryst. Growth **17**, 70 (1972).

[15] R. S. Wagner and R. J. H. Voorhoeve, *Adsorption and Growth of Cadmium on Polycrystalline Tungsten*, J. Appl. Phys. **42**, 3948 (1971).

[16] R. J. H. Voorhoeve and R. S. Wagner, *Adsorption, Nucleation, and Growth of Cadmium on Tungsten Covered with Oxygen or Hydrogen*, Metall. Trans. **2**, 3421 (1971).

[17] D. W. Bassett and M. J. Parsley, *Field Ion Microscope Observations of Cluster Formation in Metal Deposits on Tungsten Surfaces*, Nature **221**, 1046 (1969).

[18] D. W. Bassett and M. J. Parsley, *Field Ion Microscope Studies of Transition Metal Adatom Diffusion on (110), (211), and (321) Tungsten Surfaces*, J. Phys. **D3**, 707 (1970).

[19] D. W. Bassett, *The Use of Field Ion Microscopy in Studies of the Vapour Deposition of Metals*, Surf. Sci. **23**, 240 (1970).

[20] T. T. Tsong, *Direct Observation of Interactions between Individual Atoms on Tungsten Surfaces*, Phys. Rev. **B6**, 417 (1972).

[21] T. T. Tsong, *Surface Diffusion and Cluster Binding Energy of Individual Atoms on Tungsten Surfaces*, Phys. Rev. **B7**, 4018 (1973).

[22] W. R. Graham, D. A. Reed, and F. Hutchinson, *Epitaxy at Low Temperatures by Vapor Deposition of Pd, Pt, Rh, and Ir Observed by Field Ion Microscopy*, J. Appl. Phys. **43**, 2951 (1972).

[23] V. N. E. Robinson and J. L. Robins, *Nucleation Kinetics of Gold Deposited Onto UHV Cleaved Surfaces of NaCl and KBr*, Thin Solid Films **20**, 155 (1974).

[24] J. L. Robins and A. J. Donohoe, *An Experimental Study of the Growth Kinetics of Vapour-Deposited Thin Metal Films*, Thin Solid Films **12**, 255 (1972).

[25] H. Schmeisser and M. Harsdorff, *Note on "Rate Equation Approaches to Thin Film Nucleation Kinetics" by J. A. Venables*, Phil. Mag. **27**, 739 (1973).

[26] H. Schmeisser, *Growth and Mobility Effects of Gold Clusters on Rocksalt (100) Surfaces Studied with the Method of Quantitative Image Analysis, Part II: Spatial Distribution of Clusters*, Thin Solid Films **22**, 99 (1974).

[27] J. M. Corbett and F. W. Boswell, *Experimental Investigation of the Nucleation of Silver on Molybdenite*, J. Appl. Phys. **40**, 2663 (1969).

[28] H. Poppa, K. Heinemann, and A. G. Elliot, *Epitaxial Orientation Studies of Gold on UHV-Cleaved Mica During Early Stages of Nucleation and Growth*, J. Vac. Sci. Technol. **8**, 471 (1971).

[29] W. L. Morris and R. L. Hines, *Nucleation of Gold on Muscovite Mica*, J. Appl. Phys. **41**, 2231 (1970).

[30] B. A. Joyce and R. R. Bradley, *A Study of Nucleation in Chemically Grown Epitaxial Silicon Films using Molecular Beam Techniques I. – Experimental Methods*, Phil. Mag. **14**, 289 (1966).

[31] B. A. Joyce, J. H. Neave, and B. E. Watts, *The Influence of Substrate Surface Conditions on the Nucleation and Growth of Epitaxial Silicon Films*, Surf. Sci. **15**, 1 (1969).

[32] H. M. Kramer and J. A. Venables, *Epitaxial Growth of Rare Gas Crystals*, J. Cryst. Growth **17**, 329 (1972).

[33] T. A. McLauchlan, R. S. Sennett, and G. D. Scott, *Continuous Observations with the Electron Microscope on the Formation of Evaporated Films of Silver, Gold, and Tin*, Can. J. Res. **28A**, 530 (1950).

[34] H. Poppa, *Heterogeneous Nucleation of Bi and Ag on Amorphous Substrates (In Situ Electron Microscopy Studies)*, J. Appl. Phys. **38**, 3883 (1967).

[35] V. Halpern, *Cluster Growth and Saturation Island Densities in Thin-Film Growth*, J. Appl. Phys. **40**, 4627 (1969).

[36] J. W. Matthews, *The Role of Contaminants in the Epitaxial Growth of Gold on Sodium Chloride*, Phil. Mag. **12**, 1143 (1965).

[37] J. D. Weeks, G. H. Gilmer, and K. A. Jackson, *Analytical Theory of Crystal Growth*, J. Chem. Phys. **65**, 712 (1976).

[38] J. F. Hamilton, D. R. Preuss, and G. R. Apai, *Nucleation and Growth of Vacuum-Deposited Metal Aggregates Studied by Electron Microscopy*, Surf. Sci. **106**, 146 (1981).

[39] G. Apai, J. F. Hamilton, J. Stohr, and A. Thompson, *Extended X-Ray–Absorption Fine Structure of Small Cu and Ni Clusters: Binding-Energy and Bond-Length Changes with Cluster Size*, Phys. Rev. Lett. **43**, 165 (1979).

[40] J. M. Burkstrand, *Core-Level Spectra of Chromium and Nickel Atoms on Polystyrene*, J. Appl. Phys. **50**, 1152 (1979).

[41] W. F. Egelhoff, Jr. and G. G. Tibbetts, *Growth of Copper, Nickel, and Palladium Films on Graphite and Amorphous Carbon*, Phys. Rev. **B19**, 5028 (1979).

[42] R. C. Baetzold, M. G. Mason, and J. F. Hamilton, *Determination of the Particle Size Required for Bulk Metallic Properties*, J. Chem. Phys. **72**, 366 (1980).

[43] C. Chapon and C. R. Henry, *Mobility Effects of Submicroscopical Particles During the Deposition of Ultrathin Gold Films on Alkali Halide*, Surf. Sci. **106**, 152 (1981).

[44] J. F. Hamilton and P. C. Logel, *Nucleation and Growth of Ag and Pd on Amorphous Carbon by Vapor Deposition*, Thin Solid Films **16**, 49 (1973).

[45] J. F. Hamilton and P. C. Logel, *Vapor Deposition of Silver, Gold and Palladium on Carbon and Silicon Dioxide in Ion-Pumped Vacuum*, Thin Solid Films **23**, 89 (1974).

[46] J. F. Hamilton and P. C. Logel, *Vapor Deposition of Silver, Gold and Palladium on Carbon and Silicon Dioxide in Ion-Pumped Vacuum*, Thin Solid Films **29**, L24 (1975).

[47] E. B. Prestridge, G. H. Via, and J. H. Sinfelt, *Electron Microscopy Studies of Metal Clusters: Ru, Os, Ru-Cu, and Os-Cu*, J. Catal. **50**, 115 (1977).

[48] R. T. K. Baker and J. A. France, *Growth Characteristics of Supported Palladium Particles in Gaseous Environments*, J. Catal. **39**, 481 (1975).

[49] J. G. Allpress and J. V. Sanders, *The Structure and Orientation of Crystals in Deposits of Metals on Mica*, Surf. Sci. **7**, 1 (1967).

[50] R. Niedermayer, *Formation of Ad-Layers and Clusters on Condensation of Metal Vapors on Solid Surfaces*, Angew. Chem. Int. Ed. Engl. **14**, 212 (1975).

[51] J. A. Venables, *Nucleation and Growth Processes in Thin Film Formation*, J. Vac. Sci. Technol. **B4**, 870 (1986).

[52] D. J. Mikalsen, R. A. Roy, D. S. Yee, S. A. Shivashankar, and J. J. Cuomo, *Superconducting Thin Films of the Bi-Sr-Ca-Cu-O System Prepared by Multilayer Metal Deposition*, J. Mater. Res. **3**, 613 (1988).

[53] C. -A. Chang, C. C. Tsuei, C. C. Chi, M. R. Scheuermann, D. S. Yee, and J. P. Berosh, *Formation of Thin Film YBaCuO Superconductors from $Cu/BaO/Y_2O_3$ Layer Structures*, Mater. Res. Soc. Symp. Proc. **99**, 315 (1988).

[54] C. -A. Chang, C. C. Tsuei, C. C. Chi, and T. R. McGuire, *Thin-Film YBaCuO Superconductors Formed by $Cu/BaO/Y_2O_3$ Layer Structures*, Appl. Phys. Lett. **52**, 72 (1988).

118

[55] M. Volmer and A. Weber, *Keimbildung in übersättigten Gebilden*, Zeitschr. f. physik. Chemie **119**, 277 (1926).

[56] R. Becker and W. Döring, *Kinetische Behandlung der Keimbildung in übersättigten Dämpfen*, Ann. d. Phys. Lpz. **24**, 719 (1935).

[57] J. P. Hirth and G. M. Pound, **Condensation and Evaporation: Nucleation and Growth Kinetics** (Pergamon Press, Oxford, 1963).

[58] B. Lewis and D. S. Campbell, *Nucleation and Initial-Growth Behavior of Thin-Film Deposits*, J. Vac. Sci. Technol. **4**, 209 (1967).

[59] J. Frenkel, *Theorie der Adsorption und verwandter Erscheinungen*, Zeit. Phys. **26**, 117 (1924).

[60] D. Walton, *Nucleation of Vapor Deposits*, J. Chem. Phys. **37**, 2182 (1962).

[61] G. Zinsmeister, *A Contribution to Frenkel's Theory of Condensation*, Vacuum **16**, 529 (1966).

[62] G. Zinsmeister, *Theory of Thin Film Condensation – Part B: Solution of the Simplified Condensation Equation*, Thin Solid Films **2**, 497 (1968).

[63] G. Zinsmeister, *Theory of Thin Film Condensation – Part C: Aggregate Size Distribution in Island Films*, Thin Solid Films 4, 363 (1969).

[64] B. Lewis, *Bond Energy Formulations of Heterogeneous Nucleation Theory*, Thin Solid Films 1, 85 (1967).

[65] R. M. Logan, *Saturation Density of Nuclei on a Surface from the Microscopic Rate Equations*, Thin Solid Films 3, 59 (1969).

[66] K. Takeuchi and K. Kinosita, *Mobility of Gold Clusters on a-C Substrates*, Thin Solid Films **75**, L1 (1981).

[67] K. Takeuchi and K. Kinosita, *Mobility of Gold Clusters on Amorphous Carbon Substrates I: Analysis of Cluster Density Versus Time Relations*, Thin Solid Films **90**, 27 (1982).

[68] H. D. Velfe and M. Krohn, *Root Function Solutions in a Nucleation Theory Considering Small Cluster Mobility*, Thin Solid Films **98**, 125 (1982).

[69] B. K. Chakraverty, *Grain Size Distribution in Thin Films – 2: Non-Conservative Systems*, J. Phys. Chem. Solids **28**, 2413 (1967).

[70] K. J. Routledge and M. J. Stowell, *Nucleation Kinetics in Thin Film Growth – I: Computer Simulation of Nucleation and Growth Behavior*, Thin Solid Films **6**, 407 (1970).

[71] J. B. Adams, W. N. G. Hitchon, and L. M. Holzmann, *Kinetics of Growth Coalescence of In/GaAs*, J. Vac. Sci. Technol. A**6**, 2029 (1988).

[72] W. B. Hillig, *A Derivation of Classical Two-Dimensional Nucleation Kinetics and the Associated Crystal Growth Laws*, Acta. Metall. **14**, 1868 (1966).

[73] M. Hayashi, *Improved Theory of the Growth of Perfect Crystals*, Phys. Soc. Jpn. J. **35**, 614 (1973).

[74] U. Bertocci, *The Influence of Step Motion and Two-Dimensional Nucleation on the Rate of Crystal Growth: Some Computer Simulation Experiments*, Surf. Sci. **15**, 286 (1969).

[75] J. D. Weeks and G. H. Gilmer, *Dynamics of Crystal Growth*, Adv. Chem. Phys. **40**, 157 (1979).

[76] J. A. Thornton, *Influence of Apparatus Geometry and Deposition Conditions on the Structure and Topography of Thick Sputtered Coatings*, J. Vac. Sci. Technol. **11**, 666 (1974).

[77] A. Sedehi, Z. H. Meiksin, and J. R. Blachere, *Real-Time Simulation of Nucleation and Growth of Vacuum-Evaporated Thin Metallic Films*, Thin Solid Films **98**, 49 (1982).

[78] R. A. Outlaw and J. H. Heinbockel, *Summary Abstract: Atomistic Simulation of Thin Film Nucleation and Growth of Au/NaCl (100)*, J. Vac. Sci. Technol. **A3**, 820 (1985).

[79] A. C. Adams and K. A. Jackson, *Computer Simulation of Vapor Deposition*, J. Cryst. Growth **13-14**, 144 (1972).

[80] S. H. Bauer and D. J. Frurip, *Homogeneous Nucleation in Metal Vapors – 5: A Self-Consistent Kinetic Model*, J. Phys. Chem. **81**, 1015 (1977).

[81] A. C. Hindmarsh, **GEAR: Ordinary Differential Equation System Solver** (Lawrence Livermore Laboratory, UCID-30001 Rev-1, Computer Documentation, 1972).

[82] C. F. Clement and M. H. Wood, *Equations for the Growth of a Distribution of Small Physical Objects*, Proc. R. Soc. Lond. **A368**, 521 (1979).

[83] J. A. Thornton, *The Microstructure of Sputter-Deposited Coatings*, J. Vac. Sci. Technol. **A4**, 3059 (1986).

[84] H. H. Andersen and H. L. Bay, *Sputtering Yield Measurements*, in **Sputtering by Particle Bombardment I: Physical Sputtering of Single-Element Solids**, edited by R. Behrisch (Springer-Verlag, Berlin, 1981), p. 145.

[85] H. E. Roosendaal, *Sputtering Yields of Single Crystalline Targets*, in **Sputtering by Particle Bombardment I: Physical Sputtering of Single-Element Solids**, edited by R. Behrisch (Springer- Verlag, Berlin, 1981), p. 219.

[86] B. L. Cain, personal communication (University of Illinois-Urbana, October 24, 1988).

[87] J. E. Greene, S. A. Barnett, J.-E. Sundgren, and A. Rockett, *Low-Energy Ion/Surface Interactions During Film Growth from the Vapor Phase: Effects on Nucleation and Growth Kinetics, Defect Structure, and Elemental Incorporation Probabilities*, in **Plasma-Surface Interactions and Processing of Materials**, edited by O. Auciello, A. Gras-Marti, J. A. Valles-Abarca, and D. L. Flamm (Kluwer Academic Publishers, The Netherlands, 1990), p. 281.

[88] J. E. Greene and S. A. Barnett, *Ion-Surface Interactions During Vapor Phase Crystal Growth by Sputtering, MBE, and Plasma-Enhanced CVD: Applications to Semiconductors*, J. Vac. Sci. Technol. **21**, 285 (1982).

[89] J. E. Greene, *Epitaxial Crystal Growth by Sputter Deposition: Applications to Semiconductors, Part 2*, CRC Critical Reviews in Solid State and Materials Sciences **11**, 189 (1983).

[90] J. E. Greene, T. Motooka, J.-E. Sundgren, D. Lubben, S. Gorbatkin, and S. A. Barnett, *The Role of Ion/Surface Interactions and Photo-Induced Reactions During Film Growth from the Vapor Phase*, Nucl. Instrum. Meth. in Physics Research **B27**, 226 (1987).

[91] E. Krikorian and R. J. Sneed, *Nucleation, Growth, and Transformation of Amorphous and Crystalline Solids Condensing from the Gas Phase*, Astrophys. Space Sci. **65**, 129 (1979).

[92] M.-A. Hasan, S. A. Barnett, J.-E. Sundgren, and J. E. Greene, *Nucleation and Initial Growth of In Deposited on Si_3N_4 Using Low-Energy ($\leq$ 300 eV) Accelerated Beams in Ultrahigh Vacuum*, J. Vac. Sci. Technol. **A5**, 1883 (1987).

[93] T. C. Huang, G. Lim, F. Parmigiani, and E. Kay, *Effect of Ion Bombardment During Deposition on the X-ray Microstructure of Thin Silver Films*, J. Vac. Sci. Technol. **A3**, 2161 (1985).

[94] B. F. Usher and J. L. Robins, *The Initial Nucleation and Growth of Gold on Sodium Chloride for Substrate Temperatures Between 123 and 448 K*, Thin Solid Films **155**, 267 (1987).

[95] H. Schmeisser, *Growth and Mobility Effects of Gold Clusters on Rocksalt (100) Surfaces Studied with the Method of Quantitative Image Analysis, Part I: Cluster Size Distributions*, Thin Solid Films **22**, 83 (1974).

[96] B. F. Usher and J. L. Robins, *The Role of Preferred Surface Sites in the Nucleation and Growth of Gold on Sodium Chloride I: The Influence of Low Energy Electrons*, Thin Solid Films **149**, 351 (1987).

[97] B. F. Usher and J. L. Robins, *The Role of Preferred Surface Sites in the Nucleation and Growth of Gold on Sodium Chloride II: Reanalysis of Two Comprehensive Studies*, Thin Solid Films **149**, 363 (1987).

[98] B. Lewis and M. R. Jordan, *Nucleation and Epitaxy of Gold Deposits on Sodium Chloride Substrates During Electron Bombardment*, Thin Solid Films **6**, 1 (1970).

[99] B. N. Chapman and D. S. Campbell, *Condensation of High-Energy Atomic Beams*, J. Phys. **C2**, 200 (1969).

[100] G. E. Lane and J. C. Anderson, *The Nucleation and Initial Growth of Gold Films Deposited Onto Sodium Chloride by Ion-Beam Sputtering*, Thin Solid Films **26**, 5 (1975).

[101] G. E. Lane and J. C. Anderson, *Features of the Initial Growth of Gold Films Deposited on Rock-Salt Substrates by Ion Beam Sputtering*, Thin Solid Films **57**, 277 (1979).

[102] M. Harsdorff and W. Jark, *Nucleation and Growth Kinetics of Gold Films Deposited Onto Rock Salt Single-Crystal (100) Surfaces by RF Sputtering with Helium*, Thin Solid Films **128**, 79 (1985).

[103] G. M. McCracken and P. E. Stott, *Plasma-Surface Interactions in Tokamaks*, Nuclear Fusion **19**, 889 (1979).

[104] W. M. Stacey, **Fusion: An Introduction to the Physics and Technology of Magnetic Confinement Fusion** (John Wiley & Sons, Inc., New York, NY, 1984), p. 96.

[105] M. F. Smith and J. B. Whitley, *Coatings in Magnetic Fusion Devices*, J. Vac. Sci. Technol. **A4**, 3038 (1986).

[106] P. Sigmund, *Sputtering by Ion Bombardment: Theoretical Concepts*, in **Sputtering by Particle Bombardment I: Physical Sputtering of Single-Element Solids**, edited by R. Behrisch (Springer- Verlag, Berlin, 1981), p. 9.

[107] P. Sigmund, *Theory of Sputtering I: Sputtering Yield of Amorphous and Polycrystalline Targets*, Phys. Rev. **184**, 383 (1969).

[108] R. J. MacDonald, *The Ejection of Atomic Particles from Ion Bombarded Solids*, Advan. Phys. **19**, 457 (1970).

[109] M. T. Robinson, *Theoretical Aspects of Monocrystal Sputtering*, in **Sputtering by Particle Bombardment I: Physical Sputtering of Single-Element Solids**, edited by R. Behrisch (Springer- Verlag, Berlin, 1981), p. 73.

[110] J. N. Brooks, *Erosion and Redeposition Analysis for Limiter and Divertor Impurity Control Systems*, J. Nucl. Mater. **111-112**, 457 (1982).

[111] J. N. Brooks and R. T. McGrath, *Redeposition of the Sputtered Surface in Limiters*, in **Proc. 9**[th] **Symp. on Engineering Problems of Fusion Research** (IEEE Pub. 81CH1715-2, 1981), vol. 1, p. 495.

[112] W. Eckstein and J. P. Biersack, *Reflection of Low-Energy Hydrogen from Solids*, Appl. Phys. **A38**, 123 (1985).

[113] M. I. Baskes, *Dynamical Calculation of Low Energy Hydrogen Reflection*, J. Nucl. Mater. **128-129**, 676 (1984).

[114] R. Behrisch and W. Eckstein, *Ion Backscattering from Solid Surfaces*, in **Physics of Plasma-Wall Interactions in Controlled Fusion**, edited by D. E. Post and R. Behrisch (Plenum Press, New York, 1986), p. 413.

[115] J. P. Biersack and L. G. Haggmark, *A Monte Carlo Computer Program for the Transport of Energetic Ions in Amorphous Targets*, Nucl. Instrum. Meth. **174**, 257 (1980).

[116] J. P. Biersack and W. Eckstein, *Sputtering Studies with the Monte Carlo Program TRIM.SP*, Appl. Phys. **A34**, 73 (1984).

[117] P. Chou and N. M. Ghoniem, *Precipitate Dissolution by High Energy Collision Cascades*, J. Nucl. Mater. **117**, 55 (1983).

[118] P. S. Chou and N. M. Ghoniem, *Collisional Aspects of Preferential Sputtering Using the Monte Carlo Method*, J. Nucl. Mater. **141-143**, 216 (1986).

[119] P. S. Chou and N. M. Ghoniem, *Applications of the Monte Carlo Code TRIPOS to Surface and Bulk Ion Transport Problems*, Nucl. Instrum. Meth. **B28**, 175 (1987).

[120] O. Vancauwenberghe, personal communication (Massachusetts Institute of Technology, October 8, 1990).

[121] M. S. Daw and M. I. Baskes, *Semiempirical, Quantum Mechanical Calculation of Hydrogen Embrittlement in Metals*, Phys. Rev. Lett. **50**, 1285 (1983).

[122] M. S. Daw and M. I. Baskes, *Embedded-Atom Method: Derivation and Application to Impurities, Surfaces, and Other Defects in Metals*, Phys. Rev. **B29**, 6443 (1984).

[123] J. F. Ziegler, J. P. Biersack, and U. Littmark, **The Stopping and Range of Ions in Solids** (Pergamon Press, New York, NY, 1985), Ch. 3, *Electronic Stopping Cross-Sections*.

[124] S. P. Chou and N. M. Ghoniem, *Molecular Dynamics of Collision Cascades With Composite Pair / Many-Body Potentials*, to be published in Phys. Rev. **B**.

[125] A. K. Prinja, personal communication (University of New Mexico, November 22, 1988).

[126] P. Chou, personal communication (University of California, Los Angeles, August, 1990).

[127] J. L. Katz and M. D. Donohue, *A Kinetic Approach to Homogeneous Nucleation Theory*, Adv. Chem. Phys. 40, 137 (1979).

[128] J. Frenkel, **Kinetic Theory of Liquids** (Oxford Press, New York, 1946), Ch. VII, *Kinetics of Phase Transitions*.

[129] F. C. Goodrich, *Nucleation Rates and the Kinetics of Particle Growth II: The Birth and Death Process*, Proc. R. Soc. Lond. **A277**, 167 (1964).

[130] W. G. Wolfer, L. K. Mansur, and J. A. Sprague, *Theory of Swelling and Irradiation Creep*, in **Proceedings of the International Conference on Radiation Effects in Breeder Reactor Structural Materials**, edited by M. L. Bleiberg and J. W. Bennett (TMS-AIME, New York, 1977), p. 841.

[131] N. M. Ghoniem and S. Sharafat, *A Numerical Solution to the Fokker-Planck Equation Describing the Evolution of the Interstitial Loop Microstructure During Irradiation*, J. Nucl. Mater. **92**, 121 (1980).

[132] N. M. Ghoniem, *Stochastic Theory of Diffusional Planar-Atomic Clustering and its Application to Dislocation Loops*, Phys. Rev. **B39**, 11810 (1989).

[133] C. A. Stone and N. M. Ghoniem, *Modeling the Early Stages of Thin Film Formation by Energetic Atom Deposition*, Metall. Trans. A **20A**, 2609 (1989).

[134] C. A. Stone and N. M. Ghoniem, *The Effects of Cluster Size-Dependent Aggregation on Thin Film Formation*, Vacuum **41**, 1111 (1990).

[135] C. A. Stone and N. M. Ghoniem, *The Influence of Low-Energy Particle-Surface Interactions on the Initial Stages of Thin Film Formation*, to be published in J. Vac. Sci. Technol. A, May/June 1991.

[136] M. Kendall and A. Stuart, **The Advanced Theory of Statistics: Volume 1 – Distribution Theory**, 4th edition (Charles Griffin & Company Limited, London, 1977), Ch. 6, *Systems of Distributions.*

[137] F. C. Goodrich, *Nucleation Rates and the Kinetics of Particle Growth I: The Pure Birth Process*, Proc. R. Soc. Lond. **A277**, 155 (1964).

[138] F. C. Goodrich, *Approximate Solutions to the Pure Birth Process*, Nature **198**, 220 (1963).

[139] M. Kendall and A. Stuart, **The Advanced Theory of Statistics: Volume 1 – Distribution Theory**, 4th edition (Charles Griffin & Company Limited, London, 1977), Ch. 3, Sec. 3, *Calculation of Moments.*

[140] K. B. Winterbon, P. Sigmund, and J. B. Sanders, *Spatial Distribution of Energy Deposited by Atomic Particles in Elastic Collisions*, Det Kongelige Danske Videnskabernes Selskab Matematisk-fysiske Meddelelser **37**, 14 (1970).

[141] M. Vicanek, *Derivations and Solution Methods of Evolution Equations for Surface Atomic Clustering*, UCLA/ENG-9025, PPG-1321 (August 1990).

[142] E. T. Jaynes, *Information Theory and Statistical Mechanics*, Phys. Rev. **106**, 620 (1957).

[143] E. T. Jaynes, *Information Theory and Statistical Mechanics II*, Phys. Rev. **108**, 171 (1957).

[144] E. T. Jaynes, *Prior Information and Ambiguity in Inverse Problems*, in **Inverse Problems**, edited by D. W. McLaughlin (American Mathematical Society, Providence, RI, 1984), p. 151.

[145] W. T. Grandy, Jr., *Incomplete Information and Generalized Inverse Problems*, in **Maximum-Entropy and Bayesian Methods in Inverse Problems**, edited by C. R. Smith and W. T. Grandy, Jr. (D. Reidel Publishing Company, Dordrecht, Holland, 1985), p. 1.

[146] E. T. Jaynes, *Prior Probabilities*, IEEE Trans. Syst. Sci. Cybern. **SSC-4**, 227 (1968).

[147] Vadim I. Rakhovsky, personal communication (Head of Department, All-Union Research Centre for Surface and Vacuum Investigations, Gosstandart, Moscow, USSR, October 7, 1990).

For the inquisitive reader that has taken an interest in this source, I must enlighten you with a few details about my encounter. Professor Rakhovsky and I met on a bus that took us from the Toronto (YYZ) airport to our downtown hotels in Toronto where we were both presenting papers at the 37th Annual American Vacuum Society Symposium. He sat down beside me and we started talking about all sorts of things in general when I suddenly realized that here was a man, 40 years my senior, who had seen things that I will probably never experience. The same for me; I have probably done things that Vadim could only dream about doing. With all the crazy politics going on in the world at the time, I thought, why in the hell are people always fighting something or someone? On a global scale, no two individuals are any different and no single person deserves any more rights or freedoms than another. Anyway, we said our good-byes and will probably never see one another again. Although I am a better individual for the encounter, the world still spins off-axis. It seems as though only science and music transcend the political boundaries that shackle the human spirit.

[148] B. F. Usher and J. L. Robins, *The Mobility of Gold Clusters on Sodium Chloride at Temperatures Between 123K and Ambient*, Thin Solid Films **90**, 15 (1982).

[149] A. D. Gates and J. L. Robins, *Summary Abstract: A Comprehensive Explanation of Existing Gold on NaCl Nucleation Data*, J. Vac. Sci. Technol. **A5**, 1742 (1987).

[150] B. Lewis and J. C. Anderson, **Nucleation and Growth of Thin Films** (Academic Press, Inc., New York, NY, 1978), Ch. 8, *Nucleation and Growth on Preferred Sites*.

[151] M. Marinov, *Effect of Ion Bombardment on the Initial Stages of Thin Film Growth*, Thin Solid Films **46**, 267 (1977).

[152] S. A. Barnett, H. F. Winters, and J. E. Greene, *The Interaction of Sb_4 Molecular Beams with Si (100) Surfaces: Modulated-Beam Mass Spectrometry and Thermally Stimulated Desorption Studies*, Surf. Sci. **165**, 303 (1986).

[153] S. A. Barnett, H. F. Winters, and J. E. Greene, *Influence of Ion Bombardment on the Interaction of Sb with the Si (100) Surface*, Surf. Sci. **181**, 596 (1987).